UNIVERSIDAD DE CHILE
FACULTAD DE CIENCIAS FÍSICAS Y MATEMÁTICAS
DEPARTAMENTO DE INGENIERÍA ELÉCTRICA

MODELING LOSSES IN MICROSTRIP TRAVELING WAVE KINETIC INDUCTANCE PARAMETRIC AMPLIFIERS USING THE FOUR AND THREE WAVE MIXING EFFECT

TESIS PARA OPTAR AL GRADO DE
MAGÍSTER EN CIENCIAS DE LA INGENIERÍA, MENCIÓN ELÉCTRICA

DANIEL ALEJANDRO VALENZUELA HENRÍQUEZ

PROFESOR GUÍA:
PATRICIO MENA MENA

MIEMBROS DE LA COMISIÓN:
CLAUDIO FALCON BEAS
DIANA DULIC
VINCENT DESMARIS

Este trabajo ha sido financiado por CONICYT a través del proyecto FONDECYT 1180700

SANTIAGO DE CHILE
2020

RESUMEN

MODELING LOSSES IN MICROSTRIP TRAVELING WAVE KINETIC INDUCTANCE PARAMETRIC AMPLIFIERS USING THE FOUR AND THREE WAVE MIXING EFFECT

El rendimiento de un amplificador esta basado en su ganancia y ruido. Para minimizar el ruido a altas frecuencias, se han estado desarrollando los *amplificadores paramétricos superconductores*. Estos son sistemas que usan un proceso no lineal y una fuerte referencia para transferir la energía a la señal original y a sus armónicos. En esta tesis son discutidos dos tipos de procesos, los Four-wave mixing (FWM) y Three-wave mixing (TWM).

Una implementación de este tipo de dispositivo es el *amplificador paramétrico de onda viajera e inductancia cinética* (TKIPA). Este consiste en una línea de transmisión superconductora, el cual utiliza un elemento no lineal para transferir la energía hacia la señal objetivo. Con el diseño apropiado, se pueden rechazar los armónicos indeseables para concentrar la energía en la señal (y no en los armónicos). La primera implementación de un TKIPA utilizó guia de onda coplanar (CPW), donde impedancias cercanas a los $50\,\Omega$ son difíciles de obtener. En esta tesis, un TKIPA fue diseñado utilizando una línea microstrip. Una microstrip de $50\,\Omega$ es más fácil de obtener, resolviendo el problema de acoplamiento con la electrónica de salida.

Hemos presentado dos diseños de un TKIPA basados en línea microstrip superconductora, soportando FWM y TWM, respectivamente. Los resultados muestran que línea rechaza en gran parte los armónicos, mientras se obtiene apróximadamente una línea de $50\,\Omega$. Las pérdidas en el dispositivo no deterioran significativamente el rendimiento del dispositivo.

ABSTRACT

MODELING LOSSES IN MICROSTRIP TRAVELING WAVE KINETIC INDUCTANCE PARAMETRIC AMPLIFIERS USING THE FOUR AND THREE WAVE MIXING EFFECT

The performance of an amplifier is based on a high gain and a low noise. To minimize the noise problem at high frequencies, the *superconducting parametric amplifier* has been developed. It is a system that uses a non-linear process and a strong reference to transfer the energy to the original signal and their harmonics. Two types of processes are discussed in this thesis, the Four and Three-wave mixing (FWM and TWM).

One implementation is the travelling-wave kinetic inductance parametric amplifier (TKIPA). It consists of a superconducting transmission line (TL), which uses its non-linear inductance to transfer the energy to the input signal. With the appropriated design, the blocking of undesirable harmonics to concentrate the power in the signal (and not in the harmonics) is possible. The first implementation of the TKIPA used a coplanar wave-guide (CPW), where impedances near $50\,\Omega$ are difficult to achieve. In this thesis, a TKIPA was designed using a microstrip. A $50\,\Omega$ microstrip line is easier to obtain, circumventing the problem of impedance mismatch with output electronics.

We have presented two designs of a TKIPA based on superconducting microstrip, supporting FWM and TWM, respectively. Simulation results show that the designs blocked the undesirable frequencies, while obtaining a $\approx 50\,\Omega$ line. The losses in the device do not deteriorate significantly the performance of the device.

My earnest gratitude to all the people whose help and support made this work possible

Contents

List of Figures

List of Tables

Chapter 1

Introduction and state of the art

1.1 Amplifiers in Radio astronomy

In order to understand the origin of the celestial objects and their evolution, a variety of telescopes have been developed during the years. They can be classified, loosely, in optical and radio telescopes. While optical telescopes gather and focus the light from the visible part of the electromagnetic spectrum to create an image, radio telescopes are used to receive the radio waves from astronomical sources in the sky. In a radio telescope, the reception of the signals is usually achieved by heterodyne receivers placed at the focal plane of the antenna. The typical block diagram of a heterodyne receiver is shown in Fig. 1.1**a**. The external signal is amplified by a radio-frequency low-noise amplifier (LNA), then, it is mixed with a reference signal to change the frequency ranging to a lower one (down-conversion), ending in an intermediate frequency (IF). Then, the output signal is once more amplified by an IF low noise amplifier. However, one of the main problems of the receivers is the noise. It obscures part of the desired signal, and therefore makes it difficult to analyse. The frequency of operation of current state-of-the-art LNAs do not exceed 120 GHz, which results in a lower signal-to-noise ratio (SNR)[1]. Therefore, according to Friis noise law, the first amplifier is usually removed to minimize the noise as shown in Fig. 1.1**b**.

Researchers have developed a myriad of amplifier devices to minimize the noise. For instance, the High Electron-Mobility-Transistor (HEMT) has been especially useful in astronomy. This type of FET device has contributed to the discovery of multiple phenomena, such as the confirmation that the geometry of the universe is flat [2]. Amplifiers based on it are reliable, stable, and can work in an octave or higher bandwidth without increasing the noise significantly [3]. At millimeter waves combined with Schottky diodes, they even have the potential to achieve similar noise levels of conventional SIS mixers [4]. Nonetheless, the noise temperature achieved with those amplifiers is still high for applications in Radio Astronomy with signals with frequencies higher than 120 GHz. Above this frequency, its gain diminishes and the noise contribution increases rapidly. As a result, new technologies are being studied, such as the *superconducting parametric amplifiers*. These amplifiers are potential candidates to

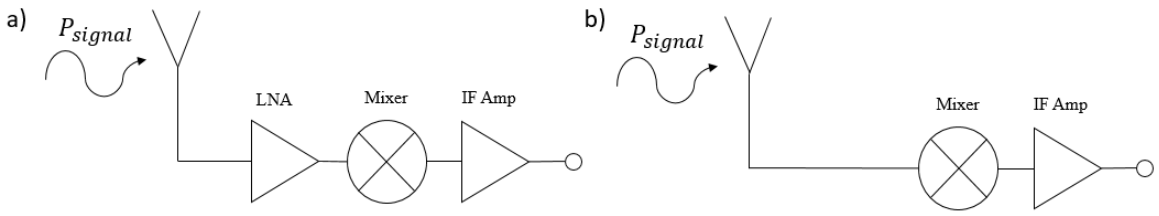

Figure 1.1: a) Block diagram of an active heterodyne detector using an RF LNA, a Schottky mixer, and a low noise intermediate frequency (IF) HEMT amplifier. b) Schematic without a RF LNA to minimize the noise resulting from losing SNR at frequencies above 120 GHz.

replace the SIS receivers and the IF amplifiers, given that they promise operating at quantum noise conditions and high frequencies [5].

1.2 Superconducting parametric amplifiers

A parametric amplifier (paramp) is a harmonic modulator based on a parametric non linear process, which describes the exchange of energy between some parameters of the system. The two types of parametric process that are discussed in this thesis are Four-wave mixing (FWM) and Three-wave mixing (TWM), which will be discussed in the following chapters. This type of amplifier has its roots in parametric oscillators, which drive harmonic oscillations by varying a characteristic of the system with a harmonic of the natural frequency in the oscillator. The theory was first introduced in 1956 by A.L.Cullen, where he used a series of low-pass filters [6].

Various types of parametric amplifiers have been developed over the years. Nonetheless, one of the most important types is the *superconducting paramp*, because of its noise and/or bandwidth performance [7]. This type of amplifier uses the kinetic inductance L_k as the non-linear parameter to generate the amplification. In superconductors, L_k is the dominant inductance compared with the geometric inductance L_m. In particular, large kinetic inductances can be achieve if films of niobuim titanuim nitride (NbTiN) are used, which, because of its London depth penetration and high resistivity in the normal state, it is useful to avoid parasitic inductances [8].

There exist different types of paramps. The first type is the Lumped-element Josepshon Parametric Amplifier (LJPA). It uses the nonlinear behaviour of the kinetic inductance to amplify a parameter in a LC resonator. However, its main limitations are bandwidth and input power saturation. More recent versions of paramps, such as the Josepshon Travelling-Wave Parametric Amplifier (JTWPA) [9] and the Travelling-Wave Kinetic Inductance Parametric Amplifier (TKIPA) [7], attack these problems.

The JTWPA uses a Coplanar wave-guide (CPW) lumped-element transmission line and a nonlinear kinetic inductance. The line behaves as a filter composed of deep-subwavelength elements acting as a resonator. This introduces a coupling capacitor, which has an ad-

ditional degree of freedom to independently couple the resonator to the transmission line. On other hand, the TKIP uses a travelling-wave CPW geometry and a non-linear kinetic inductance produced by a high-resistivity superconductor NbTiN. This device generates a practical parametric gain, which can operate with 3.4 photons at 9.4 GHz. Both amplifiers are made by using CPW transmission lines, where an impedance near 50 Ω is difficult to obtain with practical dimensions. Because of the difference in impedance between the line and the ports, an impedance matching is needed. This coupler matches only in the operation frequency and, therefore generates reflections, causing ripples in the parametric gain in the rest of bandwidth. In this thesis, we introduce a TKIPA implemented on of a microstrip geometry. By using practical dimensions, it is possible to obtain a 50 Ω, circumventing the problem of impedance matching.

1.3 Objectives

This thesis focuses on modelling a superconducting microstrip TKIPAs. Two designs are presented using four and three-wave mixing, respectively. Each design is simulated adding losses to have more realistic results.

1.3.1 Main objectives

Our main objectives are as follows:

1. Design and study a TKIPA using FWM.

2. Design an engineered transmission line, by using the concept of TWM, and comparing it with the design made by using FWM.

1.3.2 Specific objectives

To accomplish the main objectives, the specific objectives are:

1. Achieve an engineered transmission line, with a particular characteristic impedance Z_L and a wave number γ that satisfies given requirements of bandwidth and the location of the stop bands.

2. Design a superconducting microstrip line that matches Z_L and γ.

3. Obtain the main characteristics of the amplifier, such as parametric gain, dispersion relation, Bloch impedance and S parameters.

4. Repeat all the aforementioned steps including losses in substrate.

1.4 Hypothesis

The hypothesis of this work can be summarized as:

- The coupled mode equations that model the evolution of the amplitude of the signal amplified can support the addition of losses, that is to say, a complex propagation constant.
- The implementation of TWM travelling-wave amplifiers is possible by deducing a new set of coupled mode equations and designing an engineered transmission line to obtain amplification.

1.5 Outline

The outline of this thesis is the following:

- **Chapter 2** introduces the basic background and steps needed to understand and analyse microwave filters, types of transmission lines and properties of superconductivity.
- **Chapter 3** explains the theory and design of a TKIPA superconducting microstrip by using four-wave mixing. Its main characteristics are described, the dispersion relation, Bloch impedance and S parameters. Finally, the resulting parametric gain is obtained and explained. An analysis of harmonics and frequency sensitivity of the pump frequency are included to validate our design.
- **Chapter 4** extends theory and describes the design of a TKIPA by using three-wave mixing. Moreover, the results are compared with the design that uses the four-wave mixing effect.
- **Chapter 5** summarizes the general conclusions that resulted from discussions of the previous results and proposes the future work.

Chapter 2

Fundamental concepts

In this chapter, the basic theoretical background needed to understand the fundamentals of a traveling-wave kinetic inductance parametric amplifier (TKIPA) is presented. We focus on the description of the main processes that describe the operation of a TKIPA: *traveling-wave*, *kinetic inductance* and *parametric amplification*. The first section describes the first process *traveling-wave*, discussing the steps to design a Dispersion-Engineered Transmission Line (DETL). Its function is to suppress undesirable harmonic frequencies of the pump signal, f_p, and the target signal f_s. To connect the real world with the theory of the dispersion-engineered transmission line, the microstrip line is chosen.

The second section goes into detail about the second process *kinetic inductance*, which generates the non-linearity needed to perform the FWM and TWM. To explain the kinetic inductance, first, the basic theory of superconductivity is discussed. Later, the kinetic inductance is introduced. Furthermore, because a superconductor behaves different than a perfect conductor, the modelling of the superconducting microstrip lines is discussed. Finally, the final section explains the *parametric amplification*, where the concepts of four and three-wave mixing are presented. Both forms of mixing transfer the energy from the pump source to the target signal, generating the parametric amplification. By using a superconductor with a high kinetic inductance, and using the appropriate DETL, the parametric process can generate a desirable amplification in the device.

2.1 Traveling-wave: Dispersion-Engineered Transmission Line

The first process consists on designing a DETL, which is an ideal network segments of transmission lines. By manipulating its characteristic impedance, propagation constant and length, the manipulation the group velocity of the signals inside the network is possible. In other words, the DETL can behave as a filter. A filter is a two-port circuit used to regulate the frequency output of a system, removing frequencies outside of the desired bandwidth. For example, a low-pass filter removes the spectrum above a particular frequency, only passing frequencies below [7]. In particular, the DETL designed in this thesis is based on periodic

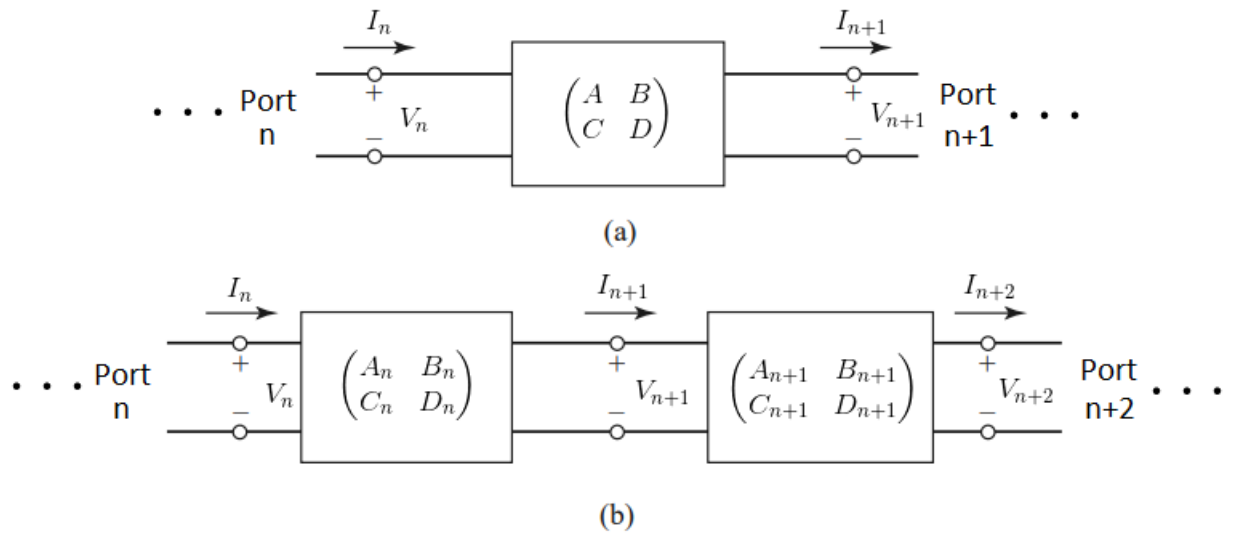

Figure 2.1: a) A two-port network; b) A connection of two-port networks [10].

filters, due to their successful microwave applications. Previous applications in paramps have demonstrated that can exhibit stop bands of a large attenuation [7, 9, 11].

In this section, the basics of microwave network analysis related with periodic filters is introduced. Subsequently, the microstrip transmission line is introduced as the connection between the theory and the experimental results. In this work, a superconducting microstrip line is used as the DETL, which is discussed thoroughly in this chapter. One of the reasons for which the microstrip line is widely used is because it is possible to achieve low values of characteristic impedances, in particular $50\,\Omega$, without restricting excessively the dimensions of the line. This is difficult to obtain by using, for example, coplanar waveguides (CPW). As a result, a good impedance matching to the external ports is expected to be achieved.

2.1.1 Transmission (ABCD) matrix

A network with an indefinite number of ports can be described using Z and S parameters. However, in case of a connection of multiple networks in cascade, defining the *ABCD matrix* is more appropriated. This concept is a relation between voltages and current that can be written as

$$\begin{bmatrix} V_n \\ I_n \end{bmatrix} = \begin{bmatrix} A & B \\ C & D \end{bmatrix} \begin{bmatrix} V_{n+1} \\ I_{n+1} \end{bmatrix}, \tag{2.1}$$

where the left-hand side represents the current and voltage at port n, and the other side are the current and voltage at port $n+1$. From Eq. (2.1) we have,

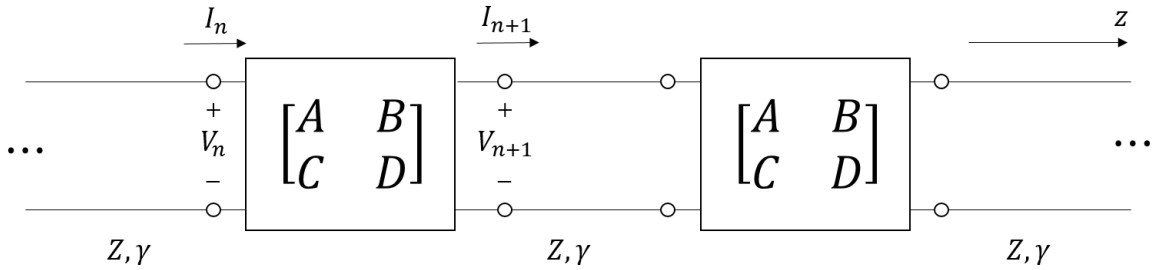

Figure 2.2: DETL represented by its transmission line and perturbations [10].

$$A = \left.\frac{V_n}{V_{n+1}}\right|_{I_{n+1}=0} \;,\; B = \left.\frac{V_n}{I_{n+1}}\right|_{V_{n+1}=0} \;,\; C = \left.\frac{I_n}{V_{n+1}}\right|_{I_{n+1}=0} \;,\; D = \left.\frac{I_n}{I_{n+1}}\right|_{V_{n+1}=0}. \quad (2.2)$$

Although an ABCD matrix can be obtained with any two-port type microwave network, in this thesis, we are only using transmission lines because only the design of a DETL is needed. The ABCD matrix of a transmission line is given by

$$\begin{bmatrix} A & B \\ C & D \end{bmatrix} = \begin{bmatrix} \cosh(\gamma \mathrm{d}) & Z\sinh(\gamma \mathrm{d}) \\ \frac{1}{Z}\sinh(\gamma \mathrm{d}) & \cosh(\gamma \mathrm{d}) \end{bmatrix}, \quad (2.3)$$

where γ is its propagation constant, Z is the characteristic impedance and d its length. The ABCD matrix of a system between the port n and $n+1$ is shown in Fig. 2.1**a**, while Fig. 2.1**b** shows a connection of two different system with their own ABCD matrix to represent the relation between the voltages and currents at the port n and $n+2$. Under these conditions, the relation between the components of current and voltage of the port $n+2$ with the port n is of the form

$$\begin{bmatrix} V_n \\ I_n \end{bmatrix} = \begin{bmatrix} A_n & B_n \\ C_n & D_n \end{bmatrix} \begin{bmatrix} A_{n+1} & B_{n+1} \\ C_{n+1} & D_{n+1} \end{bmatrix} \begin{bmatrix} V_{n+2} \\ I_{n+2} \end{bmatrix} = \begin{bmatrix} A_{n+2} & B_{n+2} \\ C_{n+2} & D_{n+2} \end{bmatrix} \begin{bmatrix} V_{n+2} \\ I_{n+2} \end{bmatrix}. \quad (2.4)$$

A DETL can be designed as a TL periodic filter. It consists in a transmission line of characteristic impedance Z and propagation constant γ. By perturbing the line with periodically distributed as shown in Fig. 2.2, it is possible to adjust the frequency behaviour of the DETL.

2.1.2 Bloch impedance

In a periodic filter, it has to be noticed that the current and voltages waves only have a meaning when they are measured in the terminals of the cell, not within it. This is because the propagation of these waves is similar to the elastic waves (*Bloch waves*) through

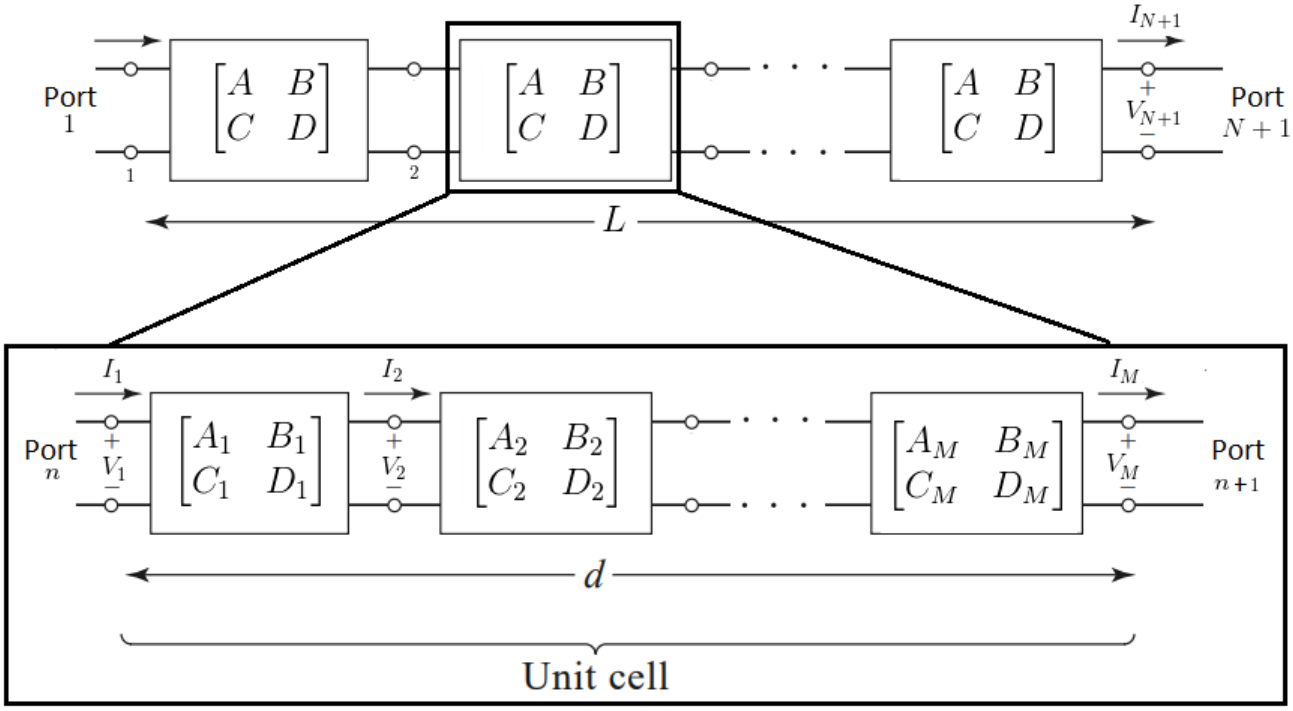

Figure 2.3: Periodically loaded transmission line with N cells and $N+1$ ports. Each cell is composed of M elements, represented by their respective $ABCD$ matrices [10].

a periodic lattice. Therefore, instead of using the characteristic impedance of the cell, the *Bloch impedance* $Z_B^{\pm}$ is used, which is defined as

$$Z_B = Z_0 \frac{V_{n+1}}{I_{n+1}}, \tag{2.5}$$

where I_{n+1} and V_{n+1} are the current and voltage of the terminal of the nth cell. The Bloch impedance can be written in terms of the ABCD matrix coefficients as

$$Z_B^{\pm} = \frac{-2BZ}{A - D \mp \sqrt{(A+D)^2 - 4}}, \tag{2.6}$$

with A, B and D the elements of the transmission matrix. The $\pm$ solutions corresponding to the Bloch impedance of a wave that travels in the $+z$ direction and $-z$ direction, respectively.

2.1.3 Scattering parameters

In non-TEM lines, currents and voltages are difficult to be defined, because their measurement is related with magnitude and phase of a wave traveling in a given direction or of

a standing wave. Therefore, they are impractical at high frequencies [10]. As a result, the *scattering matrix* is defined, which describes completely a network of N-ports. This matrix can be written as

$$\begin{pmatrix} V_1^- \\ V_2^- \\ \vdots \\ V_N^- \end{pmatrix} = \begin{pmatrix} S_{11} & S_{12} & \dots & S_{1N} \\ S_{21} & S_{22} & & S_{2N} \\ \vdots & & & \vdots \\ S_{N1} & S_{N2} & & S_{NN} \end{pmatrix} \begin{pmatrix} V_1^+ \\ V_2^+ \\ \vdots \\ V_N^+ \end{pmatrix}, \tag{2.7}$$

where V_j^+ is the voltage of the wave incident to port j. The parameter $S_{\mathrm{i}j}$ can be obtained individually as

$$S_{\mathrm{i}j} = \left. \frac{V_{\mathrm{i}}^-}{V_j^+} \right|_{V_k^+=0 \quad k\neq j}. \tag{2.8}$$

Other form to express the S parameters in a non-TEM line, is by its ABCD matrix. In a two-port network, the S parameters are given by

$$S_{11} = \frac{A + B/Z - CZ - D}{A + B/Z + CZ + D}, \tag{2.9}$$

$$S_{12} = \frac{2\,(AD - BC)}{A + B/Z + CZ + D}, \tag{2.10}$$

$$S_{21} = \frac{2}{A + B/Z + CZ + D}, \tag{2.11}$$

$$S_{22} = \frac{-A + B/Z - CZ + D}{A + B/Z + CZ + D}, \tag{2.12}$$

where Z is the characteristic impedance between the two ports. The transmission coefficient S_{12} in a periodic filter can be written in terms of the Bloch impedance Z_B. By using Eq. (2.9), the transmission coefficient S_{12} and the reflection coefficient can be written as

$$S_{12} = \frac{1}{\cosh(\gamma \mathrm{d}N) + \frac{Z_0^2 - Z_B^+ Z_B^-}{Z_0\left(Z_B^+ - Z_B^-\right)} \sinh(\gamma \mathrm{d}N)}, \tag{2.13}$$

$$S_{11} = \frac{-1}{\frac{Z_B^+ Z_B^- - Z^2}{\left(Z_B^+ - Z\right)\left(Z_B^- - Z\right)} + Z\frac{Z_B^+ - Z_B^-}{\left(Z_B^+ - Z\right)\left(Z_B^- - Z\right)} \coth(\gamma \mathrm{d}N)}, \tag{2.14}$$

which depend on the number of cells N, in contrast with its propagation constant γ that does not.

2.1.4 Periodic filters

A periodic filter is a transmission line periodically loaded with N subsystems or *cells* as shown in Fig. 2.3. The loading elements can be of any type, and usually are designed by discontinuities in the line itself. The idea of creating these discontinuities is to mimic a system of capacitance and inductance elements in shunt or parallel, which behaves as a filter. Periodic structures generally exhibit stopband and passband characteristic in multiple and periodic bands are determined by the nature of the structure. The behaviour of this type of filter can be described by their dispersion relation. The ABCD matrix of a cell with a connection of M transmission lines can be written as [10]

$$\begin{bmatrix} A & B \\ C & D \end{bmatrix} = \prod_{j=1}^{M} \begin{bmatrix} \cosh(\gamma_j l_j) & Z_j \sinh(\gamma_j l_j) \\ \frac{1}{Z_j} \sinh(\gamma_j l_j) & \cosh(\gamma_j l_j) \end{bmatrix}, \tag{2.15}$$

where γ_j, Z_j and l_j represents the complex propagation constant, characteristic impedance and length of the transmission line, respectively of the j-th block.

The analysis of a periodic filter begins with the deduction of its dispersion relation. The first step to obtain the dispersion relation is to calculate the equivalent propagating constant γ of the periodic filter. This is done by first defining the voltages $V(z)$ and currents $I(z)$ of a system that maintains a wave only propagating in the $+z$ direction. Then, they can be written as

$$V(z) = V(0)\mathrm{e}^{-\gamma z}, I(z) = I(0)\mathrm{e}^{-\gamma z}. \tag{2.16}$$

If the structure is infinitely large or supports only the propagation of a traveling wave, the voltage and current of the port n and $n+1$ can only differ in only the propagation factor $\mathrm{e}^{-\gamma \mathrm{d}}$. Therefore, they are given by

$$V_{n+1} = V_n \mathrm{e}^{-\gamma \mathrm{d}}, I_{n+1} = I_n \mathrm{e}^{-\gamma \mathrm{d}}. \tag{2.17}$$

Eq.(2.1) and (2.17) can be written as a system of equations of the form

$$\begin{bmatrix} V_{n+1}\mathrm{e}^{\gamma \mathrm{d}} \\ I_{n+1}\mathrm{e}^{\gamma \mathrm{d}} \end{bmatrix} = \begin{bmatrix} A & B \\ C & D \end{bmatrix} \begin{bmatrix} V_{n+1} \\ I_{n+1} \end{bmatrix}. \tag{2.18}$$

In order to obtain a non-trivial solution, the determinant of the matrix obtained from clearing the voltage V_{n+1} and current I_{n+1} must be 0. Therefore, the following relation is obtained

$$AD + \mathrm{e}^{2\gamma \mathrm{d}} - (A + D)\mathrm{e}^{\gamma \mathrm{d}} - BC = 0. \tag{2.19}$$

The system is reciprocal, since it does not contain active elements, such as transistors, or non reciprocal element, as ferrites. Therefore, the ABCD matrix must follow the condition

$$AD - BC = 1. \tag{2.20}$$

Finally, assuming $\gamma = \alpha + j\beta$ and solving the system of equations from Equations (2.19) and (2.20), the relation dispersion of the traveling wave filter can be obtained as

$$\cosh\,(\gamma \mathrm{d}) = \cosh\,(\alpha \mathrm{d})\,\cos\,(\beta \mathrm{d}) + j\,\sinh\,(\alpha \mathrm{d})\,\sin\,(\beta \mathrm{d}) = \frac{A + D}{2}, \tag{2.21}$$

where, by depending of the features of the TL, the cell could exhibit frequency response of passband or stopband.

2.1.4.1 Filters in cascade

We can notice that the ABCD matrix is diagonalizable and can be written as

$$\begin{bmatrix} A & B \\ C & D \end{bmatrix} = PDP^{-1} = \begin{bmatrix} Z_B^+ & Z_B^- \\ 1 & 1 \end{bmatrix} \begin{bmatrix} \mathrm{e}^{\gamma \mathrm{d}} & 0 \\ 0 & \mathrm{e}^{-\gamma \mathrm{d}} \end{bmatrix} \begin{bmatrix} Z_B^+ & Z_B^- \\ 1 & 1 \end{bmatrix}^{-1}, \tag{2.22}$$

where P is a matrix with the eigenvectors of the ABCD matrix and D is a diagonal matrix with its eigenvalues. Then, the ABCD matrix of a system with N cells in cascade is given by [12]

$$\begin{aligned} \begin{bmatrix} A_N & B_N \\ C_N & D_N \end{bmatrix} = \begin{bmatrix} A & B \\ C & D \end{bmatrix}^N &= \overbrace{(PDP^{-1} \cdot PDP^{-1} \ldots PDP^{-1})}^{\text{N times}} = PD^N P^{-1} \\ &= P \begin{bmatrix} \mathrm{e}^{\gamma \mathrm{d}} & 0 \\ 0 & \mathrm{e}^{-\gamma \mathrm{d}} \end{bmatrix}^N P^{-1} = P \begin{bmatrix} \mathrm{e}^{\gamma \mathrm{d}N} & 0 \\ 0 & \mathrm{e}^{-\gamma \mathrm{d}N} \end{bmatrix} P^{-1}. \end{aligned} \tag{2.23}$$

From Eq. (2.23), the propagation constant γ obtained in Eq. (2.21) has the characteristic of invariability with the number of cells added in cascade N, that is to say, the propagation constant of a system of one cell is the same as the system of an infinite-cell system. As a result, to calculate the ABCD of N cells in cascade, the eigenvalues of the ABCD matrix of a single cell are powering to the value of N, reducing the computational resources significantly.

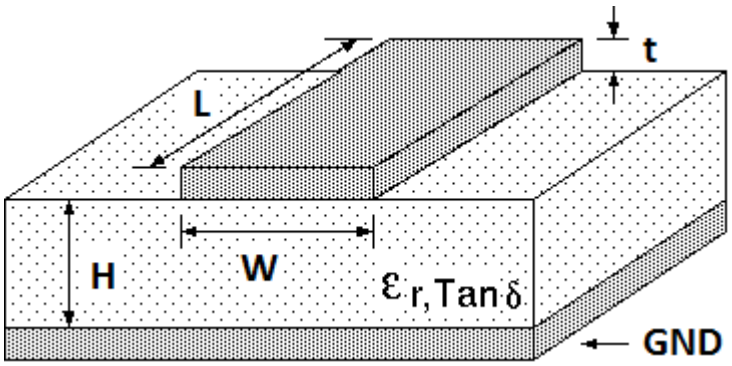

Figure 2.4: Geometry of a microstrip line, with a conduction line of length L , width W and thickness t. A substrate of height H with a relative permittivity ε_r and a tangent loss of angle δ, and in the bottom layer a ground plane [10].

2.1.5 Microstrip line

The microstrip line is one of the most used transmission lines and well characterized when compared with technologies such as CPW [13]. The geometry of this type of line is shown in Fig. 2.4 [10]. Since a current flows through the conductor, a magnetic field encircles it. The substrate lays on top of another conductor layer used as a ground, and so, the electric field goes from the conductor to the ground, passing through the substrate.

The idea of using a substrate allows the control of the characteristics of the transmission line, such as the characteristic impedance Z_L, the propagation constant γ and the effective permittivity ε_r. Because some of the electric field goes to the air while the rest is in the dielectric, the relative permittivity of the substrate does not represent the amount of charge needed to generate one unit of electric flux of the line. Therefore, the *effective permittivity* ε_{eff} is defined. However, the analysis of this type of line is also burdensome, since it has a non TEM behaviour. This problem can be overcome if the thickness of the substrate is electrically much thinner than the wavelength of the signal passing through the line ($H \ll \lambda$). As a result, the microstrip can behave as a cuasi-TEM waveguide, and their properties can be obtained as a quasi-static solutions.

There are different approximations to calculate the characteristics of a microstrip line. In this work the model given by Hammerstad and Jensen [14] is used, because it achieves more accuracy with the effective permittivity in comparison with experimental measurements. With a relative error of 0.2% for $\varepsilon_r < 128$ and $0.01 \leq W/H \leq 100$, the effective permittivity can be written as

$$\varepsilon_{eff} = \frac{\varepsilon_r + 1}{2} + \frac{\varepsilon_r - 1}{2}\left(1 + \frac{10\,H}{W}\right)^{-ab}, \tag{2.24}$$

where u is defined as $u = W/H$. The parameters a and b are of the form

$$a(u) = 1 + \frac{1}{49} \cdot \ln\left(\frac{u^4 + (u/52)^2}{u^4 + 0.432}\right) + \frac{1}{18.7} \cdot \ln\left(1 + \left(\frac{u}{18.1}\right)^3\right), \tag{2.25}$$

$$b(\varepsilon_r) = 0.564 \cdot \left(\frac{\varepsilon_r - 0.9}{\varepsilon_r + 3}\right)^{0.053}. \tag{2.26}$$

$$\tag{2.27}$$

With a relative error of 0.01% for $W/H \leq 1$ and 0.03% for $W/H \leq 1000$, the characteristic impedance Z_L is given by

$$Z_L(W, H, \varepsilon_r) = \frac{Z_{L1}(W, H)}{\sqrt{\varepsilon_{r_{eff}}}}, \tag{2.28}$$

$$Z_{L1}(W, H) = \frac{Z_0}{2\pi} \cdot \ln\left(f_u \frac{H}{W} + \sqrt{1 + \left(\frac{2H}{W}\right)^2}\right), \tag{2.29}$$

$$f_u = 6 + (2\pi - 6) \cdot \exp\left(-\left(30.666 \frac{H}{W}\right)^{0.7528}\right), \tag{2.30}$$

where Z_0 the impedance of the air. If $t > 0$, a correction on the equations is necessary. For ε_{efft}, its relation is given by

$$\varepsilon_{efft} = \varepsilon_{eff} \cdot \left(\frac{Z_{L1}(W_1, H)}{Z_{L1}(W_r, H)}\right)^2, \tag{2.31}$$

where ε_{eff} is obtained by Eq. (2.24). The change in width ΔW is expressed by two different changes $W_1 = \Delta W_1 + W$ and $W_r = \Delta W_r + W$, which are of the form

$$\Delta W_1 = \frac{t}{H\pi} \ln\left(1 + \frac{4\mathrm{e}}{\frac{t}{H} \coth^2 \sqrt{6.517W}}\right), \tag{2.32}$$

$$\Delta W_r = \frac{1}{2} \Delta W_1 \left(1 + \operatorname{sech} \sqrt{\varepsilon_r - 1}\right). \tag{2.33}$$

The corrections in the characteristic impedance can be included as

$$Z_L(W, H, t, \varepsilon_r) = \frac{Z_{L1}(W_r, H)}{\sqrt{\varepsilon_{r_{eff}}(W_r, H, \varepsilon_r)}}. \tag{2.34}$$

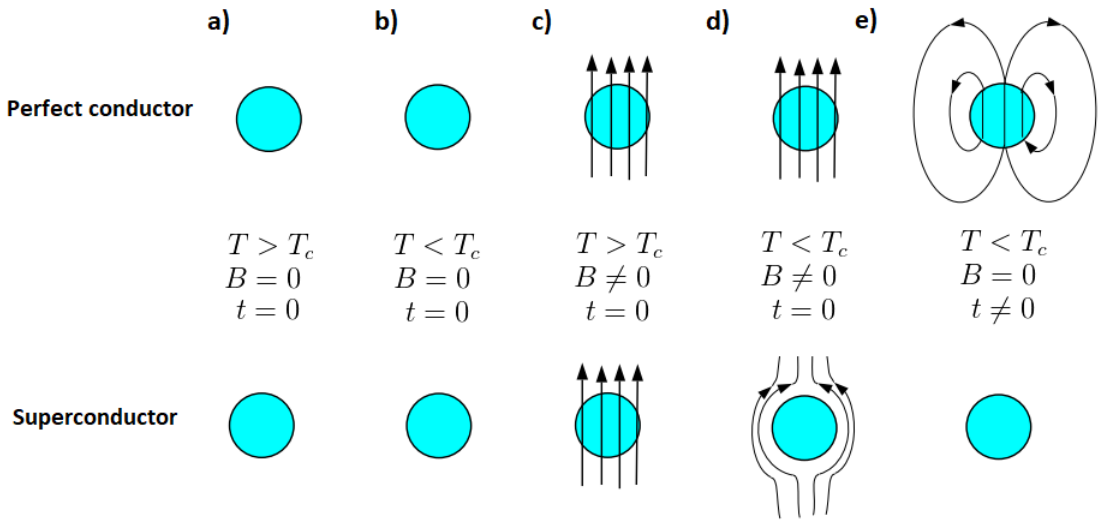

Figure 2.5: Meissner effect illustrated by a perfect conductor on top, and a superconductor on bottom. (a) Both spheres have a temperature above T_c, while a external field is not applied. (b) Temperature below T_c, external magnetic field is not applied. (c) Temperature above T_c and external field applied. (d) Temperature below T_c and external field applied. (e) With a temperature below T_c, a magnetic field was applied and it was switched off a time after [16].

2.2 Introduction to superconductors

The theory to make a general microstrip line was described in section 2.1.5. However, their non-linear effects appear when a superconducting material is used. In this section, a basic theory of superconductivity is explained. The main concepts of the kinetic inductance and superconducting microstrip line are described. Then we described how these phenomena are related with the parametric amplification.

2.2.1 Basic concepts

Some materials have a vanishing resistance below certain temperature. This phenomenon is defined as superconductivity. It was discovered by the Dutch physicist Heike Hamerlingh Onnes in 1911, when his team was studying the resistance of mercury at low temperatures [15]. The temperature at which a material becomes superconductor without the presence of a magnetic field is called *critical temperature*. In the superconducting state, there is a particular external magnetic field $B_c(T)$ that suppress the superconductivity. It was found that $B_c(T)$ is related to T by

$$B_c(T) = B_0 \left[1 + \left(\frac{T}{T_c}\right)^2\right], \tag{2.35}$$

where B_0 is the critical magnetic field at $T = 0\,\mathrm{K}$. According to Ampere's law, this behaviour also can be expressed as a *critical current* I_c, which it is the maximum electrical current that the material is able to maintain without resistance [15].

In 1933, it was discovered that superconductors are not perfect conductors. This phenomenon is known as the *Meissner-Ochosenfeld* effect. An illustration of this effect can be observed in Fig. 2.5. In the presence of an external magnetic field, perfect conductors maintain this field inside of them, while superconductors do not. This is because of the presence of persistent current that maintains a magnetic field that is opposite to the external magnetic field [16]. If the external field is removed at a time $t \neq 0$, the ideal conductor induces currents that prevents changes in the magnetic field inside it. However, the superconductor returns to its normal state, having no magnetic field outside or inside it.

2.2.1.1 Baarden-Cooper-Schrieffer theory and the two-fluid model

In 1957, the BCS theory was proposed as the first microscopic theory of superconductivity. It describes the effect produced by the condensation of the Cooper pairs into a boson state, i.e, particles where the Pauli exclusion principle does not apply. The superconducting state is produced by electrons, which collide with phonons inside the lattice, coupling a pair of two electrons in a bound state called a *Cooper pair*, with a mass $m^* = 2m$ and change $q = -2\mathrm{e}$. Phonons are more present in bad conductors when compared with good conductors, then good conductors such as copper and gold have not a superconducting state, while poor conductors often have. An illustration of the generation of the Cooper pairs is shown in Fig. 2.6. At a superconducting state, an electron flows into the material, attracting positive charges and deforming its lattice. This deformation produces a concentration of positive charges that can attract a second electron. This effect results in an indirect bonding from the second electron to the first one. Because the first electron keeps generating sources of positive charges, the second electron will "follow" the first one as a pair. All the Cooper pairs inside the superconductor are in the same quantum state and energy [18]. The condensation of the non-paired electrons of different energy values gives raise to a continuum of allowed energies bands with an energy gap Δ between them. On the contrary, the Cooper pairs are fixed to a single energy value at the Fermi surface. Therefore, the energy to break a Cooper pair is 2Δ [19].

The energy gap in the energy band of a superconductor can be calculated using the Baarden-Cooper-Schrieffer (BSC) theory. An approximation can be written as [20]

$$\Delta(T, T_c) = \Delta(0) \left(\cos \left[\frac{\pi}{2} \left(\frac{T}{T_c} \right)^2 \right] \right)^{1/2}, \tag{2.36}$$

where k_B is the Boltzmann constant [18].

The non-paired electrons in the superconductor are called *quasiparticles*, and they are produced in their majority by thermal excitation. These particles are not bosons, resulting in not being part of the condensation with the Cooper pairs to the same energy state. Thus,

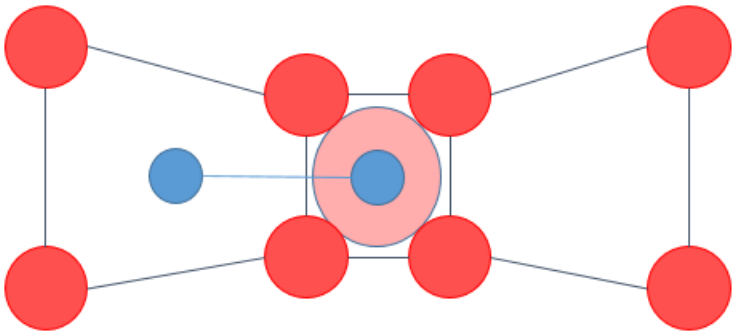

Figure 2.6: The generation of a Cooper pair produced by the deformation of the lattice. The red dots are the protons, while the blue dots represent the electrons[17].

there will be a mixture of Cooper pairs and "quasiparticles" with a total density n, which it is modelled by having two types of electron "fluids". One fluid with a normal electron density n_n, and the other fluid with Cooper pairs of density n_s.

2.2.1.2 London theory

In 1935, F. and H. London proposed a theory for the electrodynamic properties in a superconductor, which is based in the two-fluid model [22]. The current density of a normal conductor is modelled by Ohm's law,

$$J_n = \sigma_n E, \tag{2.37}$$

where the Drude model states that the conductivity is given by

$$\sigma_n = \frac{\mathrm{e}^2 n_n \tau}{m}, \tag{2.38}$$

with τ the relaxation time of the electrons inside a conductor. The superconducting current can not be properly described by the same model due to the Meissner effect. Therefore, a more general model of the supercurrent can be written as

$$J_s = -\mathrm{e} n_s v_s. \tag{2.39}$$

where v_s is the velocity of the Cooper pairs inside the superconductor. For this model, it is assumed that both densities n_n and n_s are constant in space and time at a given temperature T. By taking the time derivative part of the velocity v_s, and using Newton's law we obtain

$$\frac{\partial J_s}{\partial t} = -\mathrm{e}n_s \frac{\mathrm{d}v_s}{\mathrm{d}t} = -\mathrm{e}n_s \left(\frac{-\mathrm{e}E}{m}\right) = \frac{\mathrm{e}^2 n_s}{m} E, \tag{2.40}$$

which is defined as the *First London Equation*. It can be noted that by using the curl operator on Eq. (2.40), we have

$$\frac{\partial}{\partial t} \nabla \times J_s = \frac{\mathrm{e}^2 n_s}{m} \nabla \times E = -\frac{\mathrm{e}^2 n_s}{m} \frac{\partial B}{\partial t}, \tag{2.41}$$

where Faraday's law was used. If Eq. (2.41) is integrated, a constant appears on the right-side. To determine this constant, boundary conditions are used. In the case of a null external magnetic field, $J_s = 0$ and $B = 0$. The undetermined constant is zero. However, because of the Meissner effect, $B = 0$ independently of the situation. Therefore, Eq. (2.41) is given by

$$\nabla \times J_s = -\frac{\mathrm{e}^2 n_s}{m} B, \tag{2.42}$$

which is defined as the *Second London Equation*. The relation between the magnetic field B and the density of current can be obtained using Ampere's law as

$$\nabla \times B = \mu \left(J_s + J_n\right). \tag{2.43}$$

Thus, the operator curl can be used in Eq. (2.43) as

$$\nabla \times \nabla \times B = -\frac{-\mu \mathrm{e}^2 n_s}{m} B + \mu \sigma_n \nabla \times E = -\frac{\mu \mathrm{e}^2 n_s}{m} B - \mu \sigma_n \frac{\partial B}{\partial t}. \tag{2.44}$$

If a stationary state is assumed, then $\dot{B} = 0$. Rearranging Eq. (2.44), we obtain

$$\nabla^2 B = \frac{1}{\lambda_L} B, \tag{2.45}$$

where the *London Penetration depth* is defined as

$$\lambda_L = \sqrt{\frac{m}{\mu_0 n_s \mathrm{e}^2}}. \tag{2.46}$$

At $T = 0\,\mathrm{K}$, it is the distance between the superconductor surface and the position inside the superconductor where the magnetic field becomes e^{-1} times the one at the surface [21]. The normal state conductivity σ_n is presented as the conductivity in which the temperature is just above the critical one, T_C, before the change to the superconductor state. From Eq. (2.38) this conductivity is of the form

$$\sigma_n = \frac{n\mathrm{e}^2\tau}{m}, \tag{2.47}$$

which by the BSC theory can also be expressed as [19]

$$\sigma_n = \frac{\hbar}{\pi\Delta(0)\lambda_L^2(0)}, \tag{2.48}$$

with $\hbar$ is the normalized plank constant, $\Delta(0)$ and $\lambda_L(0)$ are energy gap and penetration depth at a temperature of absolute zero.

2.2.2 Kinetic Inductance

In the presence of a AC current, with frequency sufficiently low to maintain the Cooper pairs, the conductivity inside of a superconductor σ can be explained using the Drude model, [19]

$$\sigma = \frac{n_n\mathrm{e}^2\tau}{m(1+\omega^2\tau^2)} - \mathrm{i}\left(\frac{n_s\mathrm{e}^2}{m\omega} + \frac{n_n\mathrm{e}^2(\omega\tau)^2}{m\omega(1+\omega^2\tau^2)}\right) = \sigma_1 - \mathrm{i}\sigma_2, \tag{2.49}$$

where m and e are the electron mass and charge, respectively. n_s and n_n are the density of Cooper pairs and quasiparticles inside the superconductor, and τ is the collision time between normal electrons and the lattice. At low frequencies and using Eq. (2.46), the complex conductivity also can be written as

$$\sigma = \sigma_1 - \mathrm{i}\sigma_2 = \sigma_n(n)\left(\frac{n_n}{n}\right) - \mathrm{i}\left(\frac{1}{\omega\mu_0\lambda_L^2}\right), \tag{2.50}$$

where a direct dependence between σ_2 and λ_L is shown. The second term of the right-side of Eq. (2.49) is related with a store of energy inside the material. In particular, the energy is stored in the kinetic energy of the Cooper pairs. In normal metals, the collision time is typically 10^{-14} seconds approximately, and so the term $\omega\tau$, and the second expression, can be neglected in conductors at frequencies below 100 GHz. However, because the collision time

in superconductors is infinity, the second expression is not possible to be neglected. The additional term has into account the kinetic energy of the Cooper pairs store in the material, which can be expressed as

$$E_k = \frac{1}{2} M v_s^2, \tag{2.51}$$

with v_s the velocity of the Cooper pairs, $M = 2mn_sAl$ the total mass of the Cooper pairs, and A and l are the transversal area and length of the line, respectively. On the other hand, the current of the superconductor is given by

$$I_k = 2An_s e v_s, \tag{2.52}$$

where A is the transversal area of the superconducting line. By using Eq. (2.52), Eq. (2.51) can be written of the form

$$E_k = \frac{1}{2} \overbrace{\left(\frac{ml}{2An_s e^2} \right)}^{L_k} I_k^2. \tag{2.53}$$

This behaviour can be modelled as an inductor, which is defined as the *kinetic inductance* L_k of the superconductor. It can be demonstrated that the kinetic inductance has a quadratic dependence with the current passing through the superconductor line, which can be written as [23]

$$L_k(I) = L_{K0} \left(1 + \frac{I^2}{I_*^2} \right), \tag{2.54}$$

where $L_{K0} = \mu_0 \lambda^2 / A$ is the kinetic inductance of the superconductor at $I = 0$. I_* is a parameter that sets the nonlinearity of the device and is comparable to the critical current I_c. As a simplification, in this work it is assumed that I_* is equal to I_c. A more exact calculation of I_* can be done by measuring the non linear phase shift $\Delta\theta$ experimentally [24]. By using the non-linear effect of the kinetic inductance, a large amount of devices have been made using superconductors and operating in RF. Some examples are the kinetic inductance detectors (KID) [25], the superconducting kinetic inductance magnetometers (SKIM) [26] and parametric amplifiers.

2.2.2.1 Mattis-Bardeen complex conductivity

Even though the complex conductivity can be calculated using the two-fluid model provided by Drude, the model does not consider the effect of the separation of the Cooper pairs because of radiation absorption. Mattis and Bardeen obtained an expression of the conductivity including the latter phenomena by using the BCS weak-coupling theory [27],

$$\begin{aligned}\frac{\sigma_1}{\sigma_n} = \frac{2}{\hbar w}\int_{\Delta}^{\infty}[f(\varepsilon)-f(\varepsilon+\hbar w)]\times\frac{\varepsilon^2+\Delta^2+\hbar w\varepsilon}{\sqrt{(\varepsilon^2-\Delta^2)\cdot\left[(\hbar w-\varepsilon)^2-\Delta^2\right]^{1/2}}}\mathrm{d}\varepsilon+\cdots \\ +\frac{1}{\hbar w}\int_{\Delta}^{\hbar w-\Delta}[1-2f(\hbar w-\varepsilon)]\times\frac{\hbar w\varepsilon-\varepsilon^2-\Delta^2}{\sqrt{(\varepsilon^2-\Delta^2)\cdot\left[(\hbar w-\varepsilon)^2-\Delta^2\right]^{1/2}}}\mathrm{d}\varepsilon\end{aligned}, \tag{2.55}$$

$$\frac{\sigma_2}{\sigma_n} = \frac{1}{\hbar w}\int_{\Delta-\hbar w,-\Delta}^{\Delta}[1+2f(\hbar w-\varepsilon)]\times\frac{\hbar w\varepsilon-\varepsilon^2-\Delta^2}{\sqrt{(\varepsilon^2-\Delta^2)\cdot\left[(\hbar w-\varepsilon)^2-\Delta^2\right]^{1/2}}}\mathrm{d}\varepsilon, \tag{2.56}$$

with $f(E)$ the Fermi function defined as

$$f(E) = \frac{1}{1+\mathrm{e}^{\frac{E}{k_B T}}}, \tag{2.57}$$

which describes the probability of an electron to be in a particular state of energy. The first integral Eq. (2.55) represents the quasiparticles generated by thermal excitation, and Eq. (2.56) presents the quasiparticles created by phonons in the lattice. For $0 < T < T_c$, incident photons can produce quasiparticles by breaking Cooper pairs. Thus, by stating that the energy to break a Cooper pair is 2Δ, the radiation absorption in the Cooper pair is possible for frequencies of $\omega > 2\Delta/\hbar$.

2.2.3 Surface impedance

When an ideal conductor is immersed in an electromagnetic field, the tangential electric field is zero E_t. A current circulates near the surface of the material to maintain a magnetic field H_t and expelling all the electric field inside of it. However, in real conductors, some electric field pass through the surface of them. In order to circumvent of the difficulties of solving the Maxwell equations under these circumstances, the concept of *surface impedance* is defined [28]. It accounts for providing boundary conditions at the surface of the conductor, modelling the dissipation and storage of energy inside the material. The internal field decreases exponentially with the distance. This behaviour can be characterized by the skin depth $\delta = (2/w\sigma\mu)^{1/2}$, which is the distance inside the conductor where the field is attenuated in 1/e. For a superconductor, the tangential magnetic field penetrates the material, with a distance modelled by the London penetration depth λ_L. This depth is independent of the frequency if $\omega \ll \omega_c = 2\Delta/\hbar$.

2.2.3.1 Resistance per square

The surface impedance as well as the surface inductance can be measured *per square* ($\square$). Any fabrication process usually requires a layout, where all the features are modelled by rectangles with a specific length h and thickness d. The 1 $X/\square$ indicates one unit of X in a square. Why a square? The concept was defined by Valdes in 1954 using the four-probe method, where the sheet resistance was measured. He noticed that if a square was used to measure the resistivity of a particular material and using [29]

$$R_{\text{sheet}} = \frac{(\text{length})}{(\text{conductivity})\,(\text{cross sectional area})} = \frac{h}{\sigma h \text{d}} = \frac{1}{\sigma \text{d}}, \tag{2.58}$$

the resistance only depends of the thickness of the sheet d. The length h does not matter. Because of this fact, the term *resistance per square* is used.

2.2.3.2 Surface inductance

As the surface impedance, the surface inductance has units of H/$\square$. By using the expression of L_K given by Eq. (2.53), the kinetic inductance can also be written as

$$L_K = \frac{l}{W}\mu_0\lambda \tag{2.59}$$

where W is the width of the superconducting line. From Eq. (2.59) and stating that the inductance is modelled in a square ($W = l$), the surface kinetic inductance is $L_\square = \mu_0\lambda$.

2.2.3.3 Surface impedance models for superconductors

A.R. Kerr proposed two methods to model the surface impedance of a superconducting strip, the single conducting sheet and the pair of conducting sheets [28]. The single conducting sheet method consists on replacing the conductor for a thin sheet with surface impedance Z_S. In case of a superconductor, Z_S is given by

$$Z_S = j\omega\sqrt{\frac{\mu_0 m^*}{n^* \text{e}^{*2}}} = j\omega\mu_0\lambda_L = j\omega L_\square\ \Omega/\square, \tag{2.60}$$

where ω is the operation frequency. This result comes from surface inductance per length $L_\square = \mu_0\lambda_L$ $H/\square$. L_S is the kinetic inductance per unit of length produced in the superconductor and is modelling the energy store inside the material.

The single conducting sheet method is often used for a superconductor strip that has a penetration depth λ_L much smaller than its thickness ($\lambda_L \ll t$). As a consequence, the strip can be treated as if the thickness is infinite. Moreover, a thick conductor is not equivalent to

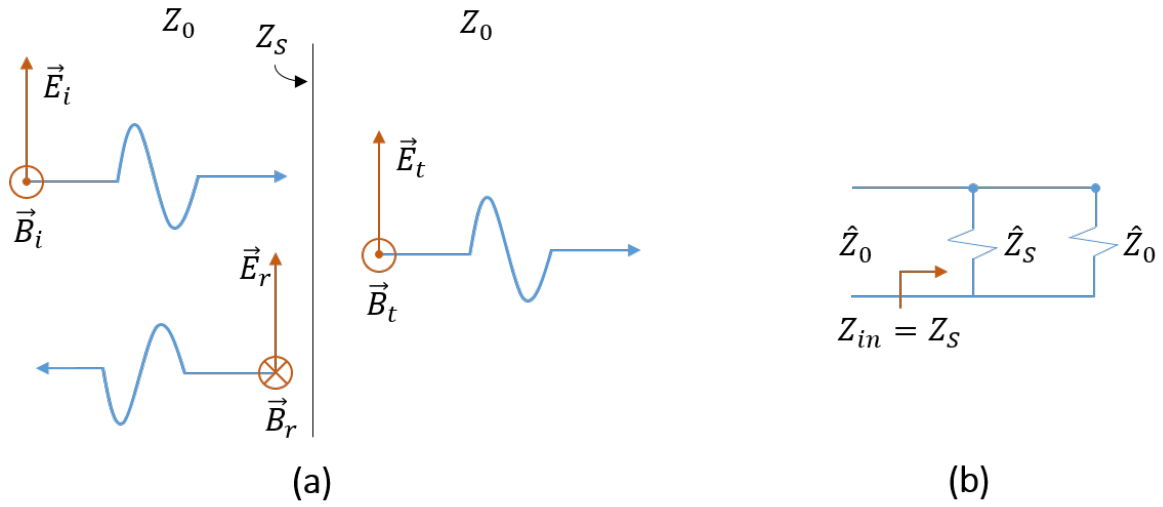

Figure 2.7: (a) Superconductor represented by a single sheet of surface impedance Z_S between the vacuum. It is assumed that the wave plane transmitted into the strip behaves similarly as in a transmission line. (b) The single sheet equivalent model, where Z_0 is the impedance of the vacuum [30].

the thin sheet, but for cases when $|Z_S| \ll 377\,\Omega/\square$, the error can be negligible. A schematic of the superconductor and its equivalent circuit are shown in Fig. 2.7, where it represents the single sheet model. Its equivalent model in a superconducting line is shown in Fig. 2.9**a**.

In case of a superconductor with a finite thickness t as presented in Fig. 2.8, the double sheet model is used. It is assumed that the penetration depth is not much smaller than the thickness t of the superconductor, so that a magnetic field of one side penetrates to the other side. Two parallel sheets are placed to a distance t. Because this time the energy stored is located between the sheets, an inductance $L = \mu_0 t$ H/m is placed in between. The surface impedance used for each sheet is of the form

$$Z_S' = j\omega\mu\lambda_L \frac{\mathrm{e}^{\frac{t}{\lambda_L}} + \frac{Z_0 - j\omega\mu\lambda_L}{Z_0 + j\omega\mu\lambda_L}\mathrm{e}^{-\frac{t}{\lambda_L}}}{\mathrm{e}^{\frac{t}{\lambda_L}} - \frac{Z_0 - j\omega\mu\lambda_L}{Z_0 + j\omega\mu\lambda_L}\mathrm{e}^{-\frac{t}{\lambda_L}}}. \tag{2.61}$$

with $Z_0 = 120\pi\,\Omega$. For the case when $Z_0 \gg \omega\mu\lambda_L$, the surface impedance is given by $Z_S = j\omega\mu\lambda_L \coth(t/\lambda_L)$. If $t \gg \lambda_L$, the previous equation reduces to $Z_S = j\omega\mu_0\lambda_L\ \Omega/\mathrm{m}$.

An additional correction β to the double sheet method is needed to get an input surface impedance of Z_S shown in Fig. 2.9**b** seen by an incident wave. The correction is given by

$$\beta = \left[1 - \frac{t}{2\lambda_L \coth t/\lambda_L} + \sqrt{1 + \left(1 + \frac{t}{2\lambda_L \coth t/\lambda_L}\right)^2}\right]. \tag{2.62}$$

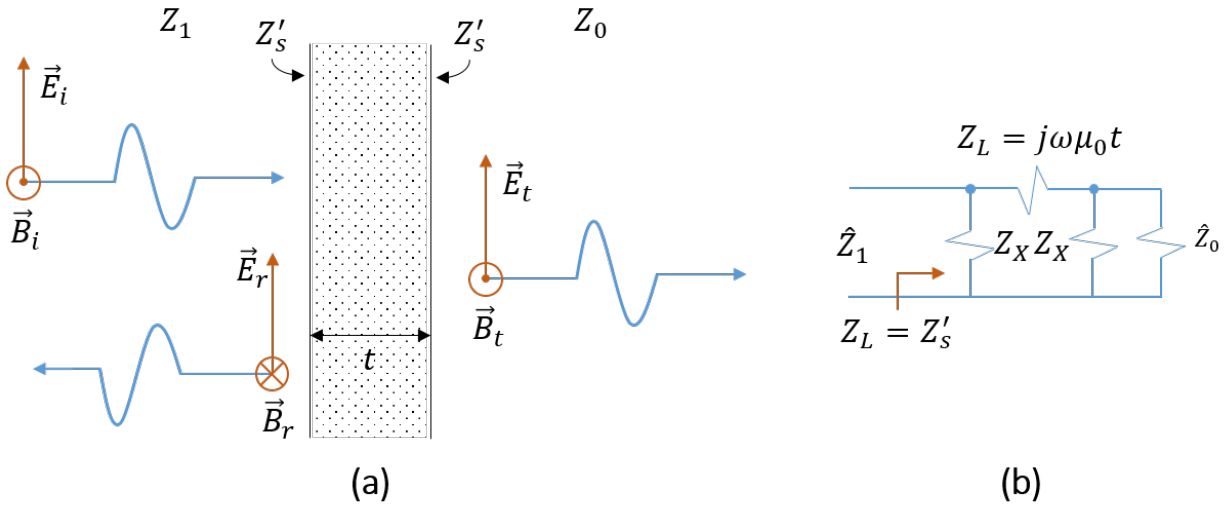

Figure 2.8: (a) Superconductor represented by a thick superconductor with two sheets of surface impedance Z_S' between the vacuum. It is assumed that the wave plane that is transmitted into the strip behaves similarly as in a transmission line. (b) The double sheet equivalent model, where Z_L models the energy store inside the superconductor. In addition, the correction Z_x is included to increase the reliability of the model [30].

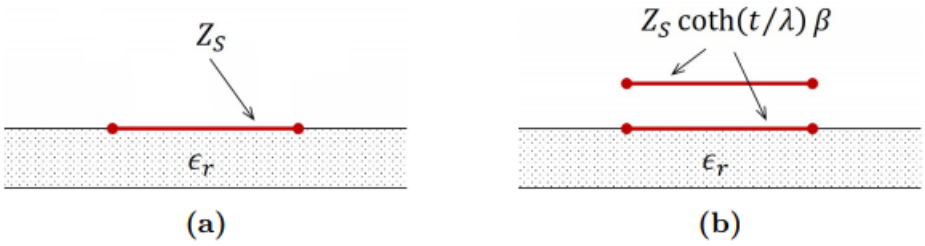

Figure 2.9: Two methods to model the surface impedance of a superconductor. (a) The single sheet model using the surface impedance Z_S. (b) The double sheet model using the coth and β correction to have more reliable results Reprinted from [30].

The effective surface impedance Z_X is of the form $Z_X = \beta Z_S$.

2.2.4 Superconducting microstrip model

In order to include the concept of surface impedance to superconducting microstrip lines, a model for superconducting millimeter and sub-millimeter-wave microstrip lines was provided by G. Yassin and S. Withington. The model provides a method to calculate the propagation constant and characteristic impedance of the assumed quasi-TEM line. In addition, it is assumed that the penetration depth λ_L of the line is much smaller than its thickness. Therefore, the model lacks accuracy with wide and thin films [31]. An additional assumption is that the strip and ground of the microstrip line are made of the same superconductor material. The series characteristic impedance Z and shunt admittance Y can be expressed as

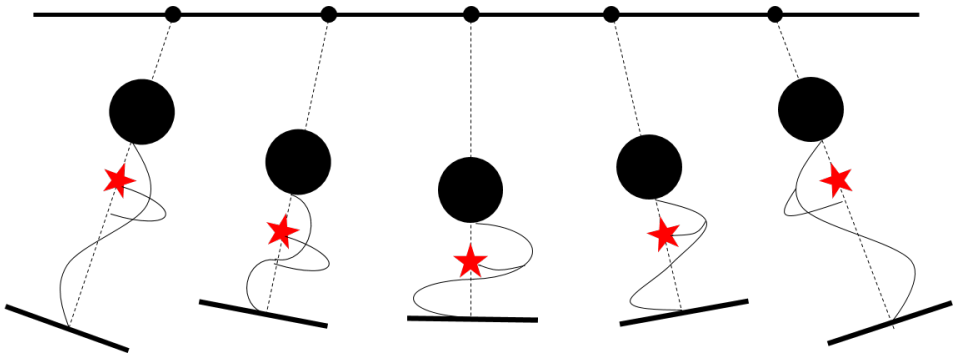

Figure 2.10: The pendulum oscillates to the natural frequency ω, while the string oscillates with a frequency 2ω [32].

$$Z = k(k_0 Z_0) g_1 + 2 g_2 Z_S, \tag{2.63}$$

$$Y = \left(\frac{k_0}{Z_0}\right)\left(\frac{\varepsilon_T}{g_1}\right), \tag{2.64}$$

where $k_0 = 2\pi f/c$ and $Z_0 = 120\pi\ \Omega$ are the wavenumber and characteristic impedance in the vacuum, $\varepsilon_T = j\varepsilon_{eff} + \varepsilon_r \tan\delta$ is the lossy effective permittivity, $\tan\delta$ is the dielectric tangent loss, and ε_{eff} is the effective permittivity without losses. The parameters g_1 and g_2 depend on the geometry of the line [31]. By using Eq. (2.63), the complex propagation constant or wavenumber can be obtained as

$$\gamma = \sqrt{ZY} = -k_0\sqrt{\varepsilon_{eff}}\left(1 - \frac{2\chi Z_S}{k_0 Z_0 H}\right)^{1/2} = \alpha + j\beta, \tag{2.65}$$

where H is the thickness of the substrate and χ is the penetration factor. The calculation of χ is further explained in [31]. Therefore, the propagation constant β, the attenuation constant α and the characteristic impedance Z_y of the lossy superconducting microstrip line can be written as

$$\beta = \beta_m \mathrm{Im}\left(1 - \frac{2j\chi Z_S}{k_0 Z_0 H}\right)^{1/2}, \tag{2.66}$$

$$\alpha = \beta_m \mathrm{Re}\left(1 - \frac{2j\chi Z_S}{k_0 Z_0 H}\right)^{1/2}, \tag{2.67}$$

$$Z_y = Z_L \mathrm{Re}\left(1 - \frac{2j\chi Z_S}{k_0 Z_0 H}\right)^{1/2}. \tag{2.68}$$

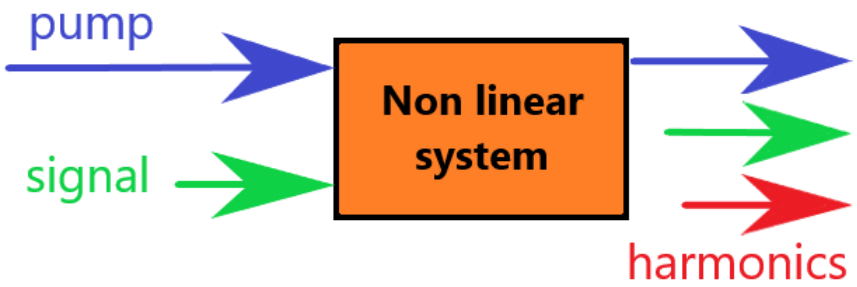

Figure 2.11: Schematic of the parametric amplification, where the pump is combined with the signal inside the non linear system to generate the transfer of energy to the combination of harmonics [33].

2.3 Parametric Amplification

The parametric amplifier is the harmonic modulation on a non linear system driven by a strong *pump*. The oscillations caused by the non linearity interaction generates the transfer of power from the pump source to a combination of states. For instance, the pendulum that is shown in Fig. 2.10 has a natural frequency ω. If it is excited with a vertical oscillation with the double of its frequency, the horizontal oscillation starts growing, similar to a swing [32]. Because a resistive element is not required in the process, energy and momentum of the system are conserved during the transfer of energy. The system has the potential to function without energy dissipation, implying the possibility to operate in quantum-limited noise conditions [7].

From the electromagnetic point of view, shown in Fig. 2.11, the parametric amplification occurs when a strong *pump* signal of frequency f_p is combined with a small target *signal* f_s inside of a non linear circuit. The output of the system are the pump source with a reduction in amplitude due to the parametric effect, the amplified target signal, and the combination of harmonics of the target signal and the pump source. This phenomenon can be analysed by using the Maxwell equations, which result in the *wave equation* or *Helmholtz equation*, written in the electric as

$$\nabla^2 \bar{E} + \gamma^2 \bar{E} = 0, \tag{2.69}$$

where $\gamma = \omega\sqrt{\mu\varepsilon}$ is defined as the *propagation constant* or *wave number*. When a TEM wave is applied to a transmission line, it can also be described in terms of the voltage and current, which are written of the form

$$\frac{\partial^2 I}{\partial z^2} - \frac{\partial}{\partial t}\left(LC\frac{\partial I}{\partial t}\right) = 0. \tag{2.70}$$

The non linear behaviour can occur in different ways. For example, A.L. Cullen introduced the theory of the parametric amplifiers by using an non linear capacitance to describe the

effect [6]. Another example is a third-order susceptibility $\chi^{(3)}$ produced by a refraction index that has a quadratic dependence with the electric field. This is often used to generate the parametric amplification, which in optics is called the *Kerr effect*. In this thesis, the *kinetic inductance* of a superconductor is used as the non linear element to generate the four and three-wave mixing effects, resulting in the parametric amplification.

2.3.1 Self-phase and cross-phase modulation

Self-Phase Modulation (SPM) and Cross-Phase Modulation (XPM) are intrinsic manifestations in an non-linear media. They are widely used in non-linear optics by using the optic Kerr effect [33]. Because those effects are not ascribed exclusively to optic fibers, they can be used in other non linear systems. In this work, these effects are used to derive the model the amplitudes of the signals involved in the parametric process.

Self-phase modulation occurs when a particular signal changes its phase to a variation in the phase velocity induced by an non linear effect. One of the first observations of this effect was in 1970, when glasses and solids were excited by using picosecond pulses [33]. Nowadays, it is used in optical fibers to generate pulses of light of different wavelengths in communication systems. In contrast, cross-phase modulation comes from the non-linear interaction of multiple waves inside the system.

2.4 Summary

In this chapter, the three fundamental processes that form the principle operation of a traveling-wave kinetic inductance parametric amplifier were discussed.

1. The DETL was defined by first discussing their main characteristics, such as the dispersion relation, bloch impedance, S parameters. Subsequently, the treatment of DETL was explained by describing one cell and adding multiple cells in cascade. Given the properties of each segment of the DETL, a microwave network analysis of it can be done. In particular, the stop-bands of the equivalent propagation constant can be located to generate the desired gain in the amplifier.

2. The fundamental of superconductors and kinetic inductance were also described. The theory of surface impedance and its use in superconducting microstrip lines had been presented. By using the dimensions and properties of the DETL, the characteristic impedance Z_j and propagation constant γ_j of each segment of the DETL are possible to be obtained.

3. Finally, the basics of parametric amplification had been explained, describing the main concepts in this process. These concepts are used to derive the equations that describe the amplitudes of the signals inside the amplifier.

This provides enough background to understand concepts such as four and three wave mixing, engineered transmission line and superconducting theory.

Chapter 3

A TKIP using four-wave mixing

The first implementation of a traveling-wave kinetic inductance parametric amplifier was developed by B.H. Eom *et al.* in 2012 [7]. The amplification was generated through the parametric process of Four-Wave Mixing (FWM). This is based on a non-linear intermodulation of different signals inside of a system, where the non-linear element is produced by the kinetic inductance of a superconductor. By using NbTiN as the superconductor, it gives a large enough kinetic inductance to provide a high parametric gain. The four-wave mixing process ideally transfers the energy from a pump source signal to the target signal. However, because of the non-linear behaviour of the system, it also transfers part of that energy to harmonics of the pump and target signals. Therefore, a filter was used to block those harmonics. Because the line does not require resistive elements, the amplifier operates in very low-noise conditions.

In this chapter, the model used to describe the effects involved in the process of amplification is explained. First, the deduction and description of the coupled mode equations are outlined. They describe the evolution of the signals in both amplitude and phase. Furthermore, an extension of the coupled mode equation is made by introducing higher order harmonics. Later, the dispersion-engineered transmission line is introduced. We describe the design and method to calculate the dimensions needed to generate stop bands at the desired frequencies. Once the cell is designed, we present simulations of the dispersion relation, the Bloch impedance and the S parameters. The parametric gain is illustrated with varying different parameters of the amplifier, for instance the pump power, pump frequency, and the behaviour of the gain with additional harmonics. To have more realistic results on the feature of the amplifier, losses in the DETL are included.

3.1 Four-wave mixing theory

The four-wave mixing, represented in Fig. 3.1, is a type of parametric process that uses the non linearity of a material to generate the transfer of energy between the signals that travel in the material. The signals involved are the following:

- Two *pump* signals of amplitudes A_{p1} and A_{p2}, and frequencies f_{p1} and f_{p2}, which are

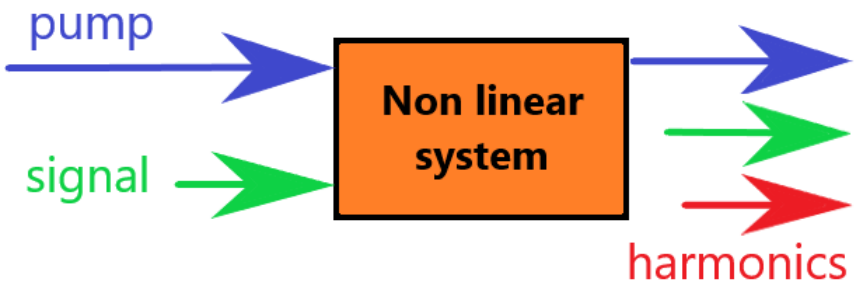

Figure 3.1: Schematic of the parametric amplification, where the pump is combined with the signal inside the non linear system to generate the transfer of energy from the pump source to the combination of harmonics [33].

used as a source to the other signals inside the amplifier.

- The target *signal* of amplitude A_s and frequency f_s, which is the signal that is amplified inside the device.
- The *idle* signal of amplitude A_i and frequency f_i, which represents the first harmonic signal that is generated.

It is assumed that all other signals do not to propagate inside the amplifier because the dispersion-engineered transmission line should filter those frequencies. The mixing of those four signals in the system gives to the process the name Four-Wave Mixing (FWM). Despite the idle signal also receives part of the power of pump signal, by conservation of photon energy, this harmonic is necessary for the generation of the FWM effect. If there is no dissipation of energy during the process, conservation of momentum and energy are satisfied, which are given by

$$f_s + f_\mathrm{i} = f_{p1} + f_{p2}, \tag{3.1}$$
$$k_s + k_\mathrm{i} = k_{p1} + k_{p2}. \tag{3.2}$$

In a degenerate four-wave mixing, both pump signals have the same characteristics. Therefore, the relations $A_{p1} = A_{p2} = A_p$ and $f_{p1} = f_{p2} = f_p$ can be assumed. Because of the non-linear behaviour of FWM, components related with self phase and cross phase modulation are also included in the analysis.

3.1.1 Deduction of gain equations using Four-Wave Mixing

The derivation of the coupled mode equations starts by using the telegraph equations described in Eq. (2.70). The wave equation for the current in a transmission line can be written as [33]

$$\frac{\partial^2 I}{\partial z^2} - \frac{\partial}{\partial t}\left[LC\frac{\partial I}{\partial t}\right] = 0, \tag{3.3}$$

with L and C the inductance and capacitance per-unit-length, respectively. If the kinetic inductance is assumed that varies slowly with respect the time, the slowly varying approximation can be used [33]. As a result, the kinetic inductance can be treated as a constant. We can write, then, Eq. (3.3) as

$$\frac{\partial^2 I}{\partial z^2} - L_T(I) C \frac{\partial^2 I}{\partial t^2} = 0, \tag{3.4}$$

where C is a constant that only depends of the geometry and properties of the transmission line. The total inductance L_T is given by

$$L_T(I) = L_0 \left(1 + \frac{\alpha I^2}{I_*^2}\right), \tag{3.5}$$

with α is the ratio between the kinetic inductance and the total inductance presented in the line. Combining Eq. (2.54) with Eq. (3.4) gives

$$\frac{\partial^2 I}{\partial z^2} - \frac{L_0}{\alpha} C_0 \left(1 + \frac{I^2}{I^{*2}}\right) \frac{\partial^2 I}{\partial t^2} = 0. \tag{3.6}$$

In an non-linear kinetic-inductance medium, the behaviour of the system can be expressed in terms of currents flowing through the material. These currents can be expressed as a sum of components of different amplitudes and phases given by

$$I(z) = \frac{1}{2} \left(\sum_{j=1}^{4} A_j(z) \exp\left(\mathrm{i}\phi_j\right) + c.c. \right), \tag{3.7}$$

where the term "$c.c$" represents the conjugated complex of the left-side term, the jth component of the current has an amplitude $A_j(z)$ and a phase $\phi_j = k_j z - \omega_j t$, and the wave number k_j is associated with its frequency ω_j and amplitude $A_j(z)$. By using the components of the current waves from Eq. (3.7) into Eq. (3.6), we obtain

$$\begin{aligned} &\frac{1}{2} \sum_{j=1}^{4} \left[\left(\frac{\partial^2 A_j}{\partial z^2} + 2\mathrm{i}k_j \frac{\partial A_j}{\partial z} - k_j^2 A_j \right) \mathrm{e}^{\mathrm{i}\phi_j} + c.c. \right] + \frac{1}{2} \left(1 + \frac{\frac{1}{4} \left(\sum_{j=1}^{4} (A_j(z) \mathrm{e}^{\mathrm{i}\phi_j} + c.c \right)^2}{I_c^{*2}} \right) \\ &\times \sum_{j=1}^{4} \left[L_0 C_0 \omega_j^2 A_j(z) \mathrm{e}^{\mathrm{i}\phi_j} + c.c. \right] = 0. \end{aligned} \tag{3.8}$$

There is a non-linear relation between k_j and ω_j that can be written as $F(\beta_j) = G(\omega_j)$, with F and G non linear functions provided by the geometry and properties of the line. On one hand, by Eq. (2.21), $F(\beta_j)$ is given by $\cosh(\beta_j \mathrm{d})$, with d the length of the line. On the other hand, $G(\omega_j)$ is given by $(A + D)/2$, where A and D are elements of the equivalent ABCD matrix of the line. By Eq. (2.15), except by resonance frequencies, we can approximate $G(\omega_j)$ by sum of phases inside a cosh [34]. Therefore, the relation between k_j and ω_j can be treated as quasi-linear, with $k_j \approx \omega_j \sqrt{L_0 C_0/\alpha}$. Furthermore, by using the slowly varying envelope approximation (SVEA), the following expression can be used

$$\frac{\partial^2 A_j}{\partial z^2} \ll k_j \frac{\partial A_j}{\partial z}, \tag{3.9}$$

which makes the neglect of the second derivative $\partial^2 A_j/\partial^2 z$ possible. By using the previous approximations, Eq. (3.8) can be rewritten as

$$\sum_{j=1}^{4} \left[\left(\frac{\partial A_j}{\partial z} \right) \mathrm{e}^{\mathrm{i}\phi_j} + c.c. \right] = \frac{\mathrm{i}}{3 I_*^{2\prime}} \left(\sum_{j=1}^{4} k_j \left(A_j(z) \mathrm{e}^{\mathrm{i}\phi_j} + c.c \right) \right)^3. \tag{3.10}$$

where $I_*^{\prime 2} = 8 I^{*2}/3\alpha$ is defined. All the components of the right side of Eq. (3.10) are presented in Appendix A. Assuming a degenerated FWM, two pump sources with only one pump frequency $\omega_1 = \omega_2 = \omega_p$, a signal frequency $\omega_3 = \omega_s$ and an idle frequency $\omega_4 = \omega_\mathrm{i}$ are present. The right-side in Eq. (3.10) can be unrolled, where the terms associated with self-phase modulation, cross-phase modulation, and FWM are selected. Self-phase and cross-phase modulation are produced due to a phase shift during the propagation of the current wave in the transmission line. This phase shift is obtained by selecting the parameters associated with $\mathrm{e}^{\mathrm{i}\phi_j}$ in the equations. The FWM effect expresses the transfer of energy between the signals, which is described by Eq. (3.1). As a result, those components give a phase shift of $\mathrm{e}^{\mathrm{i}\Delta\phi - \phi_j}$, where $\Delta\phi = \phi_\mathrm{i} + \phi_s - 2\phi_p$. These are the only important effects generated in this type of non linear system, which means that second and third harmonics $(2\omega_j, 3\omega_j)$ are neglected.

Because each component of the current is associated to its phase ϕ_j, Eq. (3.8) is a system of eight coupled equations. Each equation of the system can be written as $F(z, t, \Phi)\mathrm{e}^{\mathrm{i}\phi_j} = 0$, with Φ the group of all frequencies and wave numbers into the system. As a result, there are four equations related to ϕ_j while the other are redundant equations related to the conjugated phase $-\phi_j$. Finally, clearing all the terms except for $\mathrm{d}A_j/\mathrm{d}z$ in the left side, the coupled mode equations are given by

$$\frac{\mathrm{d}A_p}{\mathrm{d}z} = \frac{\mathrm{i}k_p}{I_*'^2}\left[\left(|A_p|^2 + 2\,|A_s|^2 + 2\,|A_\mathrm{i}|^2\right)A_p + 2A_sA_\mathrm{i}A_p^*\mathrm{e}^{\mathrm{i}\Delta\beta z}\right], \tag{3.11}$$

$$\frac{\mathrm{d}A_s}{\mathrm{d}z} = \frac{\mathrm{i}k_s}{I_*'^2}\left[\left(|A_s|^2 + 2\,|A_\mathrm{i}|^2 + 2\,|A_p|^2\right)A_s + A_\mathrm{i}^*A_p^2\mathrm{e}^{-\mathrm{i}\Delta\beta z}\right], \tag{3.12}$$

$$\frac{\mathrm{d}A_\mathrm{i}}{\mathrm{d}z} = \frac{\mathrm{i}k_\mathrm{i}}{I_*'^2}\left[\left(|A_\mathrm{i}|^2 + 2\,|A_s|^2 + 2\,|A_p|^2\right)A_\mathrm{i} + A_s^*A_p^2\mathrm{e}^{-\mathrm{i}\Delta\beta z}\right], \tag{3.13}$$

where $\Delta\beta = 2k_p - k_s - k_\mathrm{i}$ is the dispersion of the system.

3.1.2 Introducing harmonics in the gain equations

In the previous section, it was assumed that the harmonics from $3nf_p$ were blocked completely by the DETL. However, some higher order harmonics might be presented in the output of the amplifier. The analysis of higher order harmonics is presented to understand how they affect the parametric gain. A similar analysis was published by S. Chaudhuri [11], where a generalized system of coupled equations with n side band harmonics are presented. An illustration of this effect is shown in Fig. 3.2, where the side-bands up to $n = 5$ are presented. The coupled mode equations are extended to the nth harmonic, with j and m restricted to be odd, because of the cubic dependence with the current and the four wave mixing effect.

The degenerated four-wave mixing only involves the relation between four signals. However, in this case, the n side band harmonic components of the current are expressed as

$$I = \frac{1}{2}\left(\sum_{m=-n}^{n} A_m(z)\exp\left(\mathrm{i}(\omega_m t - k_m t)\right) + c.c\right). \tag{3.14}$$

The conditions to fulfill the four-wave mixing effect are conservation of energy and momentum between the side band harmonics and the pump signal. They can be described by the relations

$$\omega_m = m\omega_p - \omega_s - \omega_p, \tag{3.15}$$

$$\beta_m = m\beta_p - \beta_s - \beta_p, \tag{3.16}$$

where $\beta_m = \beta(\omega_m)$. When $m = 1$, then we have $\omega_1 = \omega_s$ and $\beta_1 = \beta_s$. If $m = -1$, $\omega_{-1} = -2\omega_p + \omega_s = -(2\omega_p - w_s)$. Because the initial phase of a signal is not significant in the parametric process, both results are equivalent, resulting in $\omega_1 = \omega_\mathrm{i} = 2\omega_p - \omega_s$. From Eq. (3.15), we obtain

$$\omega_m - \omega_{m-2} = 2\omega_p. \tag{3.17}$$

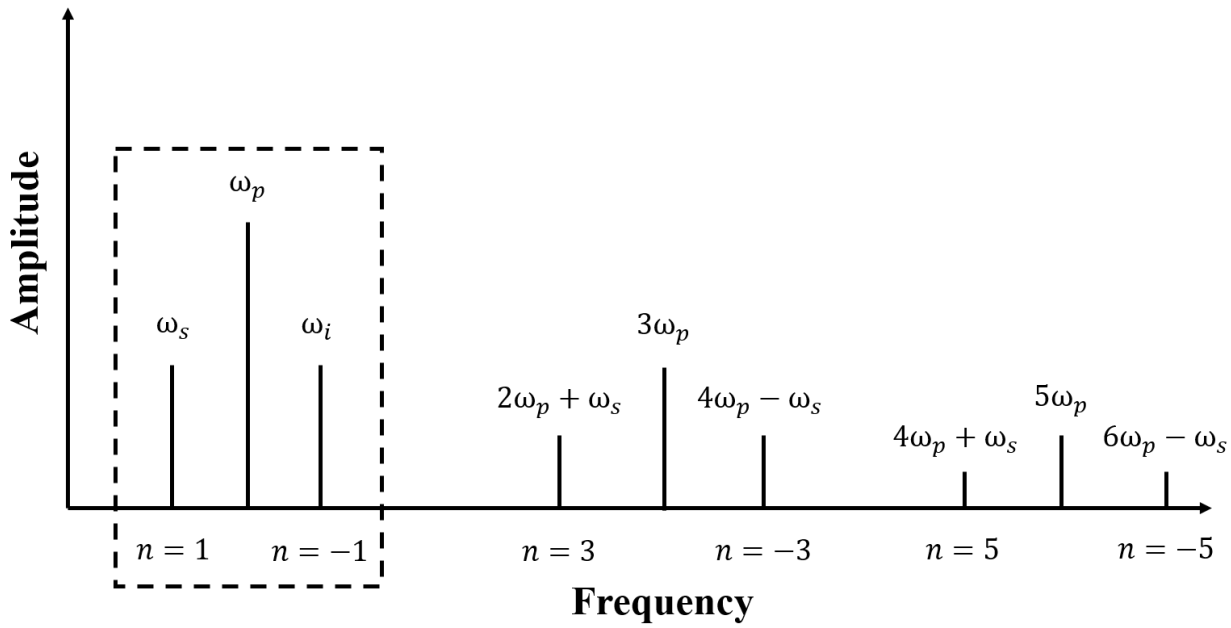

Figure 3.2: An illustration explaining the side-bands generated by harmonics of the target and pump signal, the dashed box represent the original signals of the coupled mode equations, while the other additional harmonics are included in the analysis [11].

It is assumed that the phase is not important in the amplification. Therefore, the relation of frequencies and propagation constants can be changed to

$$\omega_m + \omega_{m-2} = 2\omega_p, \tag{3.18}$$

$$\beta_m + \beta_{m-2} = \beta_p. \tag{3.19}$$

Since in Eq. (3.11), (3.12) and (3.13), the relations that domain the evolution of the signals inside the device are SPM, XPM and the parametric effect, the same analysis explained on section 3.1.1 is used. As a result, a variation of the coupled mode equations with harmonics is given by

$$\frac{\mathrm{d}A_p}{\mathrm{d}z} = \frac{\mathrm{i}k_p}{I_*'^2}\left[\left(|A_p|^2 + 2\sum_{m=-n}^{n}|A_m|^2\right)A_p + 2\left(\sum_{m=-n}^{n}A_m A_{m-2}A_p^*\mathrm{e}^{\mathrm{i}\Delta\beta_m z}\right)\right], \tag{3.20}$$

$$\frac{\mathrm{d}A_j}{\mathrm{d}z} = \frac{\mathrm{i}k_j}{I_*'^2}\left[\left(2|A_p|^2 - |A_j|^2 + 2\sum_{m=-n}^{n}|A_m|^2\right)A_j + A_{j-2}^*A_p^2\mathrm{e}^{-\mathrm{i}\Delta\beta_j z} + A_{j+2}^*A_p^2\mathrm{e}^{-\mathrm{i}\Delta\beta_{j+2} z}\right]. \tag{3.21}$$

In the case of a signal of a harmonic higher than n, the expressions are not considered.

3.1.3 Solution of the gain equations

Although the system of equations can be solved numerically. In order to have a better understanding of how the power of the signals changes during the four-wave mixing, an analytical solution can be obtained in a specific case . We will make the following assumptions [33]:

- The extraction of power from pump signal is neglected, which results in $\mathrm{d}\left|A_p\right|/\mathrm{d}z = 0$ since $A_p \gg A_s, A_\mathrm{i}$.
- The amplifier is operating in a narrow bandwidth near ω_p. As a consequence, the relation $\omega_s \approx \omega_p$ is used.
- The wave-numbers k_p, k_s and k_i are real numbers, therefore the jth propagation constant follows $k_j = k_j^*$.

By using the first assumption, the pump source can be written as

$$A_p = A_p(0)\mathrm{e}^{\mathrm{i}\Delta\theta z}, \tag{3.22}$$

where $\Delta\theta$ is a shift in the phase of the pump signal per unit of length, and $A_p(0)$ is its amplitude at the beginning of the transmission line. This shift phase can be calculated using Eq. (3.22) in Eq. (3.11). As a result we have

$$\Delta\theta = \frac{k_p}{I_c^{*2}}\left[\left|A_p(0)\right|^2 + 2\left|A_s\right|^2 + 2\left|A_\mathrm{i}\right|^2 + 2A_sA_\mathrm{i}\mathrm{e}^{-\mathrm{i}(\theta-\Delta\beta)z}\right] \approx \frac{k_p\left|A_p(0)\right|^2}{I^{*2}}. \tag{3.23}$$

The total phase of the pump source after travelling through the paramp is given by $\Delta\theta L$. By using Eq. (3.22), the pump signal can be written as

$$A_p = A_p(0)\exp\left[\frac{\mathrm{i}k_p\left|A_p(0)\right|^2 z}{I^{*2}}\right]. \tag{3.24}$$

Then, rewriting Eq. (3.12) and (3.13) in terms of power we have,

$$\frac{\mathrm{d}A_s}{\mathrm{d}z} = \mathrm{i}\gamma\left[2P_pA_s + P_pA_\mathrm{i}^*\mathrm{e}^{-\mathrm{i}(\Delta\beta-2\gamma P_p)z}\right], \tag{3.25}$$

$$\frac{\mathrm{d}A_\mathrm{i}}{\mathrm{d}z} = \mathrm{i}\gamma\left[2P_pA_\mathrm{i} + P_pA_s^*\mathrm{e}^{-\mathrm{i}(\Delta\beta-2\gamma P_p)z}\right], \tag{3.26}$$

where the parameter $\gamma_j = k_j/I^{*2} \approx \gamma$, as well as the power of the pump signal $P_p = A_p(0)^2$ are defined. This is a coupled system of non-homogeneous differential equations. By defining the variable B_j as

$$B_j = A_j \exp\left[-2\mathrm{i}\gamma P_p z\right], \tag{3.27}$$

the non-homogeneous coefficient of the coupled mode equations can be eliminated, facilitating its resolution. The resulting homogeneous equations are obtained by substituting Eq. (3.27) in Eq. (3.25) and (3.26). By taking conjugated part B_{i}^* to the resulting equation, it is found that

$$\frac{\mathrm{d}B_s}{\mathrm{d}z} = \mathrm{i}\gamma P_p B_{\mathrm{i}}^* \mathrm{e}^{-\mathrm{i}\kappa z}, \tag{3.28}$$

$$\frac{\mathrm{d}B_{\mathrm{i}}^*}{\mathrm{d}z} = -\mathrm{i}\gamma P_p B_s \mathrm{e}^{\mathrm{i}\kappa z}, \tag{3.29}$$

and the phase mismatch κ is defined as

$$\kappa = \kappa^* = \Delta\beta + 2\gamma P_p, \tag{3.30}$$

where the third assumption has been used. The detail of the resolution can be found in the Appendix B. The gain of the amplifier is given by

$$G_s = \cosh^2(gL) + \left(\frac{\kappa}{2g}\right)^2 \sinh^2(gL), \tag{3.31}$$

where g is defined as the dispersion component of the parametric gain. g can also be written as

$$g^2 = -\Delta\beta\left(\frac{\Delta\beta}{4} + \frac{k_p\left|A_p\right|^2}{I_*'^2}\right). \tag{3.32}$$

Two cases are being analysed using Eq. (3.31). If there is not dispersion, $\Delta\beta = 0$ and $g \approx 0$, then $\kappa \approx 2k_p\left|A_p\right|^2 / I_*'^2$. Therefore, the gain can be written as

$$G_s = 1 + \left(\frac{\kappa L}{2}\right)^2 = 1 + \left(\frac{k_p\left|A_p\right|^2 L}{I_*'^2}\right)^2 = 1 + (\Delta\theta L)^2. \tag{3.33}$$

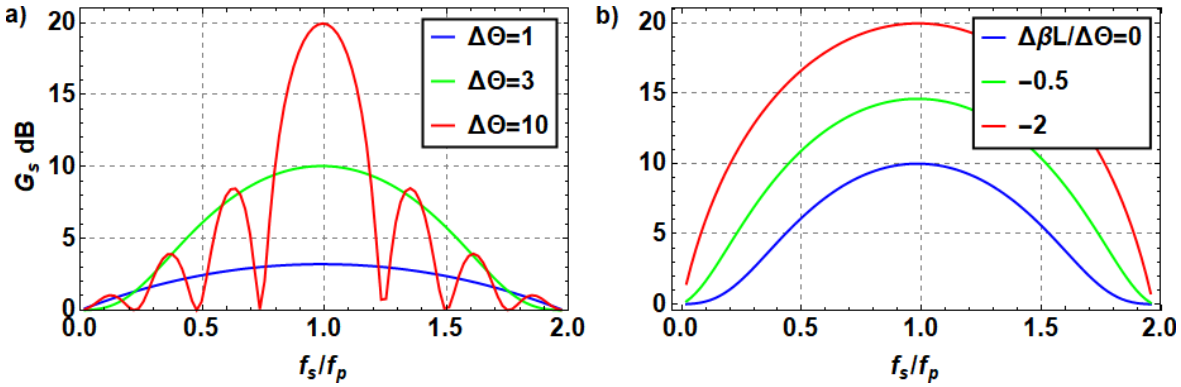

Figure 3.3: Analysis of the parametric gain calculated using Eq. (3.34), where $P_p = -48$ dBm. a) Parametric gain using a dispersion $\Delta\beta = 0$, and using different values of $\Delta\theta$. b) Illustration of the parametric gain with different and constant values of dispersion, and a phase shift of the pump tone of 3 rads [37].

If $\Delta\beta = -2\Delta\theta$, then the linear mismatch compensates with non-linear phase shift $\Delta\theta$. Thus, we have $\kappa = 0$ and $g = \Delta\theta$, and, therefore, the parametric gain can be expressed as

$$G_s = \cosh^2(gL) \approx \frac{1}{4}\exp(2\Delta\theta L), \tag{3.34}$$

which has an exponential behaviour. A basic analysis of the coupled mode equations are shown in Fig. 3.3, where in Fig. 3.3**a**, the parametric gain is illustrated with different pump phase shifts $\Delta\theta$. It can be proven from Eq. (3.32) that g is real when $-4\Delta\theta \leq \Delta\beta \leq 0$. Therefore, by using $\Delta\theta = 1$ and $\Delta\theta = 3$, we have a pure exponential gain. Furthermore, with $\Delta\theta = 10$, the parameter g is complex, generating an oscillating behaviour in the parametric gain . Fig. 3.3**b** shows the parametric gain with different values of dispersion $\Delta\beta$, where it can be observed that a decrement of the parameters increments the gain to compensate the pump phase shift of 3 rads. These results are in accordance with [37].

3.2 Engineered transmission line using microwave filters

By using the FWM effect, the desirable situation is that all the energy obtained from the pump source is transferred to the target signal, and, therefore, an important parametric gain can be generated. Nonetheless, due to non-linear parametric process, harmonics of the pump and target signal are also created by transferring part of the pump energy to those components. Thus, a system that blocks the generation of harmonics is needed. This requirement can be achieved by a DETL where, by suppressing frequencies above $3f_p$, most harmonics are filtered. In this section, based on the theoretical framework explained in the previous chapter, the design of a periodic transmission line suitable for using the FWM effect is detailed. The general design of the cell is discussed, and the methodology of obtaining the filter is presented. Later, the main features of the cell are illustrated. They are presented

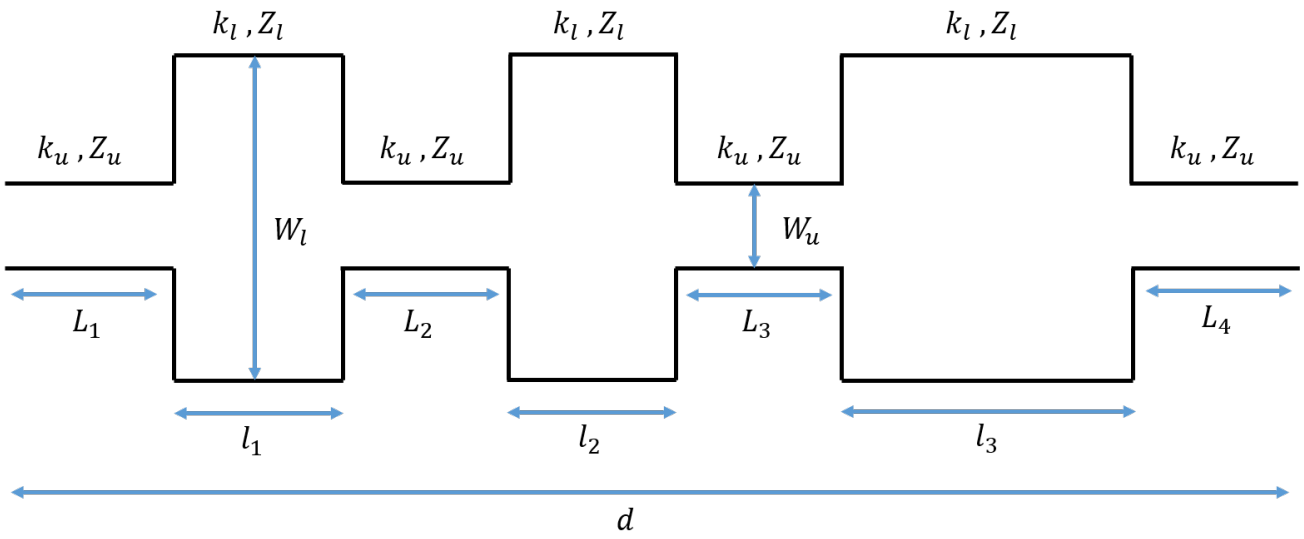

Figure 3.4: The cell design based on transmission lines. The characteristics of each line are represented with the sub-index u or *unloaded*, and the *loaded* elements with the sub-index l o *loa*ded. This filter, with the appropriate measurements, generates wider stop bands for frequencies above $3f_p$, useful when is necessary conservation of energy in four wave mixing.

Table 3.1: Dependent dimensions of the filter using a microstrip transmission line.

l_2	l_3	L_1	L_2	L_3	L_4	W_l
l_1	$2l_1$	$0.5(\mathrm{d}/3 - l_1)$	$\mathrm{d}/3 - 0.5(l_1 + l_2)$	$\mathrm{d}/3 - 0.5(l_2 + l_3)$	$0.5(\mathrm{d}/3 - l_3)$	aW_u

without and including losses.

3.2.1 Design of a periodic filter suitable for FWM

The design of the periodic filter can be observed in Fig. 3.4. It consists in a microstrip line of length d, substrate height H, and the thickness of the strip t_s and ground plane t_g. It is divided in seven transmission lines. The first four are the *unloaded* elements. These lines are used as a coupling lines to the external ports. They have lengths L_1, L_2, L_3, L_4, width W_u, propagation constant k_u and characteristic impedance Z_u. Each of them are interleaved with three perturbations (*loaded* elements) with dimensions l_1, l_2, l_3 and width $W_l = aW_u$, with a as a constant parameter. In addition, they have a propagation constant and characteristic impedance k_l and Z_l, respectively. The most important restrictions are that the first and second perturbation have the same length $l_1 = l_2$, while the third perturbation is given by $l_3 = bl_1$, with b a constant. Because of those restrictions, the generation of stop bands at $3nf_p$ is possible. As a result, there is a dependence between the parameters, by fixing the free variables d, l_1, W_u, b and a, the dependant dimensions can be calculated using Table 3.1.

The presented design generates unwanted stop bands at $(1+3(n-1))f_p$ and $(2+3(n-2))f_p$, with $n \in \mathbb{Z}^+$. These need to be as narrow as possible, because some of those frequencies are inside the operation bandwidth of the device.

Table 3.2: Properties of the superconductor.

ε_r	H	t_s	t_g	T_c	J_c	ρ_n
	nm	nm	nm	K	A/m^2	$\Omega\,cm$
10	250	60	300	14.28	1×10^{12}	1.008×10^{-6}

Table 3.3: The free parameters used to design the unit cell.

d	l_1	W_u	a	b
µm	µm	µm	–	–
2300	50	1.49	1.2	2

The requirements we impose to design the DETL are the following:

- Each cell is designed using a superconducting microstrip transmission line. The filter needs to create stop bands with a wide bandwidth at $3nf_p$, $n \in \mathbb{Z}^+$ to prevent the propagation of the signals at that frequencies.
- Minimize the width of the first two stop bands.
- Maximize the gain.
- Maximize the attenuation constant inside the stop bands.
- Avoid, if possible, large impedance changes between the unloaded and loaded lines due to possible radiation losses [35].
- A characteristic impedance Z_u of $50\,\Omega$ was needed to minimize reflection from the external ports.

The manufacturing process that will be used to fabricate the microstrip cannot produce a substrate with a height more than $0.5\,\mu$m. As a compromise to facilitate the fabrication on the superconductor, a height $H = 250\,$nm was chosen. The pump frequency was chosen as higher as possible to maximize the bandwidth of amplification, but considering the limitation of the instrumentation.

Once the requirements of the design were met, a corroboration of the resulted stop bands by using other microwave software was performed. For example, AWR can be used to compare the S parameters, where a good agreement was found by using a similar design [36].

3.2.2 Methodology

Given the requirements stated in section 3.2.1, and Eq. (2.15), the ABCD matrix of the cell can be calculated using:

- The superconducting characteristic impedance and propagation constant $\{Z_{u,l}, k_{u,l}\}$ of each part of the DETL, respectively.
- The dimensions l_j of each part of the filter, given by the dependent and free parameters in the design.

They are obtained as follows:

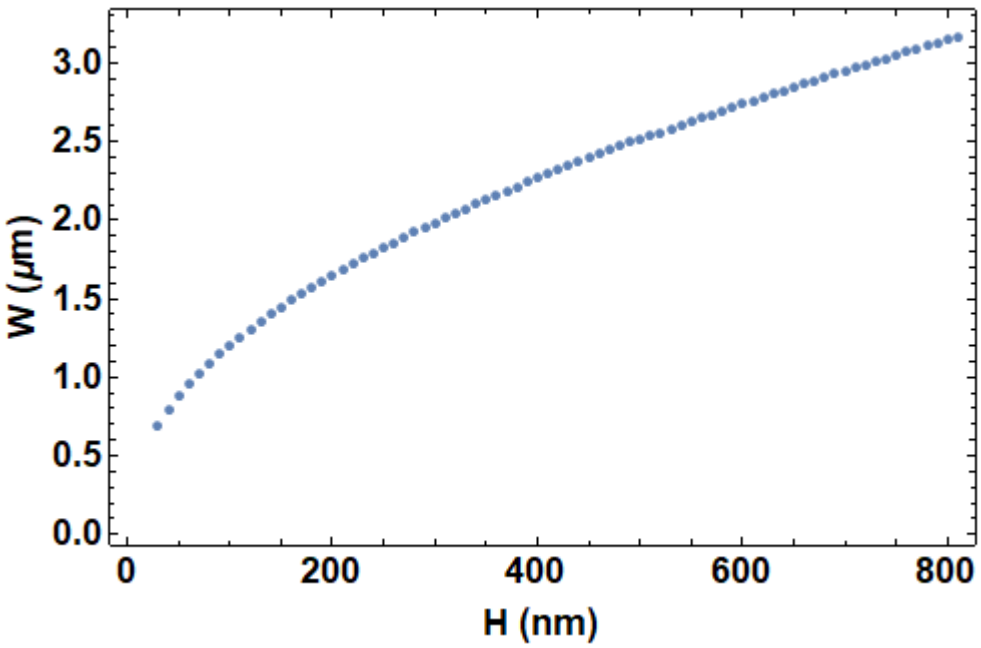

Figure 3.5: Dependence of a line width W_u with H, where a characteristic impedance of $50\,\Omega$ has been imposed Reprinted from [30].

Table 3.4: Normalized wave numbers and characteristic impedance of the engineered TL designed using the dependent and free parameters.

Z_u	k_u/k_0	Z_l	k_l/k_0
Ω	–	Ω	–
50.09	9.28	43.22	9.37

1. The superconducting characteristic impedance $Z_{u,l}$ and $k_{u,l}$ propagation constant of the microstrip line are calculated using the model of G. Yassin provided by Eq. (2.68) and (2.66), which depend on

   (a) The surface impedance Z_S modelled by Eq. (2.61), which is related to the depth penetration depth λ_L or the complex conductivity σ resulted from Eq. (2.55) and (2.56).

   (b) The height H of the substrate.

   (c) The penetration factor χ.

   (d) The effective permittivity ε_{eff} and normal characteristic impedance Z_L are obtained by the Hammerstad and Jensen model, given by Eq. (2.31) and (2.28).

   (e) The critical temperature T_c, the normal resistivity ρ_n were obtained from previous measurements [30]. These parameters and the relative permittivity ε_r are shown in Table 3.2.

By adjusting $Z_u = 50\,\Omega$, the relation between the height and the width is shown in Fig.

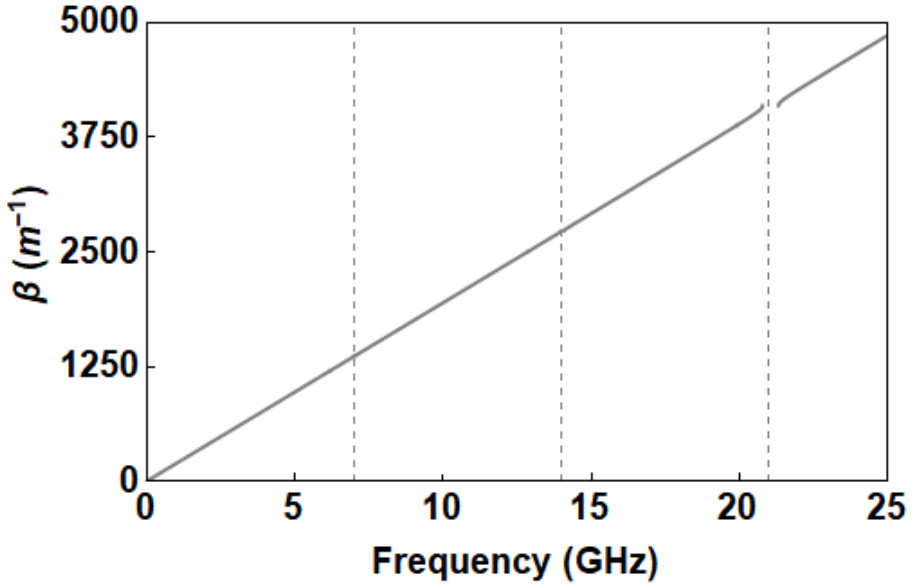

Figure 3.6: The dispersion relation created by the periodic transmission line. An important stop-band is produced at $\approx 3f_p$ to improve the amplification for FWM.

3.5 [30]. It can be seen that by using a height $H = 250\,\text{nm}$, the width of the unloaded line is $W_u = 1.49\,\mu\text{m}$.

2. The free parameters d, l_1, b and a are chosen heuristically. The other parameters are obtained according to Table 3.1.

3. Once all the parameters are obtained, the ABCD matrix of each part of the cell is calculated, and the total ABCD matrix of cell is obtained using Eq. (2.4). With the ABCD matrix of the cell the following parameters can be obtained

   (a) The equivalent propagation β and attenuation constant α_t of the TL are given by the imaginary and real part of Eq. (2.21), which uses the ABCD matrix of the cell. The parameter $\beta - k_u$ is usually plotted to eliminate its linear frequency dependence component. With this method, the stop bands created by the line are easier to observe. The equivalent attenuation constant, the reflection and transmission coefficient are used to analyse the losses. If the propagation constant β does not have wide stop bands at $3nf_p$, then, depending of their actual location, the free parameters were changed and the previous process was repeated until the requirements were met. To analyse the losses, the negative part of the attenuation constant α_t, the reflection and transmission coefficients are obtained.

   (b) The Bloch impedance is obtained using the ABCD matrix of the cell and Eq. (2.6).

   (c) The transmission and reflection coefficients S_{12} and S_{11} are calculated to analyse the losses of the entire TL. They are obtained by using Eq. (2.14) and (2.13), which depends of the N cells between the external ports. The ABCD matrix of the entire TL is calculated by using Eq. (2.23).

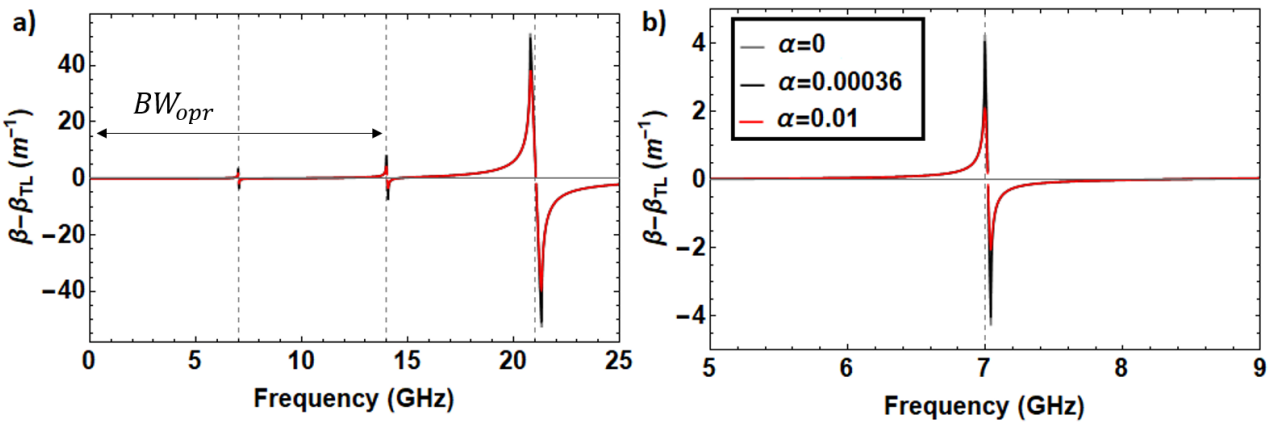

Figure 3.7: a) The dispersion relation of the cell is illustrated with different losses, with $\Delta\beta = \beta - \beta_{TL}$, where β is the propagation constant of the line, while β_{TL} is the propagation constant of an unloaded pattern. b) A close up of the first stop band is located near the pump frequency f_p at 7 GHz.

The losses are usually represented by the loss tangent $\tan\delta$. However, in this work the losses were added into the model by using attenuation constants. An attenuation constant $\alpha = \alpha_u = \alpha_l$ is used in each part of the seven transmission lines of the cell, while the propagation constant $\gamma_{u,l} = \mathrm{i}k_{u,l}$ is replaced with $\gamma'_{u,l} = \alpha + \mathrm{i}k_{u,l}$. The propagation constant $k_{u,l}$ is given by Eq. (2.66), where the modal dispersion is calculated using the effective permittivity, the surface impedance and the dimensions used by Eq. (2.68).

4. The parametric gain is calculated by using Eq. (3.11), (3.12) and (3.13) numerically. A wave number $\gamma = \alpha_t + \mathrm{i}\beta$ is used, α_t and β are the attenuation constant and propagation constant of the cell, respectively. The number of cells N is also included in the analysis, where the parametric gain grows by increasing the effective length of the line $L_{eff} = \mathrm{d}N$ (see Eq. (3.34)). The inclusion the additional harmonics are given by Eq. (3.20) and (3.21). The effective critical current $I'_* = 13.26\,\mathrm{mA}$ is obtained by using the Table 3.2, where the approximation $I_c = J_c \times A$ was used, where A is the transversal area of the line and J_c is the critical density of current inside the line. Different values of the pump power $P_{A_p} = A_p^2(0)$ and a target signal $P_{A_s} = -170$ dBm were used.

3.2.3 Simulation results of the dispersion engineered line without losses

In this section, the simulation results of the superconducting microstrip line that was designed in this work are presented. They were obtained using the software *Wolfram Mathematica*. The free parameters can be observed in Table 3.3, where, with the tuned parameters, the characteristic impedance of the unloaded and loaded parts of the cell are given by Table 3.4.

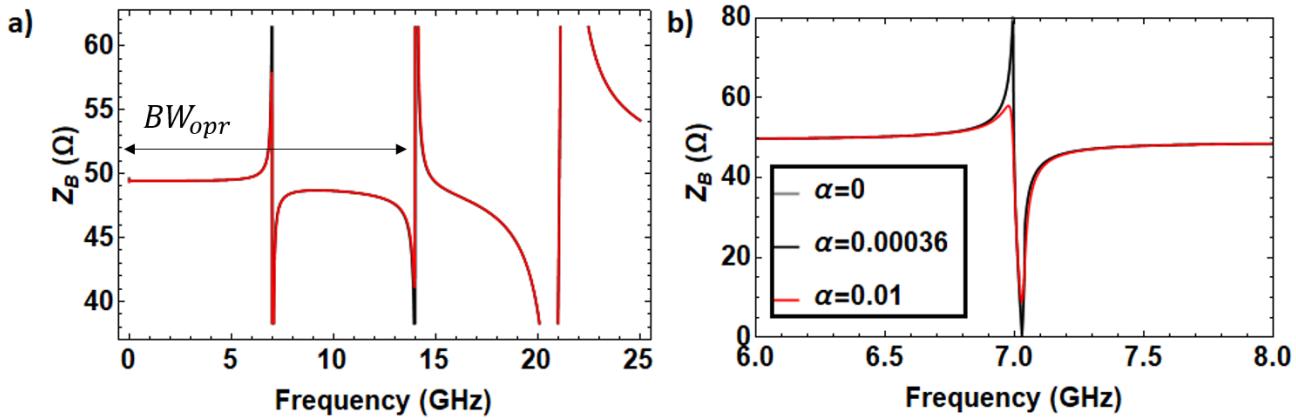

Figure 3.8: The Bloch impedance of the engineered transmission line, obtained by using different attenuation constants. a) An illustration of the Bloch impedance at the operation frequency of the amplifier. b) A close up of the first stopband located at near the pump frequency f_p.

3.2.3.1 Dispersion relation

The dispersion relation resulting from the design is shown in Fig. 3.6, where the linear behaviour of the propagation constant can be observed. The dotted gray lines represent the location of the stop bands. The pump tone was located near the stop bands to increment the dispersion during the parametric process. To appreciate the non-linear component of the dispersion, Fig. 3.7**a** is illustrated. The first stop band needs to be located very close to the chosen pump frequency, due to a higher k_s, resulting in a large dispersion $\Delta\beta = k_s + k_\mathrm{i} - 2k_p$, which by the coupled mode equations, increases the parametric gain. In addition, the bandwidth of the first stop band is desirable to be as thin as possible, so the frequency operation of the amplifier can be large. The third stop band located at $3f_p$ has a bandwidth of $\approx 500\,\mathrm{MHz}$ at $3f_p$. This bandwidth is very large when compared with the first two stop bands of $\approx 50\,\mathrm{MHz}$ and $\approx 100\,\mathrm{MHz}$, respectively, which is expected from a well designed DETL. The third stop-band is wider to prevent the rejection of the pump harmonics inside the operation bandwidth.

3.2.3.2 Bloch impedance

The other main feature of the line is the characteristic impedance Z_L. It is represented by the Bloch impedance of the cell as shown in Fig. 3.8. At frequencies below f_p, the characteristic impedance is $Z_B = 49.46\,\Omega$, which is near to the expected $50\,\Omega$. Above the pump frequency, the impedance decreases ≈ 1 percent, which generates additional reflections of 2 dB (see Fig. 3.10). Above $2f_p$, the Bloch impedance has an abrupt variation from $\approx 50\,\Omega$ to $0\,\Omega$. However, it is outside of the operating frequency, i.e does not contribute to reflections inside the amplifier.

3.2.3.3 S parameters: Transmission and reflection coefficient

Fig. 3.9**a** illustrates the transmission coefficient S_{21} of the DETL. The first stop-band has an attenuation of 2dB, while at $3f_p$, the transmission is attenuated -51 dB and having that frequency blocked. The stop-band over f_p in Fig. 3.9**b** is approximate of 100 MHz, while in

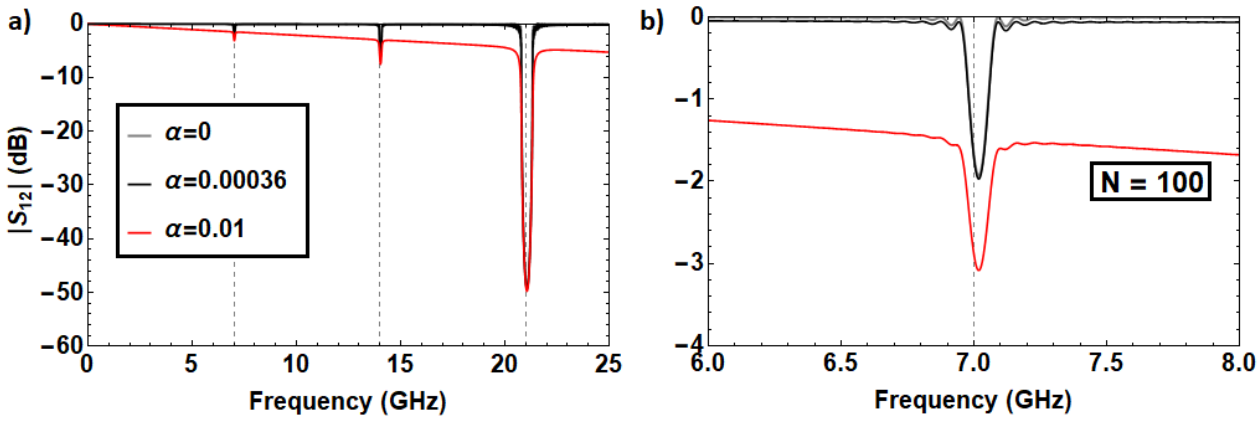

Figure 3.9: Transmission coefficient of the periodic transmission line shown in Fig. 3.4. It is introduced with different values of losses α and with a number of periodic filters (cells) in cascade N of 100. An important stop-band is produced a $3f_p$ to improve the amplification for FWM.

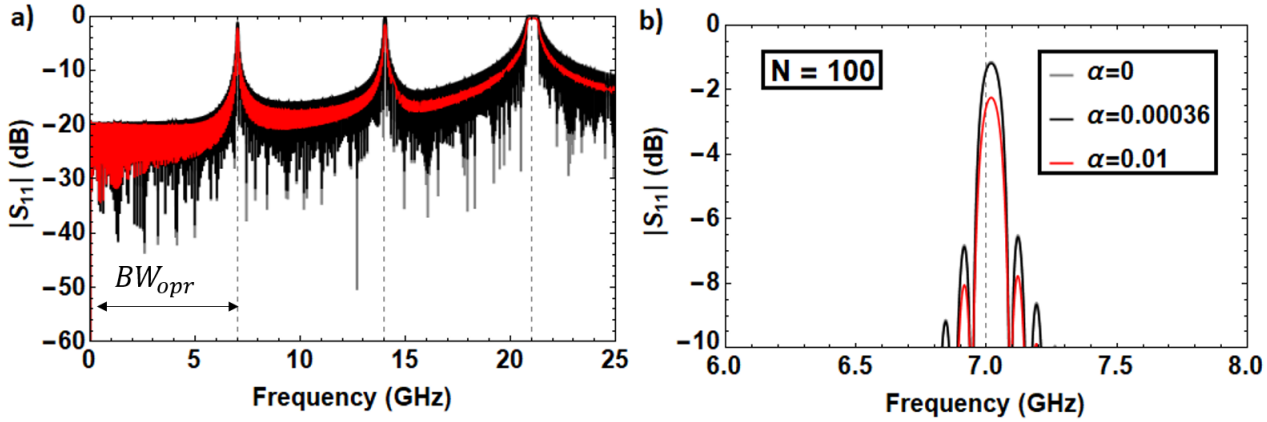

Figure 3.10: a) Reflection coefficient S_{11} of the engineered TL. It is introduced with different values of losses α and with a number of periodic filters (cells) in cascade N of 100. b) A close up of the first stopband located at near the pump frequency.

$3f_p$ the stop-band has a bandwidth of 300 MHz. There is a narrowing of the stop-band at $3f_p$ when compared with Fig. 3.7. This effect is because the number of cells not only increases the effective length of the DETL, but also affects the transmission of the signals inside the device. The idea is to minimize the stop-bands to maximize BW_{opr}, but to maximize the stop-bands to reject higher harmonics. In this thesis, a number of 100 cell in cascade were used, which was chosen arbitrary.

The reflection coefficient of line S_{11} is shown in Fig. 3.10**a**. With a Bloch impedance of 49.56 Ω, the line generates reflection near -20 dB. This indicates a good match between the device and the ports of 50 Ω. From f_p up to higher frequencies, the reflection start to increase as a result of a deviation of the characteristic impedance. The maximum amount of reflections occurs in the stop bands of the line, located at nf_p. A close up of S_{12} can be observed in Fig. 3.10**b**. At near f_p, the reflections tend to increase in conjunction with the

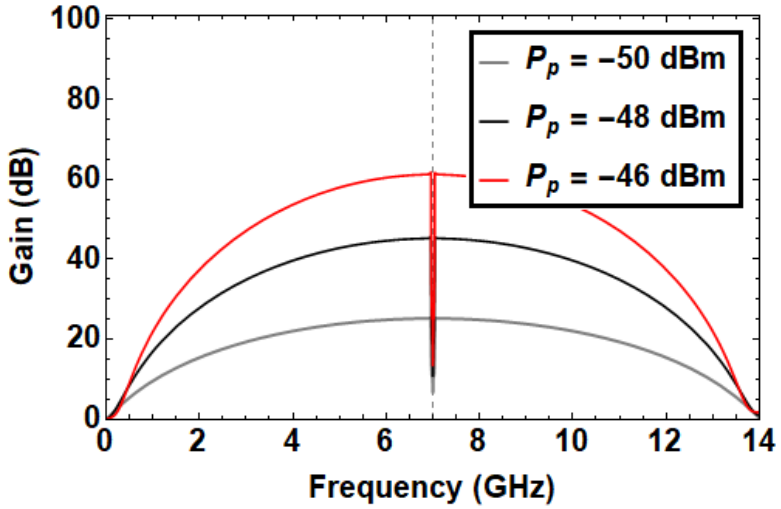

Figure 3.11: Parametric gain of the amplifier without losses and using different pump power sources.

number of cells, but losing bandwidth as a result.

3.2.3.4 Parametric gain: variation of the pump power

The parametric gain was calculated using 100 periodic patterns in cascade. This number of cells N was used to be consistent with the aforementioned transmission and reflection coefficient. The gain can be easily improved by increasing N. The number of cells not only changes the effective large L_{eff} of the amplifier, but also generates a higher rejection of harmonics, as observed in the transmission coefficient shown in Fig. 3.9.

In Fig 3.11, the parametric gain is illustrated with different values of the pump power. It can be observed that will two different power of pump signals generates a change in the parametric gain. Between a pump power of -48 dBm and -50 dBm in the device has an increment of 10.5 dBm, whereas the difference with -46 dBm and -48 dBm is approximately 8 dBm. This is expected from the result obtained in Eq. (3.34), where the pump shift $\Delta\theta$ increases in an exponential rate with respect to the gain, resulting in a quasi-linear rate in dB.

3.2.3.5 Parametric gain: variation of pump frequency

An analysis of frequency sensibility is presented to elucidate how changes in the pump frequency affects the parametric gain. Fig. 3.12 shows how the parametric gain reacts to different changes on the pump frequency f_p. The behaviour can be observed in terms of $\Delta f = f_{pe} - f_{pr}$, where f_{pe} is the frequency at the beginning of the first stop-band of the DETL, while f_{pr} is the pump frequency used in the device. When $\Delta f = 0.1\,\text{MHz}$ in Fig. 3.12**a**, the parametric gain is not reduced significantly when compared with the 32 dB of gain that can be observed in Fig. 3.11. However, when Δf increments to 1 MHz, the gain is reduced in 3 dB, i.e half of the initial parametric gain. This behaviour is produced due to the decrease of the wave number when the pump signal is moving away from the stop band, if the displacement is large enough, the pump signal can be located at the linear part of the wave

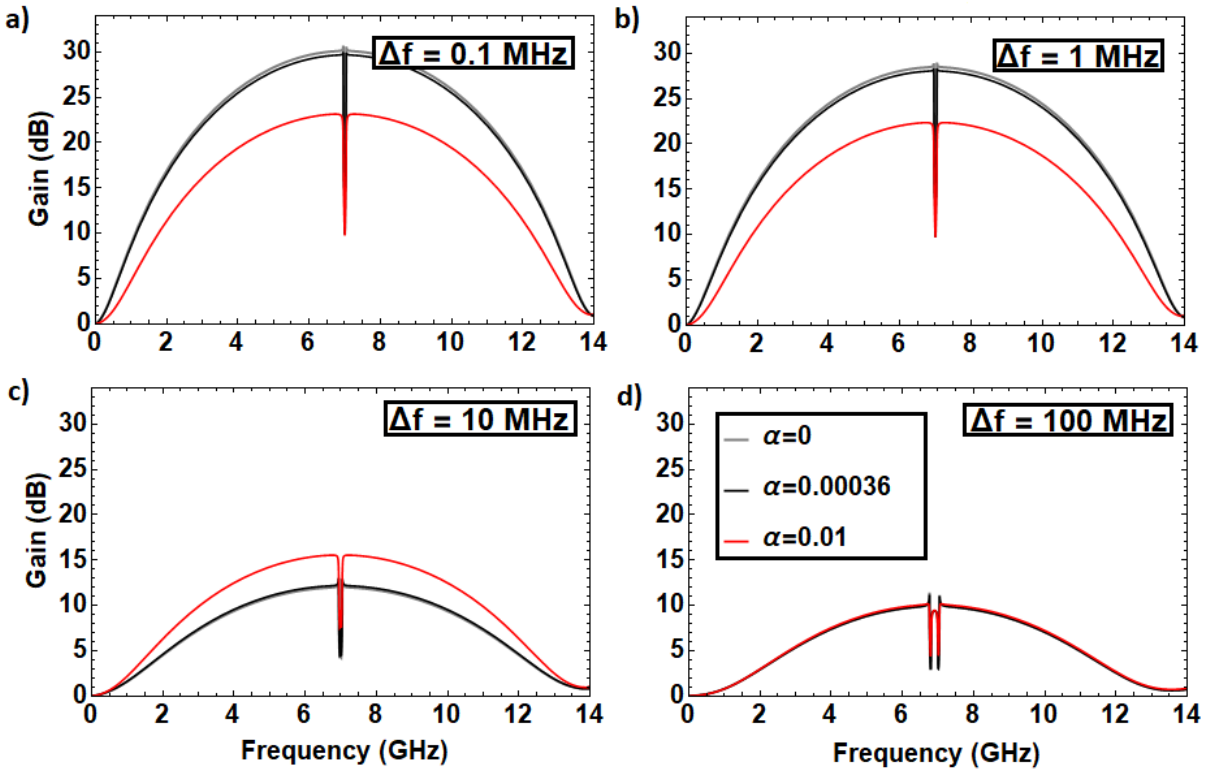

Figure 3.12: A plot illustrating the inclusion of a variation on the pump tone, by using different values of losses, from a) with Δf of 0.1MHz to d) with Δf of 100 MHz.

number. From Eq. (3.33) and Eq. (3.34), the parametric gain goes from exponential form to a quadratic relation. This phenomena can be observed in Fig. 3.12**d**, where two different tones can be observed near the pump frequency. The pump frequency $f_p = 6.9\,\text{GHz}$, and the frequency of the first stop band located at $f_p = 7\,\text{GHz}$.

3.2.3.6 Parametric gain: inclusion of higher harmonics

In this section, the parametric gain, where a third harmonics is included. The evolution of the amplitudes given by Eq. (3.20) and Eq. (3.21) can be observed in Fig. 3.13. A pump signal of 1.5 mA is introduced, which, by using a characteristic impedance of 50 Ω, represents a pump power of -46 dBm. The evolution is illustrated with respect the total length of the amplifier. It can be noticed that up to a length of 1 mm, the first harmonics domain over the third and fifth harmonic. However, from 1 mm the other components have similar amplitude, resulting in an erratic exchange of energies between the signals. This is resulting from the not conservation of amplitude, which is illustrated in Eq. (3.18). The the calculation of the parametric gain using this set of equations is meaningless.

3.2.4 Simulation results of the dispersion engineered line with losses

Losses were added to the model. To exemplify the effects, two values of losses were added.

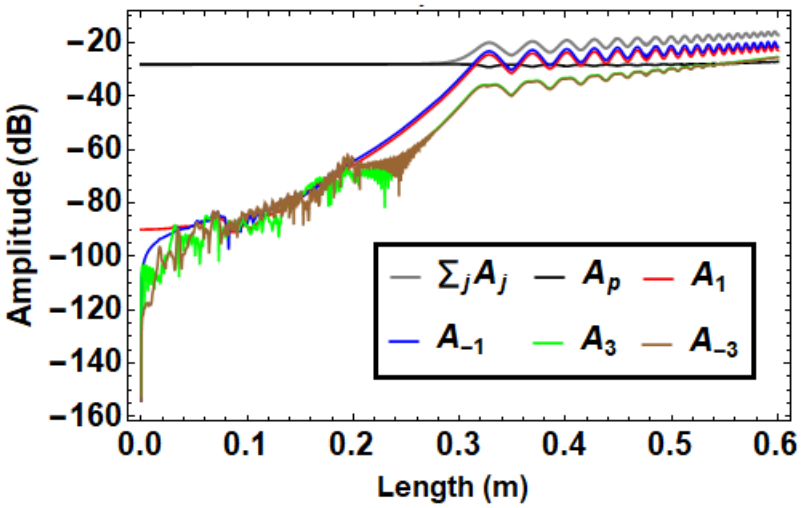

Figure 3.13: Evolution of the harmonics in the amplifier. $P_p = -46$ dBm. $\sum_j A_j$ is the sum of all the amplitudes.

- An attenuation constant of $\alpha = 0.00036$ is used because it was obtained by measuring the S parameters of a resonator using the same material properties [30].
- An attenuation constant of $\alpha = 0.01$ is introduced in the line to represent very high losses.

3.2.4.1 Dispersion relation

In Fig. 3.7**b**, the first stopband located at f_p is shown. It can be noted that an increment of the attenuation constant in the line generates a smoother curve near the stopband and is tending to zero. This behaviour can be explained as a *deterioration* of the propagation constant. The losses create a more dispersion-less transmission line, having a worse blocking of undesirable harmonics at $3f_p$. In addition, it decreases the wave number near the stop bands, resulting in a lower dispersion $\Delta\beta$.

As in the wave number, the deterioration is also presented in the equivalent attenuation constant α_t shown in Fig. 3.14**a**. A linear increment is presented due to the addition the constant loss. Fig. 3.14**b** shows a close up of the first stop-band, showing in detail the deterioration of the dispersion relation. This difference is not significant enough to hinder the performance of the filter. At f_p, the model has an increase of $\alpha_t = 1.8\,\mathrm{m}^{-1}$, which, from Fig. 3.9, gives raise to a decrease of the transmission coefficient S_{12} of -2dB, i.e a 37% of the signal is not transmitted. This behaviour is expected because adding losses to the devices produces an attenuation on the waves inside the line, which results in a dissipation of energy.

3.2.4.2 Bloch impedance

The Bloch impedance Z_B of the entire cell is presented in Fig. 3.8. A change in first stop-band is appreciated at f_p by the addition of losses, which it has the same behaviour observed in Fig. 3.7. However, the changes in deterioration of Z_B are not significant except around the stop-band.

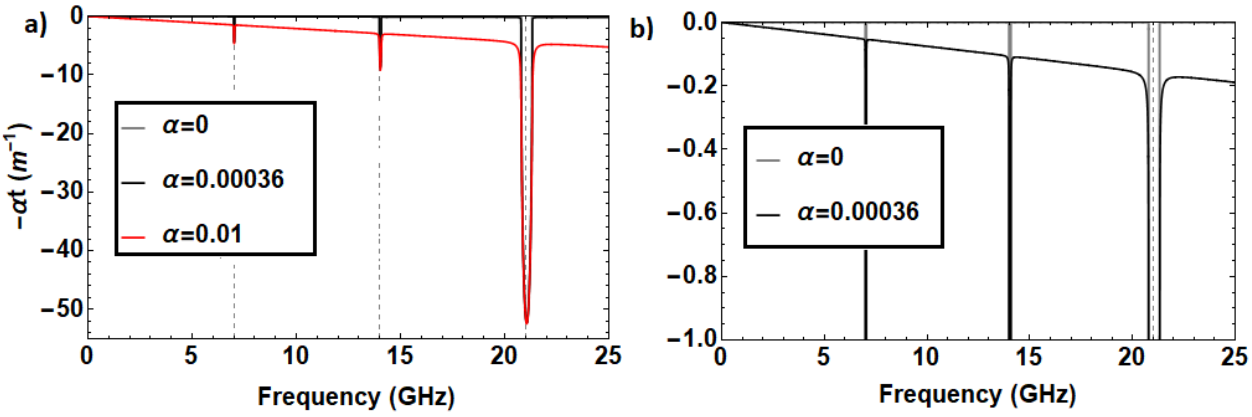

Figure 3.14: Equivalent attenuation constant α_t of the periodic transmission line shown in Fig. 3.4 with different values of losses α, it is assumed that the unloaded and loaded elements have the same amount of losses.

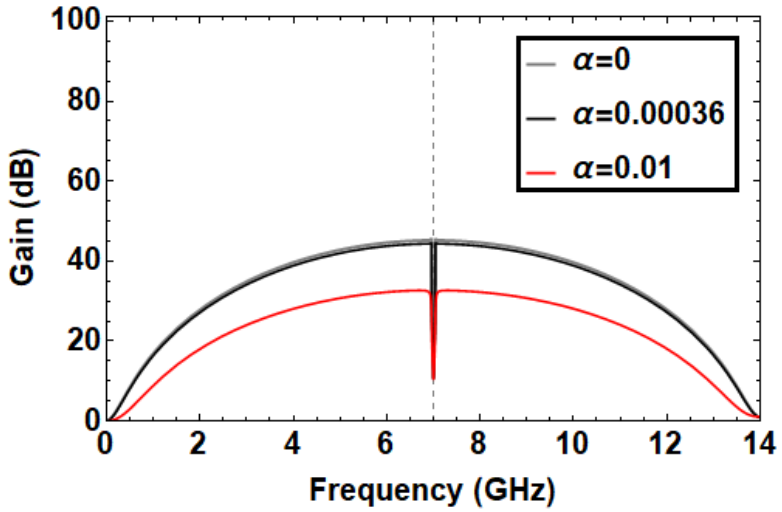

Figure 3.15: Parametric gain of the amplifier, where a pump power of -48 dBm losses and different attenuation constants are used.

3.2.4.3 S parameters: Transmission and reflection coefficient

The transmission coefficient in Fig. 3.9. The addition of $\alpha = 0.00036$ does not produce significant changes. However, the inclusion of high losses deteriorates the transmission considerably. Fig. 3.10 shows the reflection coefficient, which is plotted with different attenuation constants. The reflections tend to increase with in a linear rate with the frequency. It can be observed that an increment of the losses generates more reflections, due to the deterioration of the stop bands. On the other hand, with an increment of the frequency, the model with more losses produces less resonance, creating a thinner band of reflections. This phenomena appears because of the non oscillating behaviour of the $\cos(N\alpha_t \mathrm{d})$ term that exists in Eq. (2.13) as well. Similarly with Fig. 3.7, the close up shown in Fig. 3.10**b** emphasizes that the losses does not have important detrimental effect on the stop bands, which is an important factor to consider when the parametric gain is obtained.

3.2.4.4 Parametric gain: variation of losses

The parametric gain illustrated with a variation of losses can be observed in Fig. 3.15. When the losses increase in the amplifier, a decrease in the parametric gain appears. The decrement is due to the deterioration of the dispersion relation due to the losses. This reduction increases if more power of the pump signal is provided. For instance, in Fig. 3.15**a** which has a pump power of -12dB, the difference between without losses and 0.00036 is 9 dB, while in Fig. 3.15**b** this difference is only of 5 dB. This behaviour is expected, because more energy in the line implies more dissipation from the dielectric.

3.2.4.5 Parametric gain: variation of losses with higher harmonics

Fig. 3.16 shows the parametric gain of the amplifier with the inclusion of the third harmonic and a variation of losses. The peaks above the standard couple mode equations should not be possible because conservation of energy exists in the device. It also presents artificial noise above the parametric gain. As illustrated in Fig. 3.13, the model calculated does not represent correctly the parametric gain model with the inclusion of losses. However, the harmonics are tending to the model with $n = 1$ as the losses are increasing. This is expected, because an increment of the losses means a decrement in the exchange of energy modelled by coupled, which means that SPM and XPM are the predominant components in the parametric gain.

3.3 Conclusions

In this chapter, the design of an engineered dispersion line using the phenomenon four-wave mixing has been described:

(i) The main features of the line were analysed by using its propagation constant and S parameters. By using a pump frequency near 7 GHz, the first two harmonics are propagated while the third one is blocked.

(ii) The difference between the characteristic impedance of the unloaded segments of the DETL and its Bloch impedance generated reflections of -18 dB in the operation bandwidth, which means that the amplifier is generating a good impedance matching with the ports of 50 Ω.

(iii) The parametric gain was illustrated with different pump power and frequencies. These changes were expected from the analytical solution obtained in the chapter.

(iv) Even though the analysis did not have reliable results. It could be used for an improvement in the model.

(v) Every feature explained was described and compared with and without the addition of losses. It was noticed that an increment in the losses deteriorates the stop-band of the

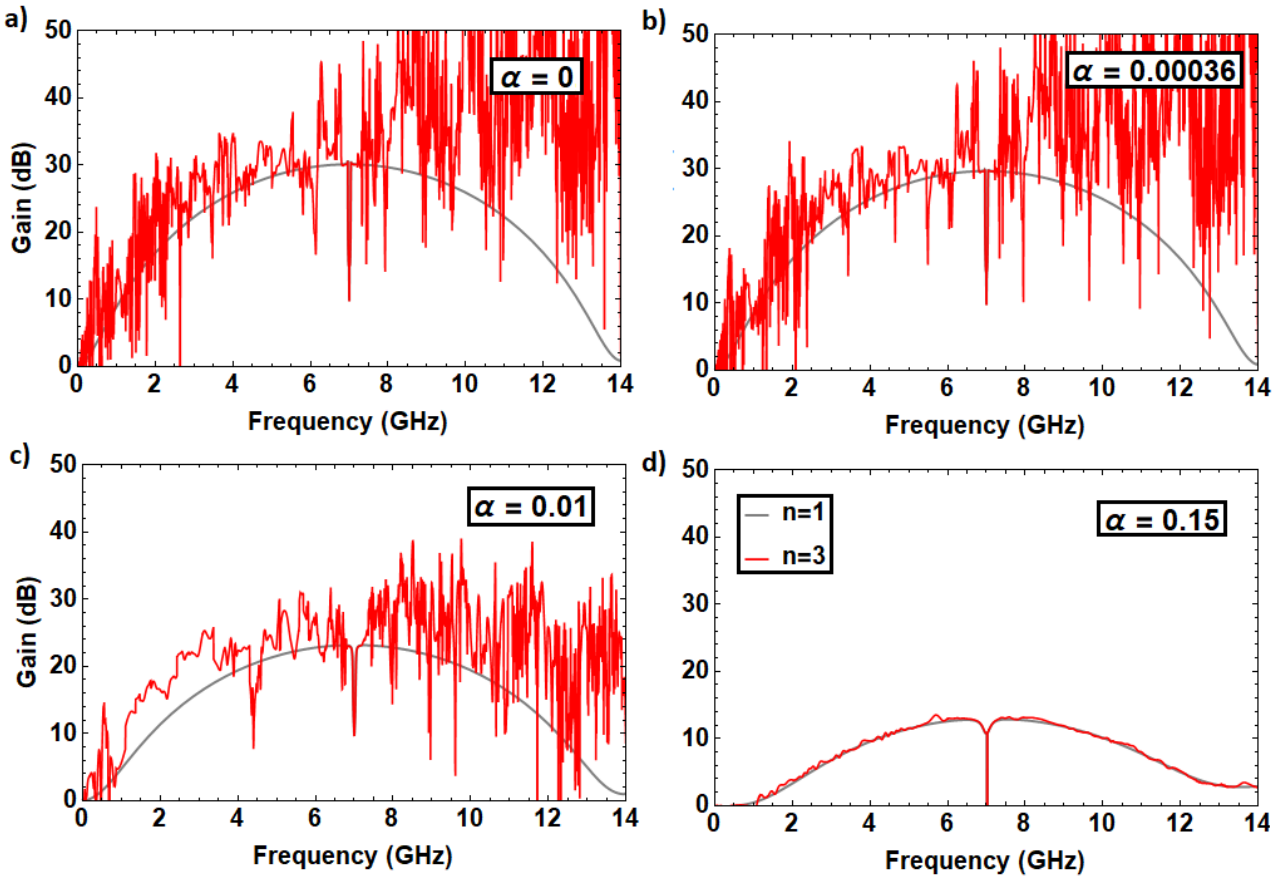

Figure 3.16: Parametric gain with a third harmonic and different values of losses, using an attenuation constant of 0, 0.00036, 0.01 and 0.15 from (a)-(d), respectively.

propagation constant, resulting worse performance of the line, and, therefore, a lower parametric gain.

Chapter 4

Modelling a TKIP amplifier using three-wave mixing

4.1 Introduction

After the development of the first TKIP, possible improvements to the device have been developed. One of the most recent implementations, developed by M. R. Vissers, uses an additional DC bias to feed the amplifier [38]. Instead of FWM, the main contribution to the amplification is the process of three-wave mixing (TWM). Therefore, a different filter is needed to block frequencies above $2f_p$ instead of $3f_p$.

In this chapter, the model involved on the process of amplification using TWM is described extensively. First, the deduction of the coupled mode equations is detailed, where an input current I_{DC} is included in system. Furthermore, an extension to the equations are included to introduce harmonics into the system. Subsequently, a different DETL design is presented, supporting the TWM effect instead, where their main features of the DETL are detailed. Furthermore, the analysis of the parametric gain with higher harmonics, and different values of the pump power and frequency are presented. The previous analysis is simulated with and without the inclusion of losses.

4.2 Three-wave mixing theory

As four-wave mixing, three-wave mixing is a parametric process that uses the non-linearity of a system to transfer of energy between a source to a target signal and their harmonics. The signals involved are the following:

- The *pump* signal of amplitude A_p and frequency f_p, which is used as a source to the signals inside the amplifier.
- The *target* signal of amplitude A_s and f_s, which is signal that is needed to be amplified.
- The *idle* signal of amplitude A_i and frequency f_i, which represents the undesirable

harmonic signal that is not blocked by the filter. It is assumed that the rest are blocked by the engineered dispersion line.

The difference with FWM is the addition of a DC bias. If a direct current I_{DC} is introduced in the amplifier, the kinetic inductance has a quadratic and linear dependence with pump current I_{RF}. By adjusting the DC bias such that $I_{DC} > I_{RF}/2$, a stronger linear relation with the mixing of the waves exists inside the device. The quadratic term that has the components of three-wave mixing dominates over the cubic term related with FWM. By assuming conservation of momentum and energy, the relation between the propagation constant and frequencies are given by

$$f_s + f_\mathrm{i} = f_p, \tag{4.1}$$
$$k_s + k_\mathrm{i} = k_p, \tag{4.2}$$

where instead of using two pump signals, only one is used. As a consequence, the filter must stop frequency bands above $2f_p$ and not $3f_p$, and the design needs to change in order to suffice this condition.

4.2.1 Deduction of gain equations using Three Wave Mixing (TWM): introducing a DC bias

Because of the additional DC current bias, a total current $I = I_{RF}(z,t) + I_{DC}$ is used. Due to the constant dependence of I_{DC}, the only meaningful change in Eq. (3.4) is the kinetic inductance given by

$$L_k(I) = L_{K0}\left[1 + \frac{I_{DC}^2}{I_*^2} + 2\left(\frac{I_{DC}I_{RF}}{I_*^2}\right) + \frac{I_{RF}^2}{I_*^2}\right]. \tag{4.3}$$

Therefore, by using the components of I^2 given by Appendix C, Eq. (3.11), (3.12) and (3.13) can be rewritten as

$$\frac{\mathrm{d}A_p}{\mathrm{d}z} = \frac{\mathrm{i}k_p}{{I'_*}^2}\left[\left(\frac{4}{3}A_{DC}^2 + |A_p|^2 + 2|A_s|^2 + 2|A_\mathrm{i}|^2\right)A_p + \frac{8}{3}A_{DC}A_\mathrm{i}A_s\mathrm{e}^{\mathrm{i}\Delta\gamma z}\right], \tag{4.4}$$
$$\frac{\mathrm{d}A_s}{\mathrm{d}z} = \frac{\mathrm{i}k_s}{{I'_*}^2}\left[\left(\frac{4}{3}A_{DC}^2 + |A_s|^2 + 2|A_\mathrm{i}|^2 + 2|A_p|^2\right)A_s + \frac{8}{3}A_{DC}A_pA_\mathrm{i}^*\mathrm{e}^{-\mathrm{i}\Delta\gamma z}\right], \tag{4.5}$$
$$\frac{\mathrm{d}A_\mathrm{i}}{\mathrm{d}z} = \frac{\mathrm{i}k_\mathrm{i}}{{I'_*}^2}\left[\left(\frac{4}{3}A_{DC}^2 + |A_\mathrm{i}|^2 + 2|A_s|^2 + 2|A_p|^2\right)A_\mathrm{i} + \frac{8}{3}A_{DC}A_pA_s^*\mathrm{e}^{-\mathrm{i}\Delta\gamma z}\right], \tag{4.6}$$

where A_{DC} is the amplitude of the DC current, I'_* is the non linear parameter, and $\Delta\beta_{DC} = k_\mathrm{i} + k_s - k_p$ is the dispersion generated using three-wave mixing.

4.2.2 Gain equations corrections deduction (TWM): introducing harmonics

As in chapter 3, to understand how the parametric gain is affected with the inclusion of higher harmonics, the coupled mode equations are generalized by introducing n harmonics into the system.

The total current of the non-linear amplifier can be written as

$$I = \frac{1}{2}\left(\sum_{m=-n}^{n} A_m(z)\exp\left(\mathrm{i}(w_m t - k_m t)\right) + c.c\right), \tag{4.7}$$

where $w_m = mw_p + w_s - w_p$ and $k_m = k(w_m)$. By using the analysis explained in section 3.2.1, a variation of the coupled mode equations with harmonics are given by

$$\frac{\mathrm{d}A_p}{\mathrm{d}z} = \frac{\mathrm{i}k_p}{I_*'^2}\left[\left(\frac{4}{3}A_{DC}^2 + |A_p|^2 + 2\sum_{m=-n}^{n}|A_m|^2\right)A_p + \frac{8}{3}A_{DC}\sum_{m=-n}^{n}A_m A_{m-2}\mathrm{e}^{\mathrm{i}\Delta\beta_m z}\right], \tag{4.8}$$

$$\begin{aligned}\frac{\mathrm{d}A_j}{\mathrm{d}z} = \frac{\mathrm{i}k_j}{I_*'^2}\Bigg[&\left(\frac{4}{3}A_{DC}^2 + 2|A_p|^2 - |A_j|^2 + 2\sum_{m=-n}^{n}|A_m|^2\right)A_j + \\ &\frac{8}{3}A_{DC}A_{j-2}^* A_p \mathrm{e}^{-\mathrm{i}\Delta\beta_j z} + \frac{8}{3}A_{DC}A_{j+2}^* A_p \mathrm{e}^{-\mathrm{i}\Delta\beta_{j+2} z}\Bigg],\end{aligned} \tag{4.9}$$

with $\Delta\beta_m = \beta_m + \beta_{m-1} - \beta_p$. All the harmonics higher than n are not considered in the derivation. Because the equations are restricted to the conservation of energy of the photons inside the device (see Eq. (4.1)), m needs to be an integer.

4.2.3 Solution of the gain equations: introducing a DC bias

We begin by solving the equations in a particular case. In addition to the assumptions mentioned in section 3.2.1., it is assumed that the DC current is much bigger than the target and idle signals ($A_{DC}, A_p \gg A_s, A_\mathrm{i}$). Therefore, the extraction of power from the DC signal is neglected. By using Eq. (3.22), the phase shift of the pump signal $\Delta\theta_{DC}$ is given by the following expression

$$\Delta\theta_{DC} = \frac{k_p}{I_c^{*2}}\left[\frac{4}{3}A_{DC}^2 + A_p^2(0)\right], \tag{4.10}$$

where $\Delta\theta_{DC}$ is the shift phase of the pump tone. By introducing Eq. (4.10) in Eq. (4.5) and (4.6), and using the assumptions provided in section 3.2.1, we have that A_s and A_i can be obtained as

$$\frac{\mathrm{d}A_s}{\mathrm{d}z} = \mathrm{i}\gamma\left[\left(\frac{4}{3}P_{DC} + 2P_p\right)A_s + \frac{8}{3}\sqrt{P_{DC}P_p}A_\mathrm{i}^* \mathrm{e}^{-\mathrm{i}(\Delta\beta_{DC} - \Delta\theta_{DC})z}\right], \tag{4.11}$$

$$\frac{\mathrm{d}A_\mathrm{i}}{\mathrm{d}z} = \mathrm{i}\gamma\left[\left(\frac{4}{3}P_{DC} + 2P_p\right)A_\mathrm{i} + \frac{8}{3}\sqrt{P_{DC}P_p}A_s^* \mathrm{e}^{-\mathrm{i}(\Delta\beta_{DC} - \Delta\theta_{DC})z}\right], \tag{4.12}$$

which is a system of non-homogeneous linear equations with non-linear coefficients. The constant P_p is defined as the power of the DC current. In order to simplify them, we define an auxiliary variable B_j as

$$B_j = A_j \exp\left[-\mathrm{i}\gamma\left(\frac{4}{3}P_{DC} + 2P_p\right)z\right] \tag{4.13}$$

to be introduced in Eq. (4.11) and (4.12). In addition, by taking conjugated part B_i^*, it is found that the previous system of coupled equations can be written as

$$\frac{\mathrm{d}B_s}{\mathrm{d}z} = \frac{8\mathrm{i}\gamma}{3}P_p B_\mathrm{i}^* \mathrm{e}^{-\mathrm{i}\kappa z}, \tag{4.14}$$

$$\frac{\mathrm{d}B_\mathrm{i}^*}{\mathrm{d}z} = -\frac{8\mathrm{i}\gamma}{3}P_p B_s \mathrm{e}^{\mathrm{i}\kappa z}, \tag{4.15}$$

where the linear phase mismatch κ can written as

$$\kappa = \Delta\beta + \gamma\left[\frac{4}{3}P_{DC} + 3P_p\right]. \tag{4.16}$$

The details about the complete solution can be found in Appendix D. The gain of the target signal G_s in the amplifier with a transmission line of length L is given by

$$G_s = \cosh^2(gL) + \left(\frac{\kappa}{2g}\right)^2 \sinh^2(gL). \tag{4.17}$$

From Eq. (4.17), two conditions are considered. First, if there is not dispersion, $\Delta\gamma = 0$ and $g \approx 0$, then $\kappa \approx 16k_p |A_p| A_{DC}/3I_*'^2$. Therefore, the gain can be written as

$$G_s = 1 + \left(\frac{\kappa L}{2}\right)^2 = 1 + \left(\frac{8k_p |A_p| A_{DC} L}{3I_*'^2}\right)^2 = 1 + (\Delta\theta L)^2. \tag{4.18}$$

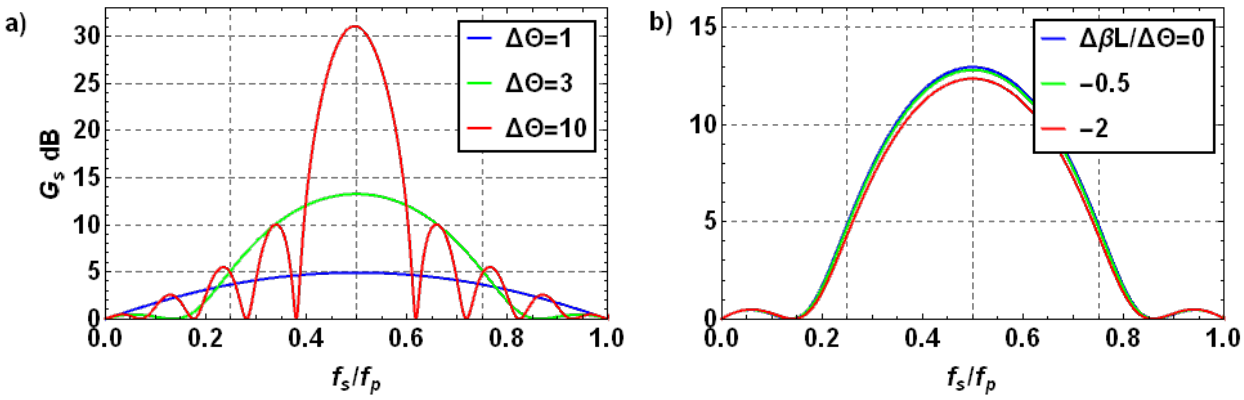

Figure 4.1: Parametric gain obtained from the coupled mode equations. A current $I_{DC} = 0.375I'_*$ was used, with $P_p = -48$ dBm. a) No dispersion ($\Delta\beta = 0$) and using different values of $\Delta\theta_{DC}$. b) Figure of the parametric gain with different constant values of dispersion, and a phase shift of the pump tone of 3 rads.

Second, if $\Delta\beta_{DC} = -2\Delta\theta_{DC} = -2\gamma P_p$, then $\kappa = 0$ and $g_{DC} = 8k_p |A_p| A_{DC}/3I'^2_*$. Thus, the parametric gain can be expressed as

$$G_s = \cosh^2(gL) \approx \frac{1}{4}\exp(2\Delta\theta L), \tag{4.19}$$

which has the same exponential behaviour than the solution obtained by the transmission line designed by using four-wave mixing effect.

The parametric gain obtained by the coupled mode equations is shown in Fig. 4.1. The parametric gain has a limit up to f_p. This limit can be explained by behaviour of the idle signal, which is governed by conservation of energy and described by Eq. (4.1). To have a similar operation bandwidth when compared with the design that used the FWM effect, a pump frequency $f_{pTWM} = 2f_{pFWM}$ is used. The DC bias used is the 37% the effective critical current obtained from the previous design. A higher gain is observed with respect Fig. 3.3, due to the high DC bias that is introduced in the coupled mode equations. In addition, as it is shown in Fig 3.3**b**, the changes in the dispersion $\Delta\beta$ are minor when compared with the design that uses FWM.

4.3 Design of a periodic filter suitable for TWM

When a direct current in the transmission line is introduced, the components that dominate the gain of the amplifier are related with the non linear effect of three wave mixing. Therefore, the cell needs to meet the following requirements:

1. The filter must block frequencies at $2nf_p$, $n \in \mathbb{Z}^+$ to hamper the transfer of energy of signals of those frequencies.

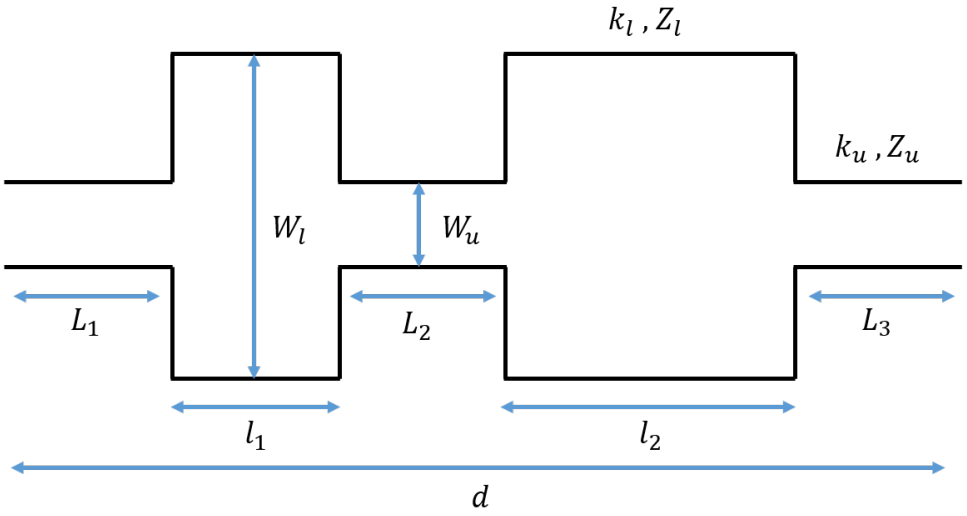

Figure 4.2: A filter design using transmission lines, where it features are represented with the sub-index u from ***u**nloaded line*, and the elements with the sub-index l from ***l**oaded line*. This filter with the appropriate dimensions, generates a wider stop bands for frequencies above f_p, useful when is necessary conservation of energy in three wave mixing.

Table 4.1: Dependant dimensions of the filter when using a microtrip transmission line.

D_{i}	l_2	L_1	L_2	L_3	W_l
d/2	bl_1	$(D_{\mathrm{i}} - l_1)/2$	$D_{\mathrm{i}} - (l_1 + l_2)/2$	$(D_{\mathrm{i}} - l_2)/2$	aW_u

2. Minimize the width of the first stop band to increase the bandwidth of the amplifier.

3. Maximize the parametric gain.

4. A characteristic impedance of the unloaded line $Z_u \approx 50\,\Omega$ is needed, which is equal to the impedance of the external ports.

4.3.1 Design and characterization of a TWM infinite filter

In order to meet the previous requirements, a modification on the design was done, which is illustrated in Fig. 4.2. The cell is divided in five transmission lines, *unloaded* and *loaded* elements. The unloaded elements have lengths L_1, L_2 , L_3, width W_u, propagation constant k_u and characteristic impedance Z_u. The loaded elements have dimensions l_1 and l_2, width W_l, propagation constant k_l and characteristic impedance Z_l. The ratio between l_1 and l_2 is b, and a the ratio between the unloaded line and the perturbations. The resulting free parameters are d, l_1, W_l, a and b, where the dependent parameters are obtained when using Table 4.1. The presented design generates stop bands at $(1+2(n-1))f_p$, with $n \in \mathbb{Z}^+$. They are maximized, as a result of maximizing the stop band at $2f_p$, achieving a larger parametric gain.

Table 4.2: Free parameters used to design a filter for three wave mixing.

d	l_1	W_u	a	b
µm	µm	µm	–	–
1151	20	1.49	1.2	2

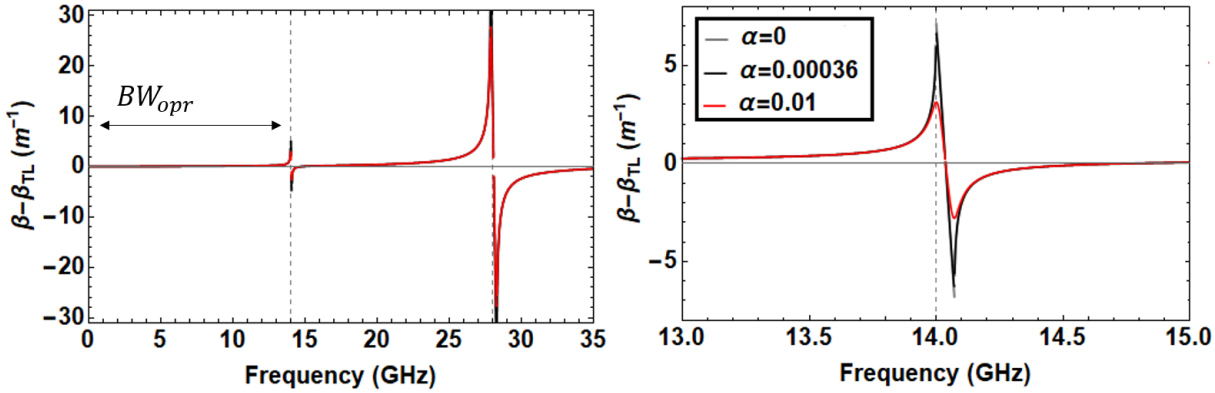

Figure 4.3: Dispersion relation of the periodic transmission line with losses shown in Fig. 4.2, with $\Delta\beta = \beta - \beta_{TL}$, where β is the propagation constant of the transmission line, while $\beta_{TL} = k_u$ is of an unloaded pattern. The first stop band is located near the pump frequency f_p at 14 GHz. An important stop-band is produced a $2f_p$ to improve the amplification for TWM.

4.3.2 Methodology

Given the requirements stated in section 3.2.1, the methodology applied to the DETL supporting the TWM effect is the following:

1. By using Eq. (2.15), the ABCD matrix of the cell is calculated by obtaining its characteristic impedance Z_j, propagation constant k_j and length l_j of each section of the cell. They can be obtained as follows:

   - The characteristic impedance $Z_{u,l}$ and normalized propagation constant $k_{u,l}$ are obtained from Table 3.4.

   - By using the design illustrated by Fig. 4.2, the free parameters are tuned, while the dependent parameters are obtained by using Table 4.1.

2. From the previous matrix, the propagation constant, Bloch impedance and S parameters are analysed.

3. The parametric gain is given by Eq. (4.4), (4.5) and (4.6), with the I_{DC} bias defined as a fraction of the critical current I_c^*. The ratio is obtained heuristically to compare the parametric gain when using the FWM effect.

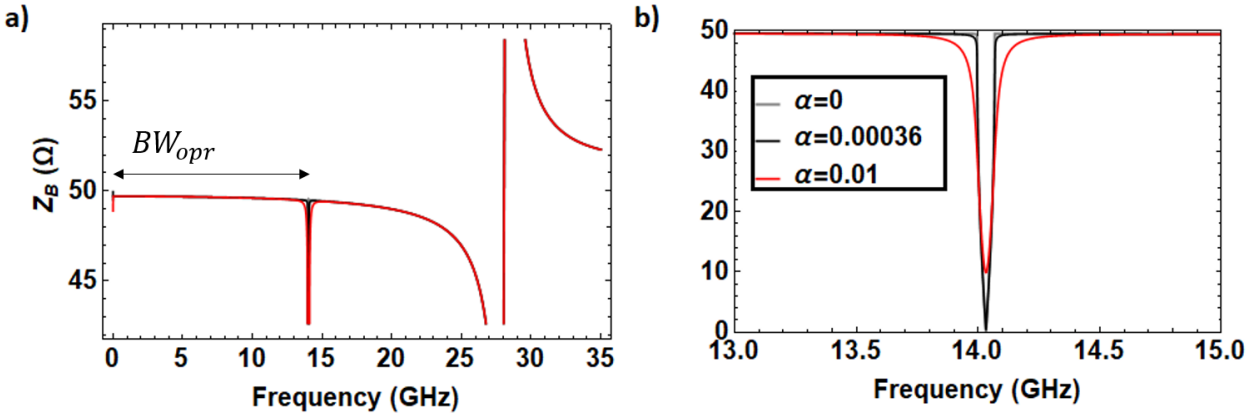

Figure 4.4: The Bloch impedance of the engineered transmission line shown in Fig. 4.2, obtained by using different attenuation constants. BW_{opr} is the operation bandwidth of the amplifier. a) The Bloch impedance in the operation frequency of the amplifier. b) The Bloch impedance in the range of the pump frequency f_p.

4.3.3 Simulation results TWM engineered transmission line without losses

In this section, we present the simulation results of the superconducting microstrip DETL that was designed to support the TWM. The free parameters are illustrated in Table 4.2. To facilitate the comparison with FWM, the characteristic impedances, and propagation constants have the same values of the design when supporting FWM. They can be observed in Table 3.4.

4.3.3.1 Dispersion relation

The equivalent propagation constant of the cell is shown in Fig. 4.3. It is illustrated without the linear component. The dotted gray lines represent the location of the stop bands. BW_{opr} indicates the frequency range of the amplifier. The stop bands can be shown in detail in panels **b** and **c**. The frequency width of the first stop band located at $f_{pTWM} = 14\,\text{GHz}$ is $\Delta f \approx 50\,\text{MHz}$, and the width of the second, located at $2f_{pTWM}$, is $\Delta f \approx 500\,\text{MHz}$. By taking into account the conservation of momentum and energy imposed on the deduction of the coupled mode equations. The idle signal is limited up to f_{pTWM} (see Eq. (4.1)). As a result, frequencies above f_{pTWM} are not important in the amplification for TWM.

4.3.3.2 Bloch impedance

The Bloch impedance is shown in Fig.4.4**a**. At frequencies below f_{pTWM}, the Bloch impedance is $Z_B = 49.68\ \Omega$, which is near from the desirable $50\,\Omega$. When compared with the design that supports FWM, the impedance is steadier in the operation bandwidth BW_{opr}, which is a desirable characteristic in the range of operation . Near f_{pTWM}, where the first harmonic is located, the impedance drops abruptly to zero. A zoom of the first stop band is presented in Fig. 4.4**b**, which it has a stop band of 20 MHz. The stop band is thinner when compared with Fig. 3.8, which can result in a better transmission when compared with the FWM

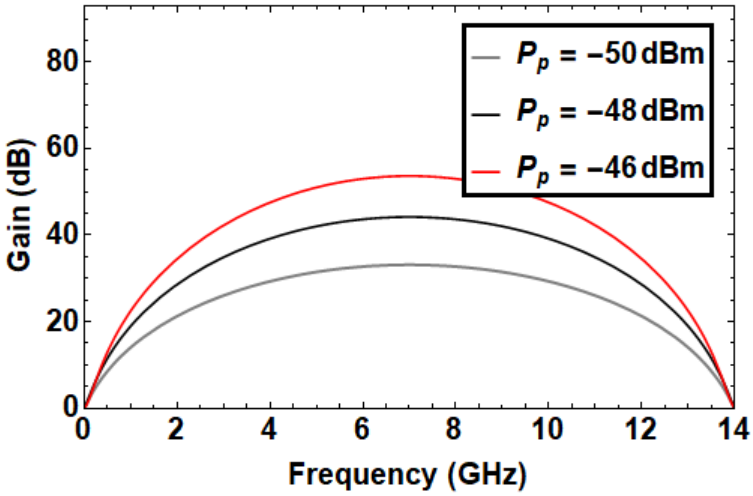

Figure 4.5: Parametric gain of the infinite transmission line of a periodic pattern shown in Fig. 4.2 with different values of the pump power P_p and with a number of periodic filters (cells) in cascade of 100. A DC bias of 13% of the effective critical current is used.

transmission line.

4.3.3.3 Parametric gain: variation of pump power

The parametric gain of the TWM DETL is shown in Fig. 4.5. The same critical current $I'_* = 13.26\,\text{mA}$ was used in FWM, because the line was design using the same material. As the design that supports FWM, the TWM DETL uses 100 periodic patterns placed in cascade. In addition, pump-signal powers of $P_{Ap} = -50$, -48 and -46 dBm were used. The DC current was used as $I_{DC} = 12\%\ I'_c$, chosen heuristically within the range permitted to make an acceptable comparison between the gain using FWM and TWM. The difference of parametric gain between the pump-powers is ≈ 10 dB. The parametric gain observed in 3.11 has an abrupt decrement in f_{pFWM}. However, in the design to support TWM, this decrement does not appear in Fig. 4.5, because the first stop-band falls outside of the operation bandwidth.

4.3.3.4 Parametric gain: variation of pump frequency

As in chapter 3, an analysis of frequency sensibility is needed to understand the frequency fluctuations in the parametric gain. These variations can be observed in terms of $\Delta f = f_{\text{pe}} - f_{pr}$, where f_{pe} is the pump frequency that the line was designed, while f_{pr} is the pump frequency applied in the device. In Fig. 4.6, the parametric gain is observed with different changes of Δf. It is observed that if there is an increment of Δf, there is a decrement in the parametric gain. Nonetheless, the effect of Δf does not generate significant changes on the parametric gain. For instance, in Fig. 4.6 $\Delta f = 1\,\text{MHz}$, there is a decrement of 1 dB, while with $\Delta f = 10\,\text{MHz}$, the difference is of 3 dB. In comparison with the DETL FWM, the difference between different values of Δf does not affect significantly the parametric gain.

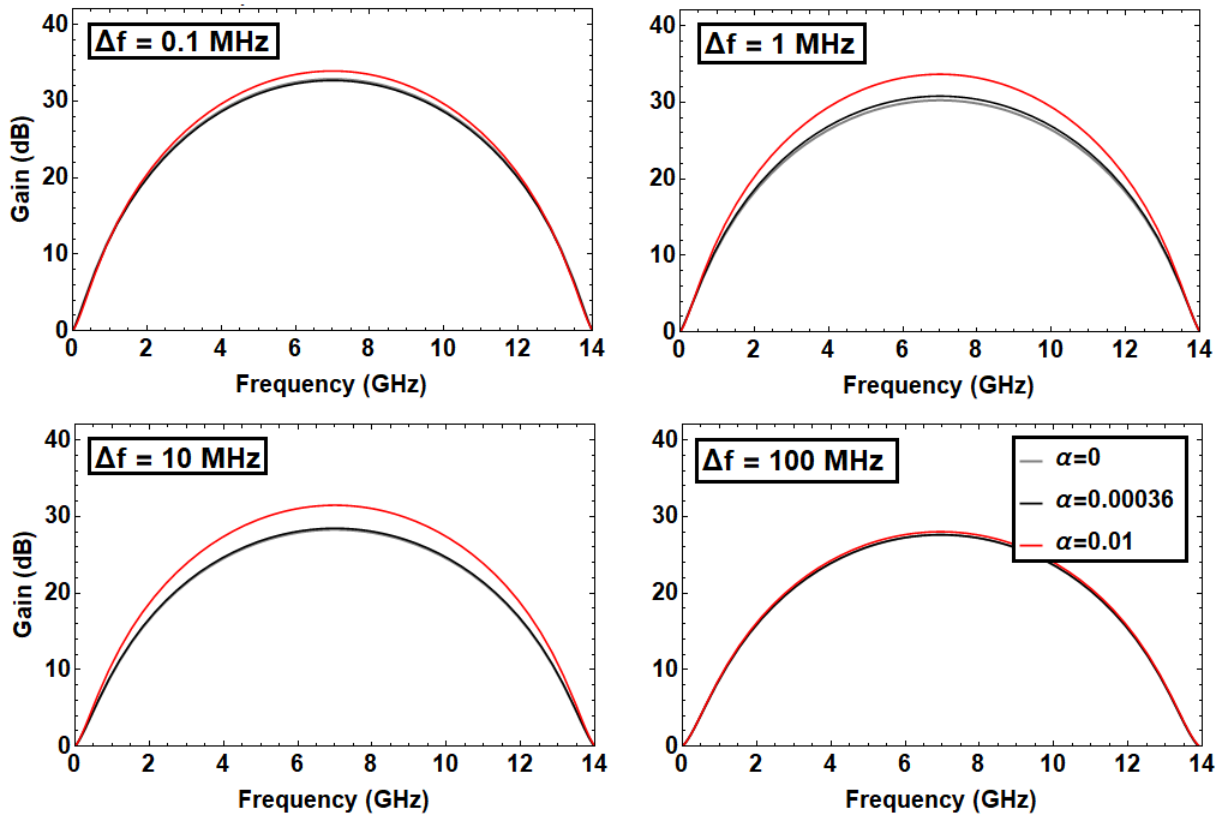

Figure 4.6: An illustration of a frequency variation on the parametric gain with TWM. Different values of losses, from a) with Δf of 0.1 MHz to d) with Δf of 100 MHz are used.

4.3.3.5 Parametric gain: addition of higher harmonics

In this design, the analysis of harmonics is also included. The first and third harmonic are illustrated. The change on the amplitudes are shown in Fig. 4.7, where in this case, the coupled mode equations were extended to a third harmonic. We define A_1 as the target signal, and A_{-1} as the idle signal. For TWM even harmonics are presented in the device such as A_2 and A_{-2}, the side bands A_3 and A_{-3} of the harmonic $3f_p$ are presented to have comparable results with section 3.2.3.6. At 0.01 m, the evolution of the amplitudes goes according to the standard equations given by Eq. (4.4), (4.5) and (4.6). In addition, with a lower amplitude, the side bands A_3 and A_{-3} grow with a similar amplitude, generating an exchange of energy between these frequencies. Once those signals reach the idle and target signals, they exchange energy between them randomly, having a noise behaviour as a result.

4.3.4 Simulation results of the engineered dispersion line with losses

4.3.4.1 Dispersion relation

In Fig. 4.3, the dispersion relation has been plotted with different attenuation constants. When the line with $\alpha = 0.000\,36$ is compared with the lossless TL, there is a decrement in the

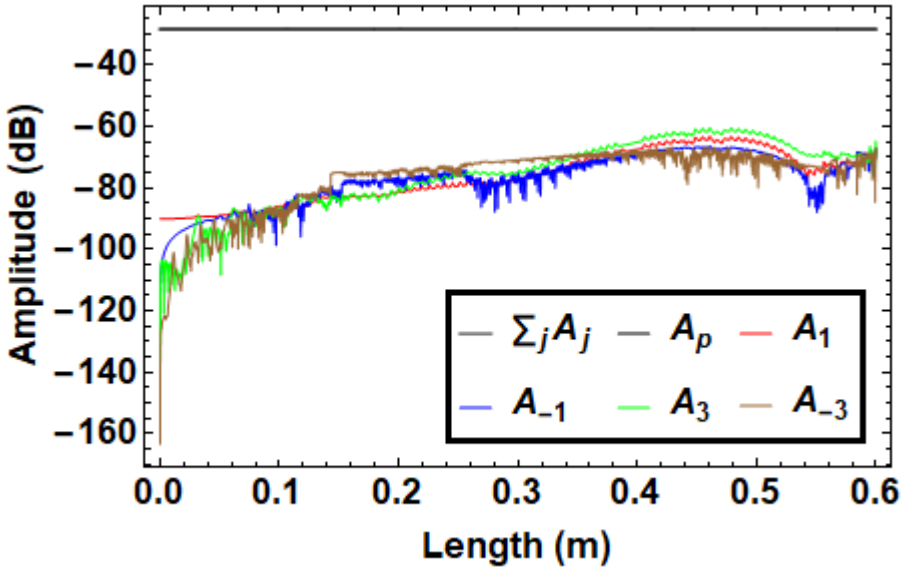

Figure 4.7: Evolution of the harmonics in the amplifier. $P_p = -46$ dBm, where $\sum_j A_j$ is the sum of all the amplitudes. Because the exchange of amplitude between the pump signal and the harmonics is very small. It results that the amplitude of the pump and all the signals have similar power. Therefore, these components are shown in the same place in the figure.

propagation constant. This behaviour is traduced as a *deterioration* of the dispersion relation. The increment of losses deteriorates the dispersion relation, and therefore, the attenuation of undesirable frequencies is decrementing. The difference between the line without losses and the line with an attenuation constant $\alpha = 0.01$ is of 43%, degrading considerably the results of the DETL. This amount of deterioration should not be acceptable when the DETL is designed, due to possible a detrimental performance on the device.

The losses in the transmission line are also observed in the equivalent attenuation constant α_t, which is presented in Fig. 4.8. The attenuation constant is shown between 0 and 30 GHz, which is slightly higher frequency than $2f_p$ in order to understand how the stop bands are generated in the strip. There is an abrupt increment located at the harmonics of the pump signal, where the stop bands are located. A close up of the first stop band is shown in Fig. 4.8**b**. A constant increment is produced while there is an increment in the attenuation constant α for each of the sub-lines that is composed the filter. It is noticeable that the introduction of losses increments in a linear rate the equivalent attenuation constant, but it deteriorates the relation dispersion. With the increase of α, the line start behaving as a line with no dispersion.

4.3.4.2 Bloch impedance

An illustration of the bloch impedance of the DETL with the addition of different attenuation constants is shown in Fig. 4.4. The deterioration caused by losses cause a difference of 0.1 Ω with the lossless TL. This difference cause an increment of 1 dB in the reflection constant. The stop band located at f_p presents a variation of 10 Ω.

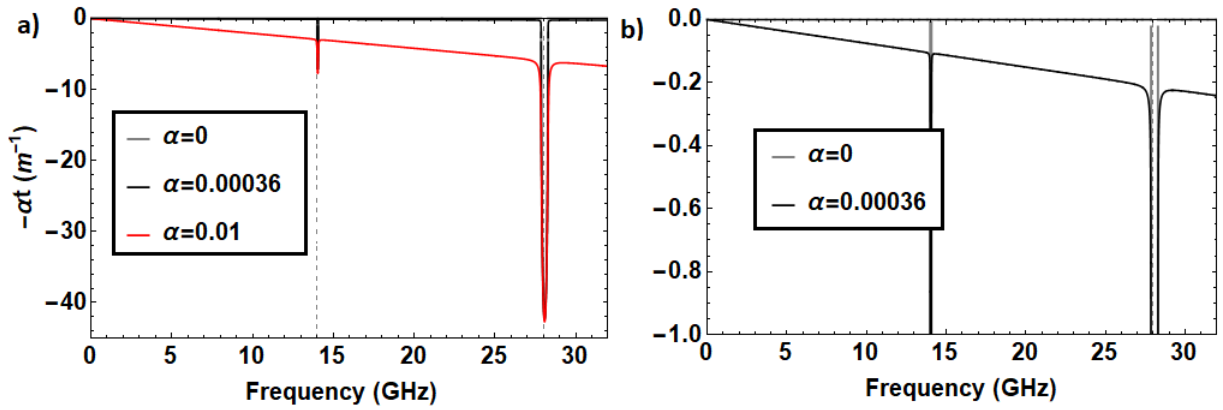

Figure 4.8: Equivalent attenuation constant α_t of the periodic transmission line shown in Figure 4.2 with different values of losses α. The negative sign of the attenuation constant is used to compare the results with the S parameters. It is assumed that as the unloaded elements as the loaded elements have the same amount of losses. An important stopband is produced at $2f_p$ to improve the amplification for TWM.

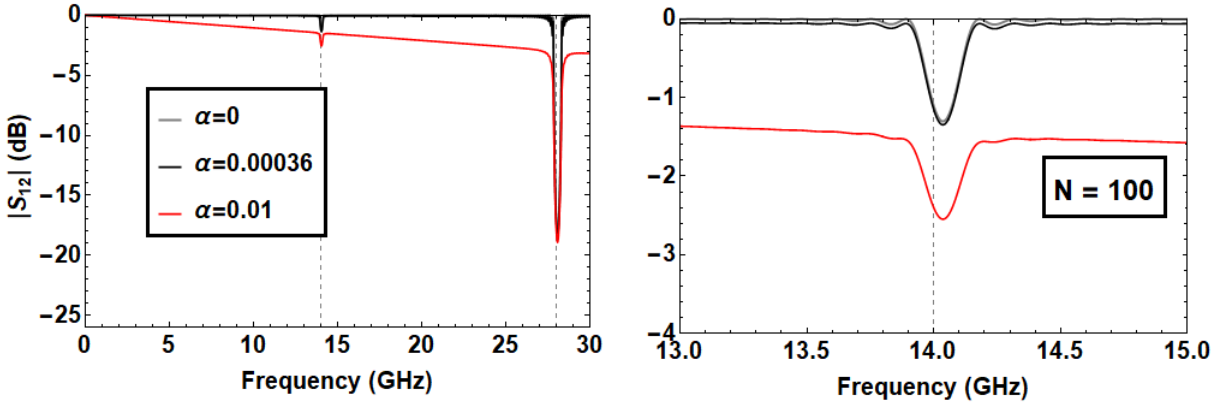

Figure 4.9: Transmission coefficient of the periodic transmission line shown in Fig. 4.2 without losses and with different number of cells in cascade. An important stop-band is produced at $2f_p$ to improve the amplification using TWM.

4.3.4.3 S parameters: Transmission and reflection coefficient

In Fig. 4.9, the transmission coefficient is plotted for different values of the attenuation constant α. Fig. 4.9 illustrates the same behaviour than in Fig. 4.8, where S_{12} drops with a similar rate. Furthermore, an important degradation is obtained from the DETL with $\alpha = 0.01$ when compared with the lossless DETL. From section 4.3.4.2, this is expected from the difference of $10\,\Omega$ obtained in the bloch impedance.

With a similar analysis, the reflection coefficient presented in Fig. 4.10 with the same values of α. The ripples of 10 dB amplitude are obtained because of the number of cells $N = 100$ included in the amplifier, where, by obtaining that are far from the 0 dB, they are increment their amplitude. Once the frequencies reach a stop band, the amplitude of the oscillations begin to decrease. With a difference of $10\,\Omega$ obtained with an $\alpha = 0.01$, the reflections were incremented in 0.75 dB, which does not generated significant differences of the parametric

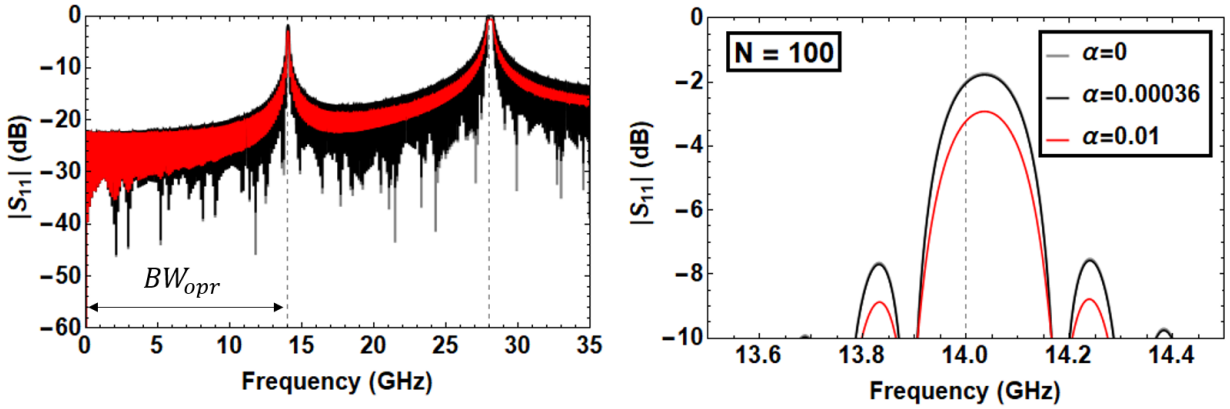

Figure 4.10: Reflection coefficient of the periodic transmission line shown in Fig.4.2 without losses and with different number of cells in cascade. An important stop-band is generated at $2f_p$ to improve the amplification for TWM.

gain.

4.3.4.4 Parametric gain: variation with losses

The slight differences of the gain can be observed in Fig. 4.11. When the attenuation constant increases, there is a loss in the parametric gain due to the deterioration of the dispersion relation. In addition, this reduction is bigger if there is more power provided by the pump signal. However, the change reduction in the gain is considerably higher in FWM, due to the considerably higher amplitude A_{DC} when compared with A_s and A_{i} in SPM and XPM.

There is an unexpected increment of gain with the addition of losses. In particular, a variation of 4 dB is obtained when compared the line with $\alpha = 0.01$ and the lossless DETL. Is this behaviour possible? The answer is **no**. However, this is discussion has not been solved yet.

4.3.4.5 Parametric gain: variation of pump frequency

In Fig. 4.6, the parametric gain with different losses and changes in the pump frequency f_p inside the strip is presented. With the introduction of losses and $\Delta f = 0.1\,\mathrm{MHz}$, differences of 4 dB are obtained. However, when Δf increases, this difference decreases. This effect is obtained due to moving the pump frequency outside of the non-linear regimen produced by the attenuation constant at the stop bands, which results in smaller variations of the parametric gain.

4.3.4.6 Parametric gain: variation with losses and higher harmonics

In Figure 4.12 is presented the analysis of the parametric gain including harmonics using Eq. (4.8) and (4.9). It also shows the results provided by the standard coupled mode equations ($n = 1$) and the equations but including a third harmonic. Every plot has its own value of attenuation constant. However, this time the combination of harmonics is different. Even

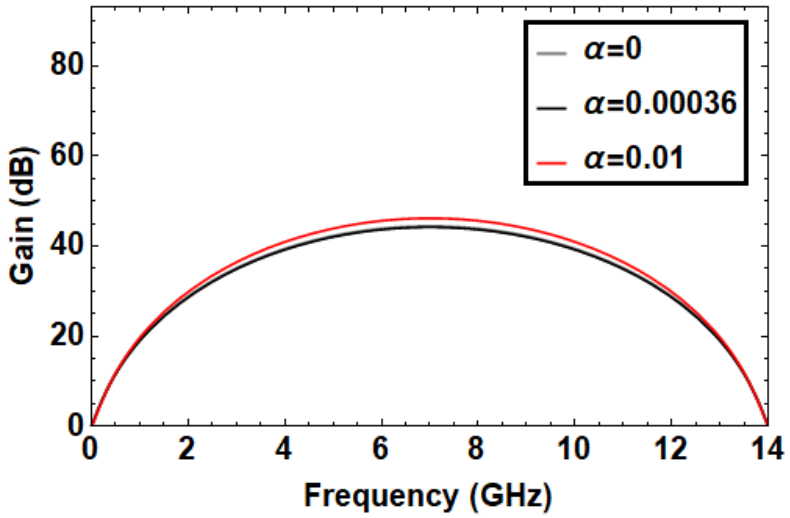

Figure 4.11: Parametric gain of the DETL supporting TWM with different values attenuation constant. The number of periodic cells in cascade is 100. A DC bias of 13% of the effective critical current is used.

though in both chapters the equation for the harmonics is the same, in FWM he domain of m is only the odd numbers, while in TWM is in the natural numbers.

Furthermore, in Fig. 4.12**a**, the peaks above the standard couple mode equations should not be possible because while more harmonics are presented in the system, more energy is transferring to them. However, in this case and in all the figures, peaks above the gain exists.

4.4 Conclusions

In this chapter, it has been explained and discussed the design of an engineered dispersion line using the three-wave mixing effect.

(i) It was compared the dispersion relation, transmission coefficient, characteristic impedance, equivalent attenuation constant and parametric gain with and without losses.

(ii) It was demonstrated that the parametric gain did not present changes as significant as in FWM by adding losses.

(iii) The slight increment of a DC current increases considerably the parametric gain. Because the increment of a continuum signal is cheaper than an alternating current, the line that uses TWM is considered as the best to manufacture the ideal amplifier.

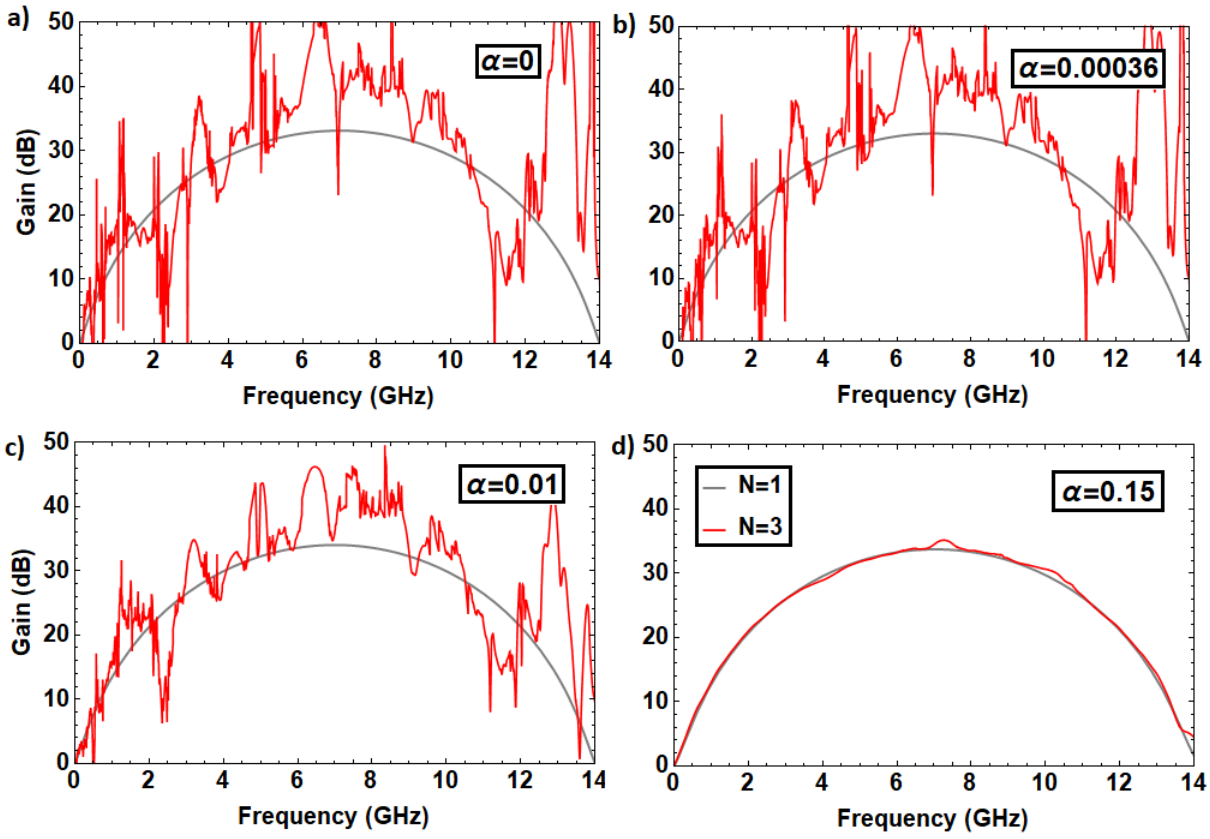

Figure 4.12: The parametric gain of the infinite transmission line with a periodic pattern shown in Fig. 4.2 with the inclusion of multiple harmonics and different attenuation constants.

Chapter 5

Conclusions and future work

This work was focused on the design of *superconducting parametric amplifiers*, which have demonstrated to have the potential to minimize the system noise of heterodyne receivers. The reduction of the system noise is obtained by using non-dissipative properties of the superconductor. The material, below the critical current, also has a non-linear inductance, which is essential to generate the amplification through one of the non-linear processes (FWM or TWM). Since these processes involve the generation of undesirable harmonics, a dispersion-engineered transmission line (DETL) was designed to concentrate the power of the reference input power to the target signal rather than the harmonics. Two designs of DETLs were presented, one design supporting the FWM effect, and the other one the TWM. The theoretical background to support these design was also presented. This results consisted on obtaining the S parameters, the Bloch impedance and the parametric gain, where an addition of losses was made to have more realistic results.

5.1 Conclusions

5.1.1 Introduction of losses in the designs

In a microstrip line, certain amount of losses are expected to be inserted due to dielectric loss. Therefore, these losses were introduced in our model to understand how they affect the characteristic of the line. This effect is represented by a normalized attenuation constant α, which is also used in each segment of the superconducting line. The features of the line were analysed without losses, with an expected value α_{e}, and with a large α_l to clearly observe the effect in the line. The losses are obtained experimentally by a resonator using the same properties, which do not present a significant deterioration [30]. Hence, an abrupt increment of loss ($\alpha_l = 0.01$) was required to observe the detrimental effects. The losses produced a deterioration of the dispersion relation β and Bloch impedance Z_B. All of this resulted in a decrement of transmission in the operation bandwidth, while a increment of transmission in the stop-bands was observed. This is particularly noticeable at $3f_p$ and above, where these harmonic should not be transmitted. As a consequence, there is a decrease in the parametric gain G_s.

5.1.2 Comparison between FWM and TWM

(i) The strip designed to support TWM has a smaller variation of its Bloch impedance and parametric gain when loss was added. Therefore, the line can be designed assuming a lossless transmission line.

(ii) In addition, the FWM dispersion-engineered transmission line has a stop-band in the middle of the range of frequencies where the amplifier could be used, and as a result, reduces the effective operation bandwidth.

(iii) The DC current added in the design that supports TWM has an additional degree of freedom to optimize the parametric gain. Similar levels of parametric gain can obtained by reducing the reference power, while adding the direct current.

Because of these advantages, the TWM dispersion engineered transmission line is the better choice.

5.1.3 The addition of harmonics to the model

The derivation of the coupled mode equations (section 4.2.2 and 3.1.2) was not complete. The main problem is that the condition of conservation of energy was not satisfied. This resulted in complications to understand how the harmonics affected the parametric gain.

5.1.4 Problem with larger gain by adding loss

The addition of losses to the coupled-mode equations has resulted in an increased parametric gain. This effect -counter-intuitive for sure- was described in section (4.3.4.5). This phenomena might results from the fact that the effect introduced by these losses do not satisfy the conservation of momentum and energy of the amplitudes in the coupled-mode equations.

5.2 Future work

(i) Including not only the combination of harmonics between the pump and target signal ($nf_p + mf_s$), but also the pump signal (nf_p) in the analysis in order to complete the coupled mode equations.

(ii) Addressing the problem of section (4.3.4.5). It can be done by obtaining an analytical solution with the inclusion of losses, it might allow us to have a better understanding of the problem.

(iii) In order to have a better performance of the device, different approaches could be studied, such as the *inverted microstrip line*. It would allows us to achieve a characteristic impedance in the line of $50\,\Omega$ with a larger line width. Another different approach is changing the design to a parametric amplifier using a coplanar wave-guide artificial transmission line [39]. This type of amplifier would be fabricated in CPW. It is easier to fabricate and a $50\,\Omega$ transmission line can be obtained.

Bibliography

[1] V. Kumar et al., "AlGaN/GaN HEMTs on SiC with fTof over 120 GHz," in IEEE Electron Device Letters, vol. 23, no. 8, pp. 455-457, Aug. 2002. doi: 10.1109/LED.2002.801303

[2] P. de Bernardis, P. A. R. Ade, J. J. Bock, J. R. Bond, J. Borrill, A. Boscaleri, K. Coble, B. P. Crill, G. De Gasperis, P. C. Farese, P. G. Ferreira, K. Ganga, M. Giacometti, E. Hivon, V. V. Hristov, A. Iacoangeli, A. H. Jaffe, A. E. Lange, L. Martinis, S. Masi, P. V. Mason, P. D. Mauskopf, A. Melchiorri, L. Miglio, T. Montroy, C. B. Netterfield, E. Pascale, F. Piacentini, D. Pogosyan, S. Prunet, S. Rao, G. Romeo, J. E. Ruhl, F. Scaramuzzi, D. Sforna, and N. Vittorio, *"A flat universe from high-resolution maps of the cosmic microwave background radiation,"* Nature 404 (2000), no. 6781, 955–959.

[3] National Radio Astronomy Observatory, "Cooled HFET amplifier development," August 1999.

[4] Tapia, Valeria & Nesti, R & Gonzalez, Alvaro & Barrueto, I & Mena, F.P. & Reyes, Nicolas & Villa, F & Cuttaia, Francesco & Yagoubov, P. (2016). An ultra-broadband optical system for ALMA Band 2+3. 10.1117/12.2233143.

[5] O. Noroozian et al., "Superconducting parametric amplifiers: The next big thing in (Sub)millimeter-wave receivers," *2018 United States National Committee of URSI National Radio Science Meeting (USNC-URSI NRSM)*, Boulder, CO, 2018, pp. 1-2.

[6] A. L. Cullen, "Theory of the travelling-wave parametric amplifier," Nature Physics 181, 332 (1958).

[7] B. H. Eom, P. Day, H. LeDuc, and J. J Zmuidzinas, "A wideband, low-noise superconducting amplifier with high dynamic range," Nature Physics 8, 623 (2012).

[8] T. Shiino, S. Shiba, N. Sakai, T. Yamakura, L. Jiang, Y. Uzawa, H. Maezawa, and S. Ya-mamoto, "Improvement of the critical temperature of superconducting NbTiN and NbN thin films using the AlN buffer layer", *Superconductor Science and Technology*, vol. 23,p. 045004, mar 2010.

[9] Christhopher Stewart Macklin, "Quantum Feedback and Traveling-wave Parametric Amplification in Superconducting Circuits," University of California, Berkeley, 2015.

[10] David M. Pozar, "Microwave engineering," 4th Edition, John Wiley & Sons Inc, pp

1-448.

[11] S. Chaudhuri, J. Gao and K. Irwin, "Simulation and Analysis of Superconducting Traveling-Wave Parametric Amplifiers," in IEEE Transactions on Applied Superconductivity, vol. 25, no. 3, pp. 1-5, June 2015, Art no. 1500705.

[12] J.Perruisseau-carrier, "Microwave periodic structures based on microelectromechanical systems (MEMS) and micromachining techniques".

[13] J. Coonrod, "Comparing microstrip and cpw performance," *Microwave Journal*, vol. 55,pp. 74–82, 07 2012.

[14] M. V. Schneider, "Microstrip Lines for Microwave Integrated Circuits," The Bell System Technical Journal, vol. 48, pp. 1421-1444, May 1969.

[15] D. Dew-Hughes, "The critical current of superconductors: an historical review," *Low Temperature Physics,* vol. 27, no. 9, pp. 713-722, 2001.

[16] "Superconductivity: The meissner effect, persistent currents, and the josephson effects mit,"2017.

[17] S. Massidda, "Superconductivity: from BSC to modern electronic structure theory", University of Cagliari, 2018.

[18] J. Bardeen, L. N. Cooper, and J, R. Schrieffer, "Theory of supercoductivity," *Phys. Rev,*, vol. 108, pp. 1175-1204, Dec 1957.

[19] C. P. McClay, S. Soares, P. S. Weitzman. "Superconducting Microwave Transmission Lines,". The MITRE Corporation Bedford, Massachusetts. 1991. pp. 3-12.

[20] R. Pöpel,"Surface impedance and reflectivity of superconductors," pp 5953, December 1989.

[21] R.L.Kautz, "Picoseconds pulses on superconducting striplines," pp 310, January 1978.

[22] C. Timm, Class Lecture, Topic: "Theory of Superconductivity," Institute of Theoretical Physics, TU Dresden, Dresden, Feb. 2016.

[23] S.M. Anlage, H.J Snortland and M.R.Beasley,"A current controlled variable delay superconducting transmission line," *in IEEE Transactions on Magnetics*, vol.25, no.2, pp. 1388-1391, March 1989.

[24] A. A. Adamyan, S. E. de Graaf, S. E. Kubatkin, and A. V. Danilov, "Superconducting microwave parametric amplifier based on a quasi-fractal slow propagation line," *Journal of Applied Physics*, vol. 119, no. 8, p. 083901, 2016.

[25] M. Calvo, J. Goupy, A. D'Addabbo, A. Benoit, O. Bourrion, A. Catalano, and A. Monafardini, "Superconducting kinetic inductance detectors for astronomy and particle physics," *Nuclear Instruments and Methods in Physics Research Section A: Accelerators,*

Spectrometers, Detectors and Associated Equipment, vol 824, pp 173-176. Frontier Detectors for Frontier Physics: Proccedings of the 13th Pisa Meeting on Advanced Detectors.

[26] J. Luomaahara, V. Vesterine, L. Grnberg, and J. Hassel, "Kinetic inductance magnetometer," *Nature Communications*, vol 5, p.4872, 09 2014.

[27] D. C. Mattis and J. Bardeen, "Theory of the anomalous skin effect in normal and superconducting metals," *Phys. Rev.*, vol. 111, pp. 412-417, Jul 1958.

[28] A. R. Kerr, "Surface Impedance of Superconductors and Normal Conductors in EM Simulators," Jan 1999.

[29] M.R. Perry and R.R Lentz, "9 - susceptors in microwave packaging, " Development of Packaging and Products for Use in Microwave Ovens," (M. W. Lorence and P. S. Pesheek, eds), pp.207-236, Woodhead Publishing, 2009.

[30] F. P. Mena, Priv. Comm. (2018).

[31] G Yassin and S Withington, "Electromagnetic models for superconducting millimeter-wave and sub-milimeter-wave microstrip transmission lines," 1995 J. Phys. D: Appl. Phys. 28 1983.

[32] P.D Nation, J.R Johansson, M.P. Blencowe, Franco Nori, "Stimulating Uncertainty: Amplifying the Quantum Vacumm with Superconducting Circuits," et al. Rev.Mod.Phys. 84 (2012).

[33] G. P. Agrawal, "Nonlinear Fiber Optics," Third Edition, Paul L. Keller, Ivan P. Kaminov, January 2001.

[34] M. Attenborough, "8 - the exponential function," in *Mathematics for Electrical Engineering and Computing* (M. Attenborough, ed), pp. 162 - 187, Oxford: Newnes, 2003.

[35] E. J. Denlinger, "Losses of microstrip lines," *IEEE Transactions on Microwave Theory and Techniques*, vol. 28, pp. 513–522, Jun 1980.

[36] D.Valenzuela, "Amplificadores parametricos de onda viajera e inductancia cinetíca," January 2018.

[37] B. H. Eom, P. Day, H. LeDuc, and J. J Zmuidzinas, "A wideband, low-noise superconducting amplifier with high dynamic range," Supplementary Information, Nature Physics 8, 623 (2012).

[38] Vissers, M.R., Erickson, R.P., Ku, H.S., Vale, L.R., Wu, X., Hilton, G.C., & Pappas, D.P. (2016). "Low-noise kinetic inductance traveling-wave amplifier using three-wave mixing". Applied physics letters, 108.

[39] S.Chaudhuri, D. Li, K. D. Irwin, C. Bockstiegel, J. Hubmayr, J. N. Ullom, M. R. Vissers, and J. Gao, "Broadband parametric amplifiers base on nonlinear kinetic inductance artificial transmission lines", *Applied Physics Letters*, vol. 110, no. 15, p. 152601, 2017.

Appendix A

Components of I^3

In the FWM effect, the current can be expressed as

$$I(z) = \frac{1}{2}\left(\sum_{j=1}^{4} A_j(z)\exp\left(\mathrm{i}\phi_j\right) + c.c.\right), \tag{A.1}$$

where I^3 is given by

$$\begin{aligned}
\frac{I^3}{3} &= A_1^2A_1^*\mathrm{e}^{\mathrm{i}\phi_1} + 2A_1A_2A_1^*\mathrm{e}^{\mathrm{i}\phi_2} + 2A_1A_3A_1^*\mathrm{e}^{\mathrm{i}\phi_3} + 2A_2A_3A_1^*\mathrm{e}^{\mathrm{i}(\phi_3+\phi_2-\phi_1)} \\
&+ 2A_1A_4A_1^*\mathrm{e}^{\mathrm{i}\phi_4} + 2A_2A_4A_1^*\mathrm{e}^{\mathrm{i}(\phi_2+\phi_4-\phi_1)} + 2A_3A_4A_1^*\mathrm{e}^{\mathrm{i}(\phi_4+\phi_3-\phi_1)} + A_1^2A_2^*\mathrm{e}^{\mathrm{i}(2\phi_1-\phi_2)} \\
&+ A_1^2A_2^*\mathrm{e}^{\mathrm{i}(2\phi_1-\phi_2)} + A_1^2A_3^*\mathrm{e}^{\mathrm{i}(2\phi_1-\phi_3)} + A_1^2A_4^*\mathrm{e}^{\mathrm{i}(2\phi_1-\phi_4)} + A_2^2A_2^*\mathrm{e}^{\mathrm{i}\phi_2} \\
&+ A_2^2A_3^*\mathrm{e}^{\mathrm{i}(2\phi_2-\phi_3)} + A_2^2A_4^*\mathrm{e}^{\mathrm{i}(2\phi_2-\phi_4)} + A_3^2A_2^*\mathrm{e}^{\mathrm{i}(2\phi_3-\phi_2)} + A_3^2A_3^*\mathrm{e}^{\mathrm{i}\phi_3} \\
&+ A_3^2A_4^*\mathrm{e}^{\mathrm{i}(2\phi_3-\phi_4)} + A_4^2A_2^*\mathrm{e}^{\mathrm{i}(2\phi_4-\phi_2)} + A_4^2A_3^*\mathrm{e}^{\mathrm{i}(2\phi_4-\phi_3)} + A_4^2A_4^*\mathrm{e}^{\mathrm{i}\phi_4} + 2A_1A_2A_2^*\mathrm{e}^{\mathrm{i}\phi_1} \\
&+ 2A_1A_2A_3^*\mathrm{e}^{\mathrm{i}(\phi_1+\phi_2-\phi_3)} + 2A_1A_2A_4^*\mathrm{e}^{\mathrm{i}(\phi_1+\phi_2-\phi_4)} + 2A_1A_3A_2^*\mathrm{e}^{\mathrm{i}(\phi_1-\phi_2+\phi_3)} + 2A_1A_3A_3^*\mathrm{e}^{\mathrm{i}\phi_1} \\
&+ 2A_1A_3A_4^*\mathrm{e}^{\mathrm{i}(\phi_1+\phi_3-\phi_4)} + 2A_2A_3A_2^*\mathrm{e}^{\mathrm{i}\phi_3} + 2A_2A_3A_3^*\mathrm{e}^{\mathrm{i}\phi_2} \\
&+ 2A_2A_3A_4^*\mathrm{e}^{\mathrm{i}(\phi_2+\phi_3-\phi_4)} + 2A_1A_4A_2^*\mathrm{e}^{\mathrm{i}(\phi_1-\phi_2+\phi_4)} + 2A_1A_4A_3^*\mathrm{e}^{\mathrm{i}(\phi_1-\phi_3+\phi_4)} \\
&+ 2A_1A_4A_4^*\mathrm{e}^{\mathrm{i}\phi_1} + 2A_2A_4A_2^*\mathrm{e}^{\mathrm{i}\phi_4} + 2A_2A_4A_3^*\mathrm{e}^{\mathrm{i}(\phi_2-\phi_3+\phi_4)} + 2A_2A_4A_4^*\mathrm{e}^{\mathrm{i}(\phi_2)} \\
&+ 2A_3A_4A_2^*\mathrm{e}^{\mathrm{i}(\phi_4+\phi_3-\phi_2)} + 2A_4A_3A_3^*\mathrm{e}^{\mathrm{i}\phi_4} + 2A_3A_4A_4^*\mathrm{e}^{\mathrm{i}\phi_3} + \\
&+ \frac{1}{3}A_1^3\mathrm{e}^{3\mathrm{i}\phi_1} + \frac{1}{3}A_2^3\mathrm{e}^{3\mathrm{i}\phi_2} + \frac{1}{3}A_3^3\mathrm{e}^{3\mathrm{i}\phi_3} + \frac{1}{3}A_4^3\mathrm{e}^{3\mathrm{i}\phi_4} + c.c.
\end{aligned} \tag{A.2}$$

From Eq. (A.2). The components related with SPM are:

$$A_1^2A_1^*\mathrm{e}^{\mathrm{i}\phi_1} + A_2^2A_2^*\mathrm{e}^{\mathrm{i}\phi_2} + A_3^2A_3^*\mathrm{e}^{\mathrm{i}\phi_3} + A_4^2A_4^*\mathrm{e}^{\mathrm{i}\phi_4}. \tag{A.3}$$

The components related with XPM are:

$$\begin{aligned}
&2A_1A_2A_1^*\mathrm{e}^{\mathrm{i}\phi_2} + 2A_1A_3A_1^*\mathrm{e}^{\mathrm{i}\phi_3} + 2A_1A_4A_1^*\mathrm{e}^{\mathrm{i}\phi_4} + 2A_4A_3A_3^*\mathrm{e}^{\mathrm{i}\phi_4} + 2A_3A_4A_4^*\mathrm{e}^{\mathrm{i}\phi_3} + \\
&2A_2A_3A_2^*\mathrm{e}^{\mathrm{i}\phi_3} + 2A_2A_4A_4^*\mathrm{e}^{\mathrm{i}\phi_2} + 2A_2A_3A_3^*\mathrm{e}^{\mathrm{i}\phi_2} + 2A_1A_2A_2^*\mathrm{e}^{\mathrm{i}\phi_1} + 2A_1A_3A_3^*\mathrm{e}^{\mathrm{i}\phi_1} + \\
&2A_1A_4A_4^*\mathrm{e}^{\mathrm{i}\phi_1} + 2A_4A_2A_2^*\mathrm{e}^{\mathrm{i}\phi_4}
\end{aligned} \tag{A.4}$$

Appendix B

Details of analytical solution: FWM coupled mode equations

Using the method of the eigenvalue and eigenvectors in Eq. (3.28), the variables B_{i}^{*} and B_s are defined as

$$B_s(z) = a_{1\lambda}\mathrm{e}^{\mathrm{i}(\lambda-\kappa/2)z}, \qquad B_{\mathrm{i}}^{*}(z) = a_{2\lambda}\mathrm{e}^{\mathrm{i}(\lambda+\kappa/2)z}, \tag{B.1}$$

where $a_{1\lambda}$ and $a_{2\lambda}$ are the eigenvectors associated with their own eigenvalue λ. The new system is solved by using Eq. (B.1) in Eq. (3.28) and (3.29). We find that the matrix system is given by

$$\begin{pmatrix} -\left(\lambda - \frac{\mathrm{i}\kappa}{2}\right) & \mathrm{i}\gamma P_p \\ -\mathrm{i}\gamma P_p & -\left(\lambda + \frac{\mathrm{i}\kappa}{2}\right) \end{pmatrix} \begin{pmatrix} a_{1\lambda} \\ a_{2\lambda} \end{pmatrix} = 0. \tag{B.2}$$

Because non trivial solutions are needed to understand the behaviour of the parametric gain, the vector $(a_{1\lambda}, a_{2\lambda})^T$ can not be zero. As a result, the determinant of the matrix shown in Eq. (B.2) must be zero. Furthermore, the eigenvalues of matrix can be written as

$$\lambda_{\pm} = \pm\sqrt{(\gamma P_p)^2 - \left(\frac{\kappa}{2}\right)^2} \equiv \pm g, \tag{B.3}$$

where g is defined as the dispersion component of the parametric gain. g can also be written as

$$g^2 = -\Delta\beta\left(\frac{\Delta\beta}{4} + \frac{k_p\left|A_p\right|^2}{I_*'^2}\right). \tag{B.4}$$

As a result, the general expressions for B_s and B_{i}^{*} are given as

$$B_s = \left(C_1 a_{\lambda+}\mathrm{e}^{gz} + C_2 a_{\lambda-}\mathrm{e}^{-gz}\right)\mathrm{e}^{-\mathrm{i}\frac{\kappa}{2}z}, \tag{B.5}$$

$$B_{\mathrm{i}}^{*} = \left(C_1 b_{\lambda+}\mathrm{e}^{gz} + C_2 b_{\lambda-}\mathrm{e}^{-gz}\right)\mathrm{e}^{+\mathrm{i}\frac{\kappa}{2}z}. \tag{B.6}$$

This means that the amplitude of the signals have an evanescence and phase part, as expected from solutions that come from the wave equation for transmission lines. By using Eq. (B.3) and (B.2), the eigenvectors are given by

$$v_{\lambda+} = \begin{pmatrix} a_{\lambda+} \\ \\ b_{\lambda+} \end{pmatrix} = \begin{pmatrix} \mathrm{i}\gamma P_p \\ \\ g - \frac{\mathrm{i}\kappa}{2} \end{pmatrix}, \tag{B.7}$$

$$v_{\lambda-} = \begin{pmatrix} a_{\lambda-} \\ \\ b_{\lambda-} \end{pmatrix} = \begin{pmatrix} g - \frac{\mathrm{i}\kappa}{2} \\ \\ \mathrm{i}\gamma P_p \end{pmatrix}. \tag{B.8}$$

Therefore, Eq. (B.5) and (B.6) can be rewritten as

$$B_s = \left(C_1 \mathrm{i}\gamma P_p \mathrm{e}^{gz} + C_2 \left(g - \frac{\mathrm{i}\kappa}{2} \right) \mathrm{e}^{-gz} \right) \mathrm{e}^{-\mathrm{i}\frac{\kappa}{2}z}, \tag{B.9}$$

$$B_{\mathrm{i}}^* = \left(C_1 \left(g - \frac{\mathrm{i}\kappa}{2} \right) \mathrm{e}^{gz} + C_2 \mathrm{i}\gamma P_p \mathrm{e}^{-gz} \right) \mathrm{e}^{\mathrm{i}\frac{\kappa}{2}z}. \tag{B.10}$$

To determine the constants C_1 and C_2, we use boundary conditions. These conditions can be obtained by stating that the power of the pump signal A_s and the target signal A_p are known at $z = 0$. The known coefficients are calculated by using Eq. (3.27), which can be written as

$$B_s(0) = A_s(0) \exp(0) = A_s(0), \tag{B.11}$$

$$B_{\mathrm{i}}^*(0) = A_{\mathrm{i}}^*(0) \exp(0) = A_{\mathrm{i}}(0). \tag{B.12}$$

By using the boundary conditions, we find that $B_s(z)$ and $B_{\mathrm{i}}^*(z)$ are given by

$$B_s(z) = \left[A_s(0)\cosh(gz) + \frac{\mathrm{i}}{g} \left(\gamma P_p A_{\mathrm{i}}(0) + \frac{\kappa}{2} A_s(0) \right) \sinh(gz) \right] \exp\left(-\frac{\mathrm{i}\kappa}{2} z \right), \tag{B.13}$$

$$B_{\mathrm{i}}^*(z) = \left[A_{\mathrm{i}}(0)\cosh(gz) - \frac{\mathrm{i}}{g} \left(\gamma P_p A_s(0) + \frac{\kappa}{2} A_{\mathrm{i}}(0) \right) \sinh(gz) \right] \exp\left(+\frac{\mathrm{i}\kappa}{2} z \right). \tag{B.14}$$

Now that every variable is obtained, an unroll of the defined variables is needed in order to obtain the complete expressions of the amplitudes of the target and pump signals. By substituting Eq. (B.13) and (B.14) in Eq. (3.27), $A_s(z)$ and $A_{\mathrm{i}}(z)$ are given by

$$A_s(z) = \left[A_s(0)\cosh(gz) + \frac{\mathrm{i}}{g}\left(\gamma P_p A_\mathrm{i}(0) + \frac{\kappa}{2}A_s(0)\right)\sinh(gz)\right]\mathrm{e}^{\mathrm{i}(2\gamma P_p - \frac{\kappa}{2})z}, \tag{B.15}$$

$$A_\mathrm{i}(z) = \left[A_\mathrm{i}(0)\cosh(gz) + \frac{\mathrm{i}}{g}\left(\gamma P_p A_s(0) + \frac{\kappa}{2}A_\mathrm{i}(0)\right)\sinh(gz)\right]\mathrm{e}^{\mathrm{i}(2\gamma P_p - \frac{\kappa}{2})z}. \tag{B.16}$$

The parametric gain of an amplifier with a transmission line of length L is given by

$$G_s = \frac{|A_s(L)|^2}{|A_s(0)|^2} \quad , \quad G_\mathrm{i} = \frac{|A_\mathrm{i}(L)|^2}{|A_\mathrm{i}(0)|^2}, \tag{B.17}$$

where $|A_s(z)|^2$ and $|A_\mathrm{i}(z)|^2$ are the power of the target and idle signals, respectively. Squaring Eq. (B.15) and (B.16) we obtain

$$|A_s(z)|^2 = A_s^2(0)\cosh^2(gz) + D^2\sinh^2(gz), \tag{B.18}$$

$$|A_\mathrm{i}(z)|^2 = A_\mathrm{i}^2(0)\cosh^2(gz) + F^2\sinh^2(gz), \tag{B.19}$$

with D^2 and F^2 defined as

$$D^2 = \frac{\kappa\gamma P_p}{g^2}A_s(0)A_\mathrm{i}(0) + \left(\frac{\gamma P_p}{g}\right)^2\left(A_s^2(0) + A_\mathrm{i}^2(0)\right) - A_s^2(0), \tag{B.20}$$

$$F^2 = \frac{\kappa\gamma P_p}{g^2}A_s(0)A_\mathrm{i}(0) + \left(\frac{\gamma P_p}{g}\right)^2\left(A_s^2(0) + A_\mathrm{i}^2(0)\right) - A_\mathrm{i}^2(0). \tag{B.21}$$

The amplitude of the idler wave is created during the amplification. As a result, there is not an idle source as input in the amplifier, i.e $A_\mathrm{i}(0) = 0$. Then, the coefficients D and F are reduced to $D = A_s(0)\kappa/2g$ and $F = A_s(0)\gamma P_p/g$.

Appendix C

Components of I^2

By using Eq. (A.1), I^2 is given by

$$
\begin{aligned}
I^2 = {} & 2A_2A_1^*e^{i(\phi_2-\phi_1)} + 2A_3A_1^*e^{i(\phi_3-\phi_1)} + 2A_4A_1^*e^{i(\phi_4-\phi_1)} \\
& + A_1A_2^*e^{i(\phi_1-\phi_2)} + 2A_1A_3^*e^{i(\phi_1-\phi_3)} + 2A_1A_4^*e^{i(\phi_1-\phi_4)} \\
& + 2A_2A_3^*e^{i(\phi_2-\phi_3)} + 2A_2A_4^*e^{i(\phi_2-\phi_4)} + 2A_3A_2^*e^{i(\phi_3-\phi_2)} \\
& + 2A_3A_4^*e^{i(\phi_3-\phi_4)} + 2A_4e^{i(\phi_4-\phi_2)} + 2A_4A_3^*e^{i(\phi_4-\phi_3)} \\
& + 2|A_1|^2 + 2|A_2|^2 + 2|A_3|^2 + 2|A_4|^2 + A_1^2e^{2i\phi_1} + A_2^2e^{2i\phi_2} \\
& + A_3^2e^{2i\phi_3} + A_1^2e^{2i\phi_4} + 2A_1A_2e^{i(\phi_1+\phi_2)} + 2A_1A_3e^{i(\phi_1+\phi_3)} \\
& + 2A_2A_3e^{i(\phi_2+\phi_3)} + 2A_1A_4e^{i(\phi_1+\phi_4)} + 2A_2A_4e^{i(\phi_2+\phi_4)} \\
& + 2A_3A_4e^{i(\phi_3+\phi_4)} + c.c.
\end{aligned}
\tag{C.1}
$$

We can observe that there are not elements related with SPM and XPM. However, the components of these effects in FWM are considered in Eq. (4.4), (4.5) and (4.6).

Appendix D

Details of analytical solution: TWM coupled mode equations

Using the method of eigenvalue and eigenvectors in Eq. (4.14), the variables B_{i}^* and B_s are defined as

$$B_s(z) = a_{1\lambda}\mathrm{e}^{\mathrm{i}(\lambda-\kappa/2)z}, \qquad B_{1\mathrm{i}}^*(z) = a_{2\lambda}\mathrm{e}^{\mathrm{i}(\lambda+\kappa/2)z}, \tag{D.1}$$

where the coefficients $a_{1\lambda}$ and $a_{2\lambda}$ are the eigenvector associated with its eigenvalue λ. Therefore, from Eq. (4.14) and (4.15), the matrix system of the coupled equations is given by

$$\begin{pmatrix} -\left(\lambda - \frac{\mathrm{i}\kappa}{2}\right) & \frac{8\mathrm{i}\gamma}{3}\sqrt{P_{DC}P_p} \\ -\frac{8\mathrm{i}\gamma}{3}\sqrt{P_{DC}P_p} & -\left(\lambda + \frac{\mathrm{i}\kappa}{2}\right) \end{pmatrix} \begin{pmatrix} a_{1\lambda} \\ a_{2\lambda} \end{pmatrix} = 0. \tag{D.2}$$

The eigenvalues λ of matrix can be written as

$$\lambda_{\pm} = \pm\sqrt{\frac{64}{9}\gamma^2 P_{DC}P_p - \left(\frac{\kappa}{2}\right)^2} = \pm g_{DC}, \tag{D.3}$$

where we define the parameter $g_{DC} = \sqrt{\frac{64}{9}\gamma^2 P_{DC}P_p - \left(\frac{\kappa}{2}\right)^2}$. As a result, the general expressions for B_s and B_s^* is given by

$$B_s = \left(C_1 a_{\lambda+}\mathrm{e}^{gz} + C_2 a_{\lambda-}\mathrm{e}^{-gz}\right)\mathrm{e}^{-\mathrm{i}\frac{\kappa}{2}z}, \tag{D.4}$$

$$B_{\mathrm{i}}^* = \left(C_1 b_{\lambda+}\mathrm{e}^{gz} + C_2 b_{\lambda-}\mathrm{e}^{-gz}\right)\mathrm{e}^{+\mathrm{i}\frac{\kappa}{2}z}. \tag{D.5}$$

The general solution to the evolution of the amplitude of the signals involved in TWM is shown in Eq. (D.4) and (D.5). By using Eq. (D.3) and (D.2), the eigenvectors are given by

$$v_{\lambda+} = \begin{pmatrix} a_{\lambda+} \\ \\ b_{\lambda+} \end{pmatrix} = \begin{pmatrix} \frac{8\mathrm{i}\gamma}{3}\sqrt{P_{DC}P_p} \\ \\ g - \frac{\mathrm{i}\kappa}{2} \end{pmatrix}, \tag{D.6}$$

$$v_{\lambda-} = \begin{pmatrix} a_{\lambda-} \\ \\ b_{\lambda-} \end{pmatrix} = \begin{pmatrix} g - \frac{\mathrm{i}\kappa}{2} \\ \\ \frac{8\mathrm{i}\gamma}{3}\sqrt{P_{DC}P_p} \end{pmatrix}. \tag{D.7}$$

Thus, Eq. (D.4) and (D.5) can be rewritten as

$$B_s = \left(C_1 \frac{8\mathrm{i}\gamma}{3}\sqrt{P_{DC}P_p}\mathrm{e}^{gz} + C_2\left(g - \frac{\mathrm{i}\kappa}{2}\right)\mathrm{e}^{-gz}\right)\mathrm{e}^{-\mathrm{i}\frac{\kappa}{2}z}, \tag{D.8}$$

$$B_{\mathrm{i}}^* = \left(C_1\left(g - \frac{\mathrm{i}\kappa}{2}\right)\mathrm{e}^{gz} + C_2 \frac{8\mathrm{i}\gamma}{3}\sqrt{P_{DC}P_p}\mathrm{e}^{-gz}\right)\mathrm{e}^{\mathrm{i}\frac{\kappa}{2}z}. \tag{D.9}$$

The determination of the constant C_1 and C_2 can be achieve by stating that the pump and target signal are known at $z = 0$. By using Eq. (4.13), those are defined as

$$B_s(0) = A_s(0)\exp(0) = A_s(0), \tag{D.10}$$

$$B_{\mathrm{i}}^*(0) = A_{\mathrm{i}}^*(0)\exp(0) = A_{\mathrm{i}}(0). \tag{D.11}$$

As a result, it is found that $B_s(z)$ and $B_{\mathrm{i}}^*(z)$ are of the form

$$B_s(z) = \left[A_s(0)\cosh(gz) + \frac{\mathrm{i}}{g}\left(\frac{8\gamma}{3}\sqrt{P_{DC}P_p}A_{\mathrm{i}}(0) + \frac{\kappa}{2}A_s(0)\right)\sinh(gz)\right]\mathrm{e}^{\left(-\frac{\mathrm{i}\kappa}{2}z\right)}, \tag{D.12}$$

$$B_{\mathrm{i}}^*(z) = \left[A_{\mathrm{i}}(0)\cosh(gz) - \frac{\mathrm{i}}{g}\left(\frac{8\gamma}{3}\sqrt{P_{DC}P_p}A_s(0) + \frac{\kappa}{2}A_{\mathrm{i}}(0)\right)\sinh(gz)\right]\mathrm{e}^{\left(+\frac{\mathrm{i}\kappa}{2}z\right)}. \tag{D.13}$$

Subsequently, Eq. (D.12) and (D.13) are introduced in (4.13) to obtain $A_s(z)$ and $A_{\mathrm{i}}(z)$, which are given by

$$\begin{aligned} A_s(z) = &\left[A_s(0)\cosh(gz) + \frac{\mathrm{i}}{g}\left(\frac{8\gamma}{3}\sqrt{P_{DC}P_p}A_{\mathrm{i}}(0) + \frac{\kappa}{2}A_s(0)\right)\sinh(gz)\right] \\ &\exp\left[\mathrm{i}\left(\gamma\left(\frac{4}{3}P_{DC} + 2P_p\right) - \frac{\kappa}{2}\right)z\right], \end{aligned} \tag{D.14}$$

$$A_{\mathrm{i}}(z) = \left[A_{\mathrm{i}}(0)\cosh(gz) + \frac{\mathrm{i}}{g}\left(\frac{8\gamma}{3}\sqrt{P_{DC}P_p}A_s(0) + \frac{\kappa}{2}A_{\mathrm{i}}(0)\right)\sinh(gz)\right] \exp\left[\mathrm{i}\left(\gamma\left(\frac{4}{3}P_{DC} + 2P_p\right) - \frac{\kappa}{2}\right)z\right]. \tag{D.15}$$

The gain of the amplifier depends on the effective length L of the transmission line, and is defined as the ratio between the amplitude of the target signal at the beginning of the device and the end of it. This ratio can be defined as following expressions

$$G_s = \frac{|A_s(L)|^2}{|A_s(0)|^2} \quad , \quad G_{\mathrm{i}} = \frac{|A_{\mathrm{i}}(L)|^2}{|A_{\mathrm{i}}(0)|^2}. \tag{D.16}$$

The evolution with respect the position $|A_s(z)|^2$ and $|A_{\mathrm{i}}(z)|^2$ are given by

$$|A_s(z)|^2 = A_s^2(0)\cosh^2(gz) + D^2\sinh^2(gz), \tag{D.17}$$
$$|A_{\mathrm{i}}(z)|^2 = A_{\mathrm{i}}^2(0)\cosh^2(gz) + F^2\sinh^2(gz), \tag{D.18}$$

where D^2 and F^2 are defined as

$$D^2 = \frac{8\kappa\gamma P_p}{3g^2}A_s(0)A_{\mathrm{i}}(0) + \left(\frac{8\gamma}{3g}\right)^2 P_{DC}P_P\left(A_s^2(0) + A_{\mathrm{i}}^2(0)\right) - A_s^2(0), \tag{D.19}$$
$$F^2 = \frac{8\kappa\gamma P_p}{3g^2}A_s(0)A_{\mathrm{i}}(0) + \left(\frac{8\gamma}{3g}\right)^2 P_{DC}P_P\left(A_s^2(0) + A_{\mathrm{i}}^2(0)\right) - A_{\mathrm{i}}^2(0). \tag{D.20}$$